SEISMIC PERFORMANCE OF MASONRY BUILDINGS SUBJECTED TO SYNTHETIC GROUND MOTIONS

A THESIS SUBMITTED TO
THE GRADUATE SCHOOL OF NATURAL AND APPLIED SCIENCES
OF
MIDDLE EAST TECHNICAL UNIVERSITY

BY

AHMET BAHADIR KOÇ

IN PARTIAL FULFILLMENT OF THE REQUIREMENTS
FOR
THE DEGREE OF MASTER OF SCIENCE
IN
CIVIL ENGINEERING

JUNE 2019

Approval of the thesis:

SEISMIC PERFORMANCE OF MASONRY BUILDINGS SUBJECTED TO SYNTHETIC GROUND MOTIONS

submitted by **AHMET BAHADIR KOÇ** in partial fulfillment of the requirements for the degree of **Master of Science in Civil Engineering Department, Middle East Technical University** by,

Prof. Dr. Halil Kalıpçılar
Dean, Graduate School of **Natural and Applied Sciences** __________________

Prof. Dr. Ahmet Türer
Head of Department, **Civil Engineering** __________________

Prof. Dr. Murat Altuğ Erberik
Supervisor, **Civil Engineering, METU** __________________

Prof. Dr. Ayşegül Askan Gündoğan
Co-Supervisor, **Civil Engineering, METU** __________________

Examining Committee Members:

Assist. Prof. Dr. Onur Pekcan
Civil Engineering, METU __________________

Prof. Dr. Murat Altuğ Erberik
Civil Engineering, METU __________________

Prof. Dr. Ayşegül Askan Gündoğan
Civil Engineering, METU __________________

Assist. Prof. Dr. Bekir Özer Ay
Department of Architecture, METU __________________

Assoc. Prof. Dr. Alper Aldemir
Civil Engineering, Hacettepe University __________________

Date: 20.06.2019

I hereby declare that all information in this document has been obtained and presented in accordance with academic rules and ethical conduct. I also declare that, as required by these rules and conduct, I have fully cited and referenced all material and results that are not original to this work.

Name, Surname: Ahmet Bahadır Koç

Signature:

ABSTRACT

SEISMIC PERFORMANCE OF MASONRY BUILDINGS SUBJECTED TO SYNTHETIC GROUND MOTIONS

Koç, Ahmet Bahadır
Master of Science, Civil Engineering
Supervisor: Prof. Dr. Murat Altuğ Erberik
Co-Supervisor: Prof. Dr. Ayşegül Askan Gündoğan

June 2019, 124 pages

Over the centuries, strong seismic activities have occurred with uncertain frequencies in the world which caused earthquake-prone regions to be severely influenced in terms of structural damage and economic losses. Therefore, seismic assessment approaches have been developed to minimize the vulnerability of structures, to carry out pre-earthquake mitigation planning and to mitigate economic losses. This study mainly focuses on the performance estimation of unreinforced masonry (URM) structures using synthetic ground motions, which are based on the simulated 1999 Düzce Earthquake. The performance values of the structural parameters for URM structures have been obtained in accordance with earthquake design specifications and literature reviews and also represent their local characteristics. The equivalent single-degree-of-freedom (SDOF) models are generated to simplify inelastic dynamic analysis by using these parameters. The synthetic ground motion records are generated in the case study Düzce region, by considering different earthquake scenarios, soil conditions and source-to-site distances. The seismic responses of structural simulations represent base shear versus displacement relationship. By comparing the results of displacement obtained from inelastic dynamic analyses and the pre-defined limit states, the damage states (DS) of URM structures are determined. At the end of the study, the sensitivity of the structural parameters, the estimation of performance levels under different magnitude and PGA values and the relationships between DS and independent variables, which comprise seismological and structural parameters, are carried out and the obtained results are interpreted by using probabilistic and statistical approaches.

Keywords: Equivalent SDOF model, Inelastic Dynamic Analysis, Limit State, Estimation of Performance Level, Relationships Between Variables

ÖZ

SENTETİK YER HAREKETLERİNE MARUZ KALMIŞ YIĞMA YAPILARIN SİSMİK PERFORMANSI

Koç, Ahmet Bahadır
Yüksek Lisans, İnşaat Mühendisliği
Tez Danışmanı: Prof. Dr. Murat Altuğ Erberik
Ortak Tez Danışmanı: Prof. Dr. Ayşegül Askan Gündoğan

Haziran 2019, 124 sayfa

Yüzyıllardır dünya üzerinde kuvvetli sismik aktiviteler belirsiz sıklıklarla meydana gelirken deprem bölgeleri yapısal hasar, can kaybı ve ekonomik kayıp yüzünden ciddi olarak etkilenmentedir. Bu sebepten dolayı sismik değerlendirme yöntemleri yapıların zarar görebilirliğini minimize etmek, güçlü depremlerden önce önlemler alabilmek ve ekonomik kayıpları azaltmak için geliştirilmektedir. Bu çalışma esas olarak donatısız yığma yapıların deprem performansının tahminine 1999 Düzce depremine bağlı olarak üretilmiş olan sentetik yer hareketlerini kullanarak odaklanmıştır. Donatısız yığma yapılara ait yapısal parametrelerin performans değerleri, deprem tasarım yönetmeliklerine ve literatür taramalarına uygun bir şekilde elde edilmiştir ve ayrıca bu tür yapıların yerel özelliklerini yansıtmaktadır. Yapısal parametreler kullanılarak oluşturulan ideal tek dereceli modeller yapısal analizi kolaylaştırmaktadır. Sentetik yer hareketi kayıtları, Düzce bölgesindeki farklı senaryo depremleri, zemin tipleri ve deprem kaynağı-kayıt yeri mesafeleri düşünülerek elde edilmiştir. Yapısal simulasyonların analitik davranışı taban kesme kuvveti tepe deplasman ilişkisini yansıtmaktadır. Donatısız yığma yapıların hasar seviyesi, elastik ötesi dinamik yapısal analizlerden elde edilen deplasman sonuçları ve önceden belirlenmiş limit durumları karşılaştırılarak belirlenmektedir. Çalışmanın son kısmında ise yapısal parametrelerin hassaslığı, deprem büyüklükleri ve yer ivme değerleri altında performans seviyelerinin tahmini ile sismolojik ve yapısal parametreleri içeren bağımsız değişkenler arasındaki ilişki olasılıksal ve istatiksel yaklaşımlar ile gerçekleştirilmiştir.

Anahtar Kelimeler: Eşdeğer Tek Dereceli Model, Elastik Ötesi Yapısal Analiz, Limit Durumu, Performans Seviye Tahmini, Değişkenler Arasındaki İlişkiler

My deepest gratitude to my family,

ACKNOWLEDGEMENTS

I would like to express my gratitude to my advisor Prof. Dr. Murat Altuğ Erberik and co-advisor Prof. Dr. Ayşegül Askan Gündoğan for supports, patience, guidance. In addition to this, the advice given by Prof. Dr. Murat Altuğ Erberik about the rest of my life is always one of my road maps. I wish them to health and happiness in the rest of their lives.

Another special and endless thank is to Dr. Shaghayegh Naghshineh for contribution to the progression of the study.

I would also like to thank my brotherlike; Çağlar Yertutan, Aziz Çiçek, Tuna Burak Yiğit and Bünyamin Toker for supports and providing to fun in my life.

I would like to express special thanks to my fellow friends; Furkan Gökmen, Orkun Karalı, Ömer Işıldak, Salih Alaca, Ertürk Tuncer, Alican Tatar, Zafer Karakaş, Volkan Emren, Harun Başaran, İhsan Eroğlu, Serhat Şencan, Mustafa Öz, Çağatay Bal for their endless support.

Other special thanks to parents of my wife İbrahim Süner, Zibiye Süner, and Mustafa Can Süner, the mother's brother Necdet Seyfeli and my cousins Rıza Seyfeli and Mustafa Seyfeli for their understanding and support.

Finally, I would like to express my deepest appreciation to my parents Mustafa Koç and İlknur Koç for their endless support and incredible patience throughout my education life. Besides, my grandfather Rıza Seyfeli and grandmother Müesser Seyfeli will remain as my heroes for their endless moral and material supports in my all life. My wife Eda Süner Koç deserves another my deepest gratitude for endless support, understanding, and patience throughout my university life.

TABLE OF CONTENTS

LIST OF TABLES

TABLES

LIST OF FIGURES

FIGURES

LIST OF ABBREVIATIONS

ABBREVIATIONS

ADRS	:	Acceleration-displacement Spectrum
ATC	:	Applied Technology Council
CDF	:	Cumulative Density Function
CSM	:	Capacity Spectrum Method
DA	:	Discriminant Analysis
df	:	Number of degrees of freedom
DS	:	Damage State
DSM	:	Mean value of damage states
EAF	:	Eastern Anatolian Fault
ESDOF	:	Equivalent Single Degree of Freedom
FEMA	:	Federal Emergency Management Agency
ICSM	:	Improved Capacity Spectrum Method
KMO	:	Kaiser-Meyer-Olkin Measure of Sampling Adequacy
LS	:	Limit State
MDOF	:	Multi Degree of Freedom
MIMK	:	Modified Ibarra-Medina-Krawinkler
MPA	:	Modal Pushover Analysis Method
MRA	:	Multiple Regression Analysis
M_w	:	Moment magnitude
NAF	:	North Anatolian Fault
PBD	:	Performance-based Design
PCA	:	Principal Component Analysis
PDF	:	Probability Density Function
PGA	:	Peak Ground Acceleration

R_{epic}	:	Distance from epicenter of earthquake to source
R_{JB}	:	Joyner-Boore Distance
R_{RUP}	:	Minimum distance from fault plane to source
$SS_{regression}$	:	Sum of squares from regression
$SS_{residual}$	:	Sum of squares from residual
TEC	:	Turkish Earthquake Code
URM	:	Unreinforced Masonry
WAF	:	West Anatolian Fault

LIST OF SYMBOLS

SYMBOLS

μ	:	Ductility ratio
A_o	:	Seismic zone coefficient
cc	:	Canonical correlation
c_n	:	Coefficient of the n^{th} independent variable for MRA
D_j	:	Displacement of ESDOF model for mode j
D_t	:	Top displacement of MDOF model
Dt*	:	Top displacement of ESDOF model
D_y^*	:	Yielding displacement of ESDOF model
e	:	Exponential value (mathematical constant)
f_c	:	Capping strength
f_r	:	Residual strength
F_{sj}	:	Base shear of ESDOF model for mode j
f_y	:	Effective yield strength
g	:	Gravitational acceleration
H	:	Height of structure
I	:	Building importance factor
k	:	Lateral stiffness
K_n	:	Score of independent variables for n^{th} independent variable for MRA
k_r	:	Post-capping stiffness
k_u	:	Post-yielding stiffness
k_{un}	:	Post-yielding stiffness for n^{th} modal shape ESDOF model
k_y	:	Initial elastic stiffness
k_{yn}	:	Yielding stiffness of the structure for n^{th} modal shape ESDOF model
m^*	:	Effective mass of ESDOF model

m_j^*	:	Effective modal mass of ESDOF model for mode j
M_w	:	Magnitude
n	:	Number of items in the sample
N	:	Number of stories
ɳ	:	Strength ratio
PF_1	:	First mode participation factor
R	:	Multiple correlation coefficient
R_μ	:	Ductility reduction factor
$R_a(T)$	:	Seismic load reduction factor
S(T)	:	Spectrum coefficient
S_a	:	Spectral acceleration of ESDOF model
S_{ae}	:	Elastic spectral acceleration
S_d	:	Spectral displacement of ESDOF model
S_{de}	:	Elastic spectral displacement
T	:	Fundamental period
T^*	:	Elastic fundamental period
T_c	:	Characteristic period of the ground motion
u	:	Roof displacement of ESDOF model
u_c	:	Capping displacement
u_{max}	:	Maximum displacement
u_r	:	Residual displacement
u_{rny}	:	Yielding displacement for n^{th} modal shape of ESDOF model
u_{tj}	:	Top displacement of MDOF model for mode j
u_y	:	Yield displacement
Λ	:	Wilks' Lambda
V_b	:	Base shear of MDOF model
V_b^*	:	Base shear of ESDOF model
V_{bj}	:	Base shear of MDOF model for mode j

V_{bny}	:	Yielding base shear for n^{th} modal shape of ESDOF model
V_y^*	:	Yielding strength of ESDOF model
W	:	Weight of structure
$\bar{x}$	:	Sample mean
x_i	:	Value of x at i^{th} sample
X_n	:	Independent variable n
Y	:	Value of the dependent variable
Y^	:	Mean of dependent variable
Y_{fit}	:	Value of the fitted model of the dependent variable
Z_i	:	Discriminant score of discriminant function i
α_m	:	Modal mass coefficient
α_n	:	Post-yielding stiffness ratio for n^{th} modal shape ESDOF model
α_r	:	Post-capping stiffness ratio
α_s	:	Strain hardening ratio
γ	:	Degradation parameter
Γ	:	Modal participation factor
Γ_j	:	Participation factor for mode j
λ	:	Residual strength ratio
λ_e	:	Eigenvalue
π	:	Pi number (mathematical constant)
σ	:	Standard deviation of distribution
σ^2	:	Variance of distribution
ϕ_{ij}	:	Modal amplitude at story level "i" for mode "j"
ϕ_{nj}	:	Top modal shape for mode j
ω_n	:	Frequency of the structure for n^{th} modal shape ESDOF model
Φ	:	Constant deformation shape vector

CHAPTER 1

INTRODUCTION

1.1. General

Earthquake is an inevitable thread within seismically active regions in the world. Turkey has major active faults as North Anatolian Fault (NAF), Eastern Anatolian Fault (EAF) and West Anatolian Fault (WAF). In the last century, Turkey has experienced serious structural damage and collapse of buildings, casualties and economic losses due to large scale earthquakes (i.e. magnitude larger than 7.0) that can be listed as Mürefte-Tekirdağ (1912), Erzincan (1939), Erbaa-Tokat (1942), Ladik-Samsun (1943), Gerede-Bolu (1944), Yenice-Çanakkale (1953), Fethiye-Muğla (1957), Abant-Bolu (1957), Manyas-Balıkesir (1964), Mudurnu-Adapazarı (1967), Gediz-Kütahya (1970), Muradiye-Van (1976), Gölcük-Kocaeli (1999), Kaynaşlı-Düzce (1999) and Tabanlı-Van (2011). In order to mitigate the potential earthquake losses and enhance safety of structures, precautions and restrictions in the form of seismic regulations have been considered in Turkey since 1940s.

Unreinforced masonry (URM) is one of the oldest known construction types where structures are constructed with the combination of mortar and masonry units, commonly termed as clay brick, concrete block, irregular stone, and adobe. Owing to their lower tensile strength capacity from the combination of mortar and masonry units, URM structures represent brittle behavior under earthquake excitation. In addition to this, their load-bearing masonry walls contribute to the structural system by carrying vertical and horizontal loads. They have high inertial responses to the earthquake action due to the existence of large mass. They are dominantly constructed up to two stories in rural areas of Turkey as illustrated in Figure 1.1. Furthermore, the design recommendations for URM structures and their quality control are not properly implemented in Turkey so that they are called as non-engineering structures, which mostly conceive severe damage or collapse after even a moderate seismic action.

Condition assessment of existing structures is an approach to identify the current performance or damage status of structures using different techniques, named as observed vulnerability, expert judgement, simple analytical (macro) modeling, score assignment and detailed structural analysis in the increasing order of computational effort, respectively (Lang, 2002).

In this study, the seismic performance of URM structures are investigated by using simplified structural modeling and dynamic analysis through simulated ground motions. Structural analyses are carried out with simulated ground motion datasets obtained from the simulated records of the 12 November 1999 Düzce earthquake as well as scenario events in Düzce and the simplified Equivalent Single Degree of Freedom (ESDOF) models of the URM structures. The simulations of the 1999 Düzce earthquake include different scenario earthquakes, source-to-site distances and site conditions. Accordingly, the damage state (DS) of a structural model due to a given seismic excitation is determined via comparing displacements obtained from the dynamic analyses with its predefined limit states. Considering these performance levels of URM structural models, the influences of different seismological and structural parameters are investigated with probabilistic approaches and statistical tools.

Figure 1.1. The pictures about URM structures from the rural area of Turkey (Tama et al., 2013)

1.2. Literature Survey on Seismic Performance Assessment of Structures

Over the last decade, methods to conduct a seismic performance assessment of structures have been developed to investigate the challenges of past methods and the details of the structural system. As mentioned in the previous part, there are five seismic performance assessment techniques for different objective in literature.

The observed vulnerability technique comprises the investigation of damages of structures by using field data from the past earthquakes. Since the application of analytical methods is difficult to constitute structural models, this technique is convenient for all structures, including URM. The approach by EERI (1996) was one of the important proposals to explain how to conduct the vulnerability assessments of buildings after an earthquake with this technique.

According to the study of Pomonis et al. (2014), the past earthquake datasets from 1986 to 2003 were used to evaluate URM structures in Greece. The past earthquake datasets were mostly composed of technical reports compiled with damage grades of the European Macroseismic Scale (EMS-98) developed by Grünthal (1998). Damage-0 means no damage, Damage-1 denotes the hairline cracks in the load-bearing walls, Damage-2 stands for the falling of larger patches of mortar from load-bearing walls, Damage-3 presents the heavy damage and distortion of load-bearing walls, and finally Damage-4 is for the partial or total collapse. By using these definitions of EMS-98, the damage assessments of URM structures were conducted.

Ingham and Griffith (2011) conducted a study about the damage estimations of URM structures after the 2010 Darfield earthquake in New Zealand (M_w=7.1). After the earthquake, 958 URM buildings were evaluated by utilizing the readily available damage assessment form constituted by local authorities. According to the results of that study, many URM buildings remained less than 10% damage. These results reveal that the existing URM buildings in New Zealand had been constructed by considering earthquake design criteria.

Another technique to conduct the seismic assessment of structures is the generation of subjective data from experts. The pioneer attempt to evaluate damage distribution of structures with this technique was carried out under the assistance of the Applied Technology Council (ATC), which was financially funded by the Federal Emergency Management Agency (FEMA). The outcome report ATC-13 (1985) included the damage probability matrices for 78 structures. 58 structures, which are selected among 78 structures in the report, were employed to predict potential vulnerability of the structures under the various intensities of seismic actions generated from the experience and knowledge of experts. In addition to this, the improved report, HAZUS (1999) funded by FEMA, was published to evaluate the vulnerability of the structures using spectral displacement-acceleration instead of the predicted intensity of seismic action.

The major problem in the vulnerability assessment of structures is the consideration of structural details. Thus, the use of a simple structural model has become popular to minimize the time-consuming computational efforts in the process of structural analyses.

D'Ayala et al. (1997) presented a case study regarding the evaluation of damage to masonry buildings in Lisbon. The collapse mechanisms were considered with the out-of-plane and in-plane failure modes. Damage functions of the masonry structures were estimated and verified with the damage report of masonry structures, which was prepared after the 1755 Lisbon earthquake.

In the study of Calvi (1999), masonry structures in Catania were solely evaluated by simplified models with the in-plane failure mode and selected structural parameters, namely the fundamental period, the type of masonry material and the number of stories. These models were used to estimate the seismic performance by using the limit states generated in terms of displacement.

Lang and Bachmann (2003) proposed considering macro models with out-of-plane and in-plane failure modes to assess the vulnerability of URM buildings in Switzerland. The limit and damage states were employed to achieve similar aims of Calvi (1999). The damage estimations were carried out by generating the fragility curve for each limit state.

Erberik (2008) carried out simplified modeling to evaluate the seismic performance of URM structures in Turkey by using in-plane failure modes only. In that study, fragility curve sets were generated using different structural parameters and observed damages to URM structures in the rural area after the 1995 Dinar (M_w=5.9) earthquake with the computational results. In field database, 140 rural URM buildings at different site conditions were examined by using standard damage evaluation form. At the end of the study, fragility curves generated from the results of structural analyses seemed to be reasonable with the results of observed damages for the URM buildings in Dinar, Turkey.

The purpose of the score assignment technique is to investigate seismically vulnerable structures located in an earthquake-prone area. Major deficiencies of structures are identified and the damage score of structures are allocated by specialists. Sucuoğlu and Yazgan (2003) carried out such a study in Istanbul by using the sidewalk survey technique (i.e. score assignment technique).

Erberik[a)] (2010) conducted vulnerability assessment of approximately 20,000 URM buildings in earthquake prone districts of Istanbul with the sidewalk survey technique, which enables rapid evaluation for a vast number of buildings. The classification of URM buildings in terms of vulnerability were fulfilled by utilizing the structural parameters of URM buildings, termed as the number of stories, plan geometry, load-bearing wall material and quality, wall length and opening length in the walls. The damage score for each URM building was obtained in order to make classifications with respect to the performance levels.

Erberik et al. (2013) focused on a field survey of URM buildings in Antakya, Turkey. The pre-selected 265 URM buildings were assigned damage scores using the evaluation form for masonry buildings presented in Figure 1.2. At the end of the study, 18 % of URM buildings were found out at high risk, 72 % at moderate risk, 10% at low risk.

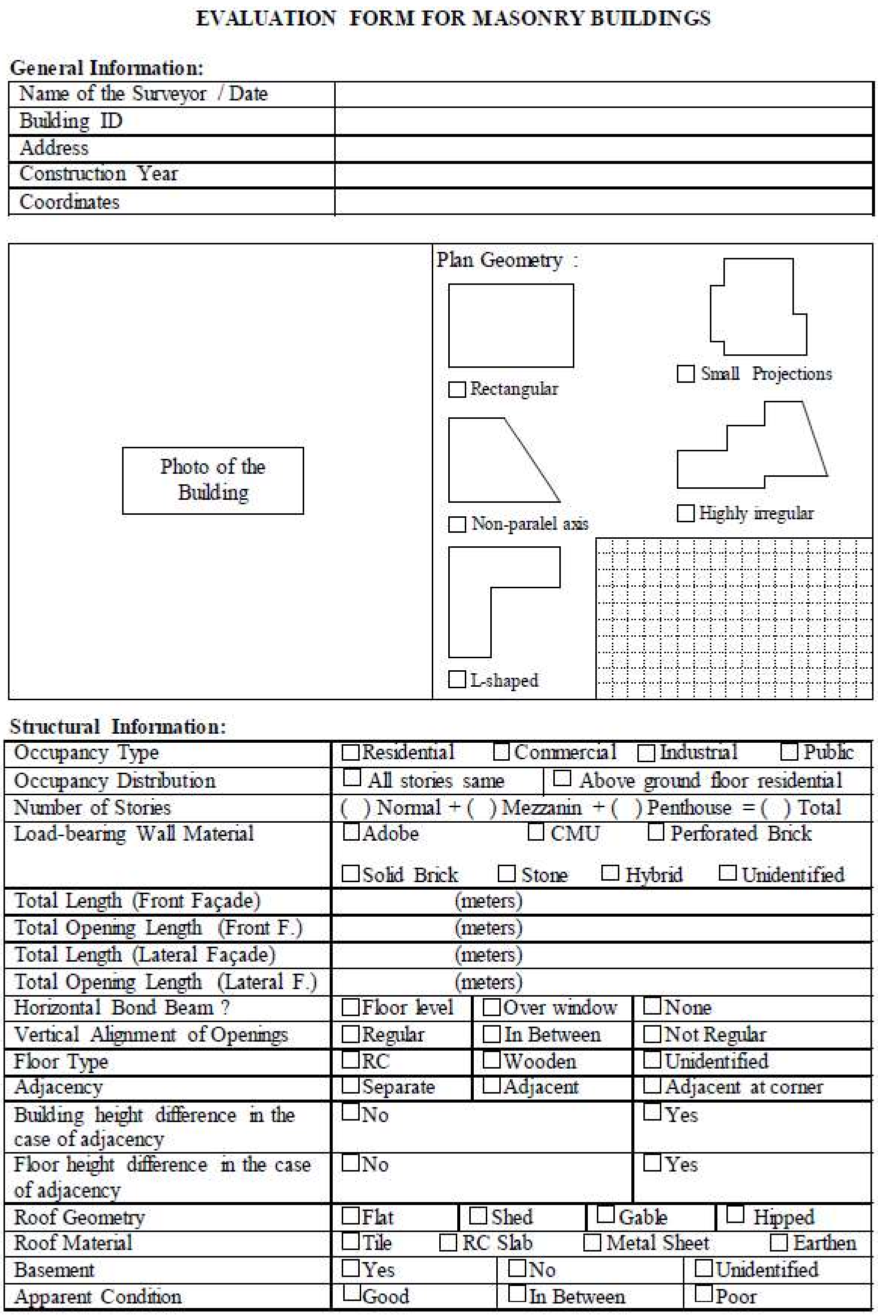

EVALUATION FORM FOR MASONRY BUILDINGS

General Information:

Name of the Surveyor / Date	
Building ID	
Address	
Construction Year	
Coordinates	

Structural Information:

Occupancy Type	☐Residential	☐Commercial	☐Industrial	☐Public
Occupancy Distribution	☐ All stories same	☐ Above ground floor residential		
Number of Stories	( ) Normal + ( ) Mezzanin + ( ) Penthouse = ( ) Total			
Load-bearing Wall Material	☐Adobe ☐CMU ☐Perforated Brick ☐Solid Brick ☐Stone ☐Hybrid ☐Unidentified			
Total Length (Front Façade)	(meters)			
Total Opening Length (Front F.)	(meters)			
Total Length (Lateral Façade)	(meters)			
Total Opening Length (Lateral F.)	(meters)			
Horizontal Bond Beam ?	☐Floor level	☐Over window	☐None	
Vertical Alignment of Openings	☐Regular	☐In Between	☐Not Regular	
Floor Type	☐RC	☐Wooden	☐Unidentified	
Adjacency	☐Separate	☐Adjacent	☐Adjacent at corner	
Building height difference in the case of adjacency	☐No	☐Yes		
Floor height difference in the case of adjacency	☐No	☐Yes		
Roof Geometry	☐Flat	☐Shed	☐Gable	☐ Hipped
Roof Material	☐Tile	☐RC Slab	☐Metal Sheet	☐Earthen
Basement	☐Yes	☐No	☐Unidentified	
Apparent Condition	☐Good	☐In Between	☐Poor	

Figure 1.2. The evaluation form of URM buildings (Erberik et al., 2013)

In Walsh et al. (2014), commercial URM buildings in Auckland, New Zealand were chosen to estimate vulnerability with taxonomies, which enable to identify the buildings in field survey in terms of the geometry of the building, the height of the building, the presence of bond beam and the type of construction material. Finally, the researchers published a report about the requirement of retrofitting and demolition of the URM buildings with considering damage score of each building. It was observed that various URM buildings in Auckland were not under high risk and retrofitting can be also a solution to remove some deficiencies of the URM buildings.

The detailed analysis technique focuses on detailed modeling of the structural system. Even though this technique enables more accurate results while assessing the vulnerability of structures, it requires more computational effort during structural analyses. With this technique, finite element model and detailed micro-modeling are utilized in some sophisticated structural models of URM structures explained as follows.

The study of Lourenco et al. (1998) was carried out with the micro-model of masonry structures generated with the anisotropic continuum model and the formulation of modern plasticity. The mechanical properties of the masonry units, mortar and the interface of masonry unit-mortar were exhibited in a micro-model. The computational results were deemed to be reasonable when compared with the experimental results in terms of base shear-displacement relationship.

Magenes (2006) focused on the evaluation of structural analysis methods, namely the linear and nonlinear static analysis, with comparing their results in terms of the distribution of internal force, overstrength ratio, and out-of-plane response. A MDOF model of URM building was constituted with finite element method based on the macro-model discretization.

In the recent study of Asteris et al. (2019), two historical URM structures in Athens, Greece were examined to determine their damage levels. The structural models were constituted with the anisotropic finite element macro-model. The fragility curves of each structural model were generated using the results of structural analyses, which represent displacements at the nodes within each mesh. Finally, the decision on whether the buildings require strengthening or not was evaluated.

1.3. Objective and Scope

The main objective of this study is to evaluate the seismic performance of URM structures with certain structural characteristics subjected to simulated ground motion records generated with well-defined seismological parameters and to investigate the influences of these seismological and structural parameters on the performance levels of URM structures using statistical tools.

MDOF masonry models are converted into equivalent SDOF masonry models to simplify the nonlinear structural dynamic analyses. The performance values of structural parameters for the ESDOF models; namely the fundamental period, strength ratio, ductility, post-yielding ratio, post-capping ratio, residual strength, and degradation parameter, are determined with the local characteristics of URM structures and also employed to identify limit states in terms of displacement. The seismic response statistics of URM structures are obtained from the nonlinear structural analyses conducted with the simulated ground motion datasets in the Düzce region. This response statistics data is employed to obtain the damage states of URM structures.

After determining performance levels for the URM structures, sensitivity analyses are carried out to observe changes in DS for each magnitude earthquake and source-to-site distance and site conditions with respect to varying performance values of each structural parameter. The estimation of performance levels of URM structures for each magnitude of earthquake and PGA value in different soil conditions are subsequently achieved by using the probabilistic distributions. Finally, statistical tools, termed as discriminant analysis, multiple regression analysis and principal component analysis, are used to obtain relationships between DS and independent variables as well as to find out the most dominant factors influencing the DS values.

The scope of this study can be explained as follows:

In Chapter 2, the ESDOF generated from MDOF models are employed to obtain force and displacement relationship under dynamic loading in a practical way.

In Chapter 3, the dummy earthquake stations, which are employed in the simulations, are randomly selected to obtain ground motion acceleration-time records and kept the same for each earthquake magnitude and site soil condition. The performance values of structural parameters are determined to carry out nonlinear structural analyses.

Chapter 4 initially presents the attainment of damage states by comparing the results of structural analyses and pre-defined limit states of URM structures. Considering the DS of each structural combination, the sensitivity analyses for each structural parameter are subsequently carried out with different seismological parameters under soft and hard soil conditions.

Chapter 5 focuses on relationships between DS and independent variables, which includes seismological and structural parameters, with using different statistical tools, named as discriminant analysis, multiple regression analysis and principal component analysis.

Chapter 6 includes the summary and conclusion of the study as well as recommended future studies.

CHAPTER 2

EQUIVALENT SINGLE DEGREE OF FREEDOM SYSTEM

2.1. General

The increasing complexity of structures both in elevation and plan, in addition to the diversity of architectural styles require complex analytical models with structure-specific members and many structural parameters to be defined. As a result, structural analysis takes time and effort and also requires well expertise in terms of the structural system. This issue becomes even more critical in the case of multiple structural simulations in order to assess seismic vulnerability of these complex structural systems. Hence, the researchers in the field generally employ simplified approaches to solve this problem. One of the most common approaches is to obtain a simple structural system from the capacity curve of a complex structure with pushover analysis. The simple structural model is called as an ESDOF model, which is illustrated in Figure 2.1. According to Graziotti et al. (2014), the main target of an ESDOF model derived from the multi degree of freedom (MDOF) model is to simplify structural complexity in a reliable manner, to obtain the structural analysis results more easily and to interpret the effect of different parameters on the structural response. This process is carried out to obtain the capacity curve with pushover analysis for MDOF model; thus, it enables to generate capacity spectrum of the ESDOF model.

There are various nonlinear static analysis methods, which utilizes ESDOF models to obtain the response statistics. The most popular ones are the Capacity Spectrum Method (CSM) first proposed by Freeman et al. (1975), the Improved Capacity Spectrum Method (ICSM) developed by Chopra and Goel (2000), the N2 method proposed by Fajfar and Fischinger (1988), and the Modal Pushover Analysis method

(MPA) initially stated by Paret et al. (1996). These methods have been stated as the conventional nonlinear static analysis methods (Themelis, 2008). The most recent nonlinear static analysis method is the energy-based approach to overcome the deficiency of the conventional pushover methods explained in the following part.

From the development of the CSM up to date, many different approaches have been proposed and some of these approaches have also been implemented into the international documents such as ATC-40 (1996), EC-8 (CEN 1995), FEMA-273 (1997). This chapter deals with the idealized structural modeling used in this study and the presentation of the parameters for the selected hysteresis model that simulates the nonlinear responses of the idealized structures.

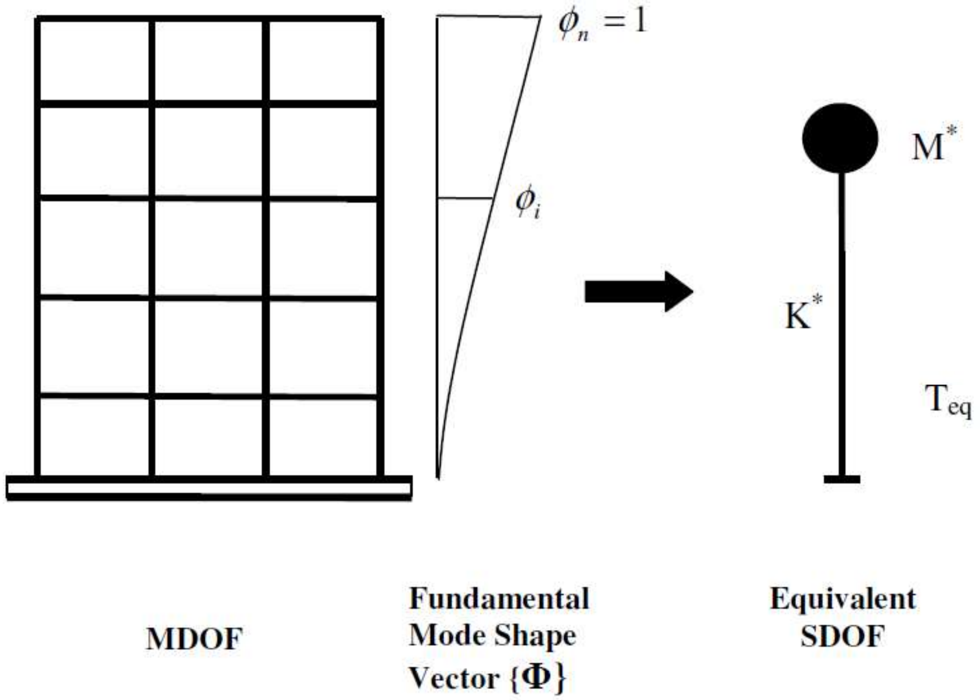

Figure 2.1. Derivation of ESDOF from MDOF (Themelis, 2008)

2.2. Previous Research on ESDOF Systems

CSM is the oldest nonlinear static analysis technique that can be used as a practical tool with the conversion of an MDOF model to an ESDOF model for the seismic assessment of multi-story structures. This method was proposed in 1970s by Freeman et al. (1975), who are the pioneers to develop the nonlinear static procedure. In CSM method, the elastic design spectrum and the capacity curve should intersect with each other to give the performance point of the selected structure under earthquake excitation. The capacity curve is obtained by using equivalent maximum base shear forces and equivalent maximum displacements. Hernandez-Montes et al. (2004) stated that capacity curve of a structure is obtained by applying incremental lateral loads with step by step nonlinear static analysis. It is converted to ESDOF model with capacity spectrum; then, the maximum displacement and maximum base shear of ESDOF model can be obtained. In CSM, the first mode of structures is dominant to estimate capacity spectrum according to the ATC-40 (1996) and FEMA-273 (1997). In order to convert an MDOF system to an SDOF system in this method, bilinearization, meaning that the capacity spectrum curve and bilinear representation are associated with the equal energy absorption capacity, is carried out.

Base shear and displacement of ESDOF nonlinear systems are obtained from the intersection point of capacity spectrum and elastic demand spectrum represented in the acceleration-displacement spectrum (ADRS) format in Figure 2.2 by utilizing the spectral acceleration and spectral displacement equations shown as follows:

$$S_a = \frac{V_b^*}{\alpha_m \ m^*} \tag{2.1}$$

$$S_d = \frac{u}{PF_1 \ \phi_{ij}} \tag{2.2}$$

$$PF_1 = \frac{\{\Phi\}^T[m^*]\{1\}}{\{\Phi\}^T[m^*]\{\Phi\}} \tag{2.3}$$

$$\alpha_m = \frac{[\sum_{j=1}^n m_i \ \phi_{ij}]^2}{\sum_{i=1}^n m_i \ \sum_{j=1}^n m_i \ \phi_{ij}^2} \tag{2.4}$$

where S_a is the spectral acceleration, S_d is the spectral displacement, V_b^* is the base shear, m^* is the effective mass, u is the roof displacement of the real model, α_m is the modal mass coefficient, ϕ_{ij} is the modal amplitude at story level "i" for mode "j", PF_1 is the first mode participation factor, Φ is the constant deformation shape vector of the equivalent SDOF model.

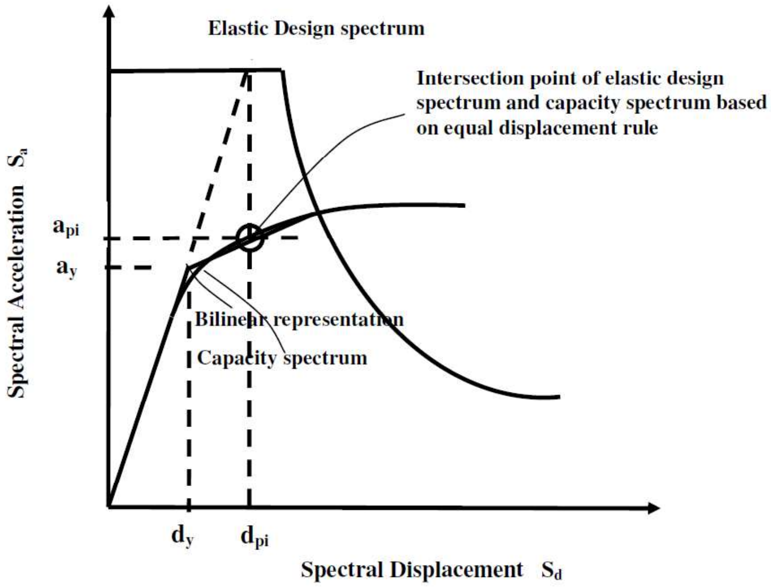

Figure 2.2. The intersection of capacity and elastic design spectrum (Themelis, 2008)

ICSM proposed by Chopra and Goel (2000) is basically a modification of the CSM. This method is distinguished from the CSM since the ICSM is conducted by using the inelastic design spectrum with constant ductility instead of the elastic design spectrum as illustrated in Figure 2.3.

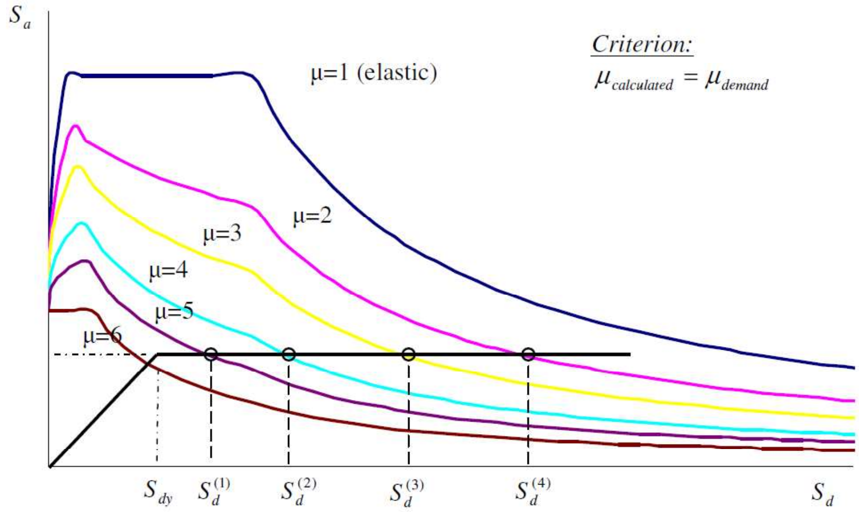

Figure 2.3. Application of the improved capacity spectrum method (Themelis, 2008)

N2 method proposed by Fajfar and Fischinger (1988) has been developed as an alternative to the CSM. The method employs base shear versus roof displacement relationships as other types of the methods, which contribute to the improvement of nonlinear seismic analysis through ESDOF model. The main assumption of the N2 method is the employment of a constant deflection shape during a ground motion excitation. After obtaining the inelastic design spectrum in the N2 method, force-displacement relationship for the nonlinear ESDOF model is developed to calculate performance-based values of ESDOF model by converting from pushover curve of the MDOF model (Fajfar, 2000). According to Fajfar and Fischinger (1988), shear force should be increased with the factor of safety to get the conservative results for the ESDOF model because they realized that nonlinear static analysis results yield higher shear forces for the MDOF model than the EDSOF model due to the higher mode effect. Inelastic spectra of ESDOF model is defined with equations as shown below:

$$S_{ay} = \frac{S_{ae}}{R_\mu} \tag{2.5}$$

$$S_d = \frac{\mu}{R_\mu} S_{de} \tag{2.6}$$

$$S_{de} = \frac{T^2}{4\pi^2} S_{ae} \tag{2.7}$$

$$R_\mu = (\mu\text{-}1)\frac{T^*}{T_c} + 1 \tag{2.8}$$

where S_{ae} is the elastic spectral acceleration, S_{ay} is the yield spectral acceleration, R_μ is the ductility reduction factor, S_{de} is the elastic spectral displacement, μ is the ductility factor and T is the fundamental period.

If elastic period value (T^*) is equal to or greater than the characteristic period of the ground motion (T_c), the equal displacement rule governs, i.e $R_\mu = \mu$.

The base shear (V_b) and the top displacement (D_t) of the MDOF model are used to calculate the base shear (V_b^*) and the top displacement (D_t^*) of the ESDOF model, respectively. The conversion from the MDOF model to the ESDOF model is carried out with the parameter Γ, called as the modal participation factor. The related relationships are shown below:

$$D_t^* = \frac{D_t}{\Gamma} \tag{2.9}$$

$$V_b^* = \frac{V_b}{\Gamma} \tag{2.10}$$

$$\Gamma = \frac{m^*}{\sum m_i \, \phi_i^2} \tag{2.11}$$

$$m^* = \sum m_i \, \phi_i \tag{2.12}$$

$$V_b = p \sum m_i \, \phi_i \tag{2.13}$$

Utilizing V_b^* and D_t^* for the ESDOF model as stated in the presented equations, yielding strength (V_y^*) and yielding displacement (D_y^*) are predicted on the idealized bilinear curve using T^* of the equivalent SDOF model as follows (Figure 2.4):

$$T^* = 2\pi \sqrt{\frac{m^* \text{ x } D_y^*}{V_y^*}} \tag{2.14}$$

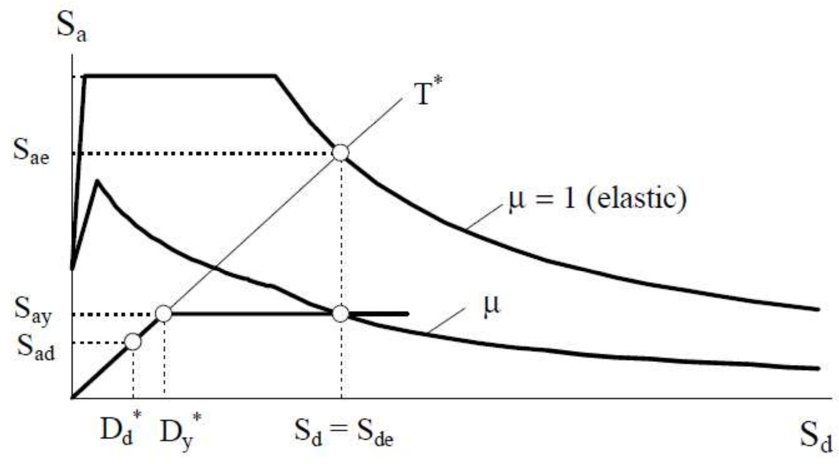

Figure 2.4. Dy* and Vy* prediction using T* of ESDOF model (Fajfar, 2000)

Another conventional pushover method proposed by Chopra and Goel (2001) is the modal pushover analysis (MPA). This method is based on the CSM contributions of modal force distributions for the selected number of modes. Owing to the weakness of the other mentioned pushover methods in terms of the effect of higher mode, MPA method can be used to get accurate results. ESDOF model for j^{th} mode can be obtained with base shear and deformation obtained by using the idealization of MDOF model pushover curve as shown in Figure 2.5 as follows:

$$V_{bj} = \frac{F_{sj}}{L_j}\, m_j^* \tag{2.15}$$

$$D_j = \frac{u_{tj}}{\Gamma_j\, \phi_{nj}} \tag{2.16}$$

where V_{bj} is the base shear of MDOF for mode j, m_j^* is the effective modal mass of mode j, F_{sj} is the base shear of ESDOF model for mode j, u_{tj} is the top displacement of MDOF model for mode j and ϕ_{nj} is the top modal shape of MDOF model for mode j, D_j which is derived from Γ_j, modal participation factor for mode j, is the displacement of ESDOF model for mode j.

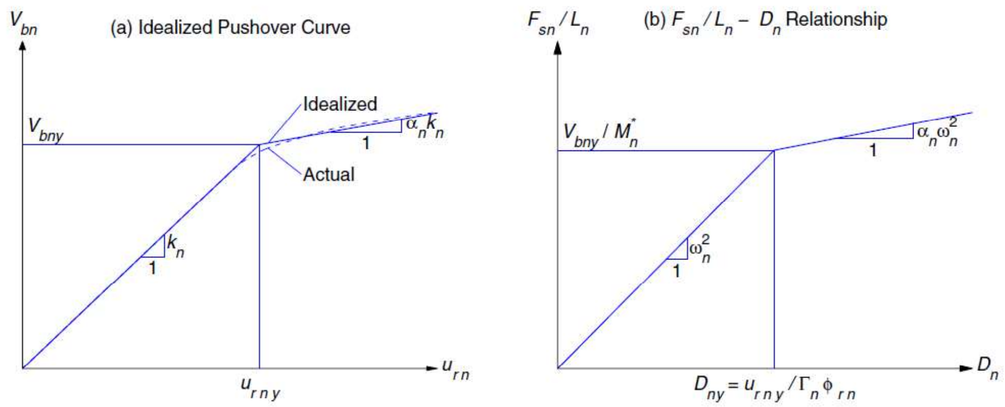

Figure 2.5. The application of MPA (Chopra and Goel, 2001)

As shown in Figure 2.5, the yielding stiffness and post-yielding stiffness values for ESDOF model are estimated according to Equations 2.17-2.19.

$$\omega_n^2 = \frac{m^*}{k_n} \tag{2.17}$$

$$k_{yn} = \frac{V_{bny}}{u_{rny}} \tag{2.18}$$

$$k_{un} = k_{yn}\alpha_n \tag{2.19}$$

where α_n is the post-yielding stiffness ratio, ω_n is the frequency of the structure, k_{yn} is the yielding stiffness, k_{un} is the post-yielding stiffness, V_{bny} is the yielding base shear, u_{rny} is the yielding displacement for the n^{th} modal shape of ESDOF model.

The contemporary approach to convert an MDOF model to an ESDOF model is the energy-based method, which eliminates the arbitrary selection of floor and roof displacement of the conventional pushover methods (Kotanidis and Doudoumis, 2008). Hernandez- Montes et al. (2004) stated that the energy-based approach fundamentally depends on the work done by lateral forces for each mode at each floor, and so shear force and displacement at each step are calculated to obtain energy-based shear force and displacement. These are represented in Figure 2.6 with the equivalent

SDOF model as the energy-based shear force and total displacement. Furthermore, the energy-based approach does not enable to the possible reversal negative displacement at the higher modal shape so that the roof displacement does not decrease with incremental lateral loads. Krawinkler and Seneviratna (1998) stated that the high sensitivity relevance for the higher mode in terms of story shear force and story drift cannot be properly examined with the conventional pushover methods.

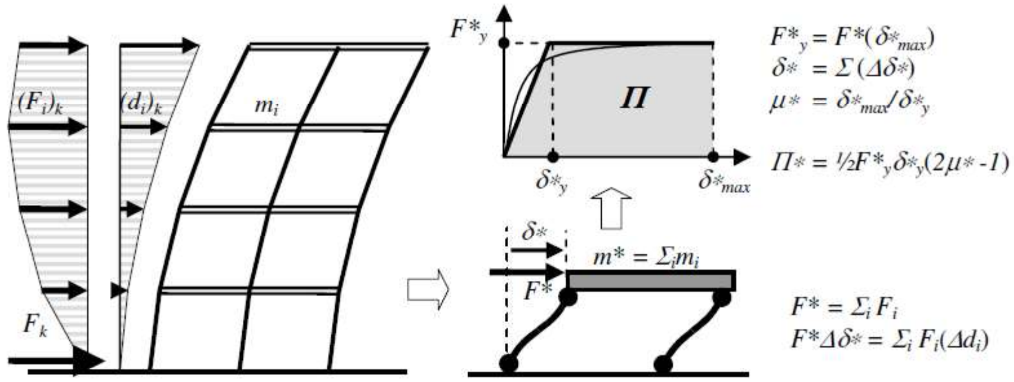

Figure 2.6. Energy-based approach through ESDOF model (Parducci et al., 2006)

As stated above, for all techniques including the conversion of an MDOF model to an ESDOF model, idealization is a common approach to observe the response of the structure under lateral load. Furthermore, structural analysis is definitely simplified by estimating an ESDOF model. Therefore, structural analyses can be carried out in a practical and simple manner in terms of the displacement and base shear with selecting a proper hysteresis model.

2.3. Hysteresis Model Used in This Study

Over the last decades, performance-based design has been popular to classify structural damages, which cause huge economic losses and human casualties with severe earthquakes, by using structural hysteresis response. Therefore, extensive research was carried out to develop hysteresis models that simulate the idealized seismic behavior of different structural systems and components. One of the first proposed hysteresis models was the elastoplastic model shown in Figure 2.7. Due to the fact that this primitive model does not have incremental load capacity after yield displacement point is exceeded, the bilinear degrading stiffness model was developed by Clough and Johnston (1966) as illustrated in Figure 2.8. In these models, unloading stiffness is parallel to the initial elastic stiffness of the structure. Taking into account the absence of strength degradation of hysteresis model suggested by Clough and Johnston (1966), various hysteresis models have been developed by researchers.

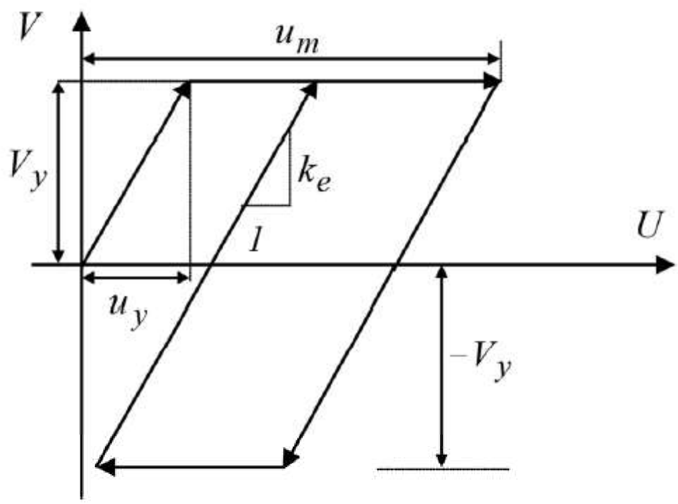

Figure 2.7. Elastoplastic hysteresis model

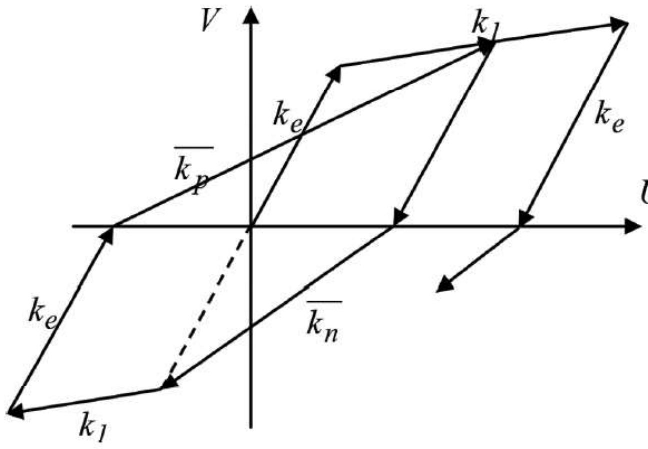

Figure 2.8. Bilinear hysteresis model by Clough and Johnston (1966)

One of the recent models is the modified Ibarra-Medina-Krawinkler (MIMK) deterioration model with peak oriented hysteresis response, which simulates all types of degradation of the structure or the component under the cyclic loading (Ibarra et al., 2005). Owing to the weakness of the original MIMK deterioration model in representing the asymmetric hysteresis behavior, the deterioration model has been further enhanced by Lignos and Krawinkler (2012). The model is presented in Figure 2.9 in the form of a cyclic moment versus chord rotation relationship. In this study, the cyclic moment versus chord rotation relationship is used by converting it into a cyclic force-displacement relationship of the ESDOF model. There are three cyclic deterioration modes in the MIMK deterioration model with peak oriented hysteretic response; basic strength deterioration, post–capping strength deterioration and unloading stiffness deterioration, respectively. Furthermore, according to this model, there are three strength limit states as the effective yield strength (f_y), capping strength (f_c) and residual strength (f_r), respectively. Accordingly, there are four displacement limit states as the effective yield displacement (u_y), capping displacement (u_c), residual displacement (u_r) and ultimate displacement (u_u) capacity, respectively.

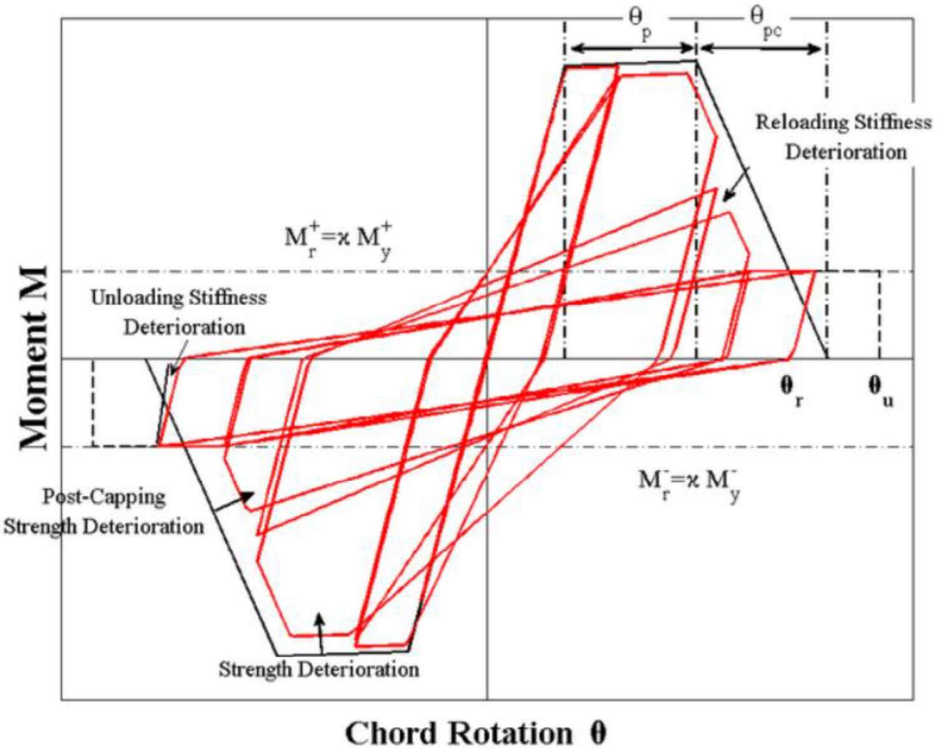

Figure 2.9. The MIMK deterioration model with peak oriented hysteretic response, Lignos and Krawinkler (2012)

The strength and displacement limit state parameters stated above can be defined in terms of stiffness values of the backbone curve as shown in Figure 2.10. These stiffness values, which are named as initial elastic stiffness (k_y), post–yielding stiffness (k_u), post–capping stiffness (k_r) are given in Equations 2.20 -2.22.

$$k_y = \frac{f_y}{u_y} \tag{2.20}$$

$$k_u = k_y \alpha_s \tag{2.21}$$

$$k_r = k_y \alpha_r \tag{2.22}$$

The strain hardening ratio (α_s) and post-capping stiffness ratio (α_r) given in Equations (2.21) and (2.22) enable to determine the post-yielding stiffness (k_u) and post–capping stiffness (k_r), respectively.

Other fundamental parameters related to strength and displacement capacities are explained in the proceeding equations. The force-based parameters, namely f_c, f_r and f_y, are directly related to the predefined structural and material properties. In Equation 2.24, parameter λ is called as the residual strength ratio.

$$f_c = k_u\left(u_c - u_y\right) + f_y \tag{2.23}$$

$$f_r = \lambda\, f_y \tag{2.24}$$

$$u_y = \left[\frac{T}{2\pi}\right]^2 \left(f_y\, g\right)/W \tag{2.25}$$

$$T = 2\pi\sqrt{\frac{m}{k_y}} \tag{2.26}$$

$$u_c = \mu\, u_y \tag{2.27}$$

$$u_r = u_c + \frac{f_r - f_c}{k_r} \tag{2.28}$$

$$u_u = c\, u_r \tag{2.29}$$

In Equation 2.25, the utilized symbols are gravitational acceleration (g) and structural weight (W), which is depending on the selected size of the structural plan and material. The symbol c in Equation 2.29 is used to estimate ultimate displacement on the hysteretic model.

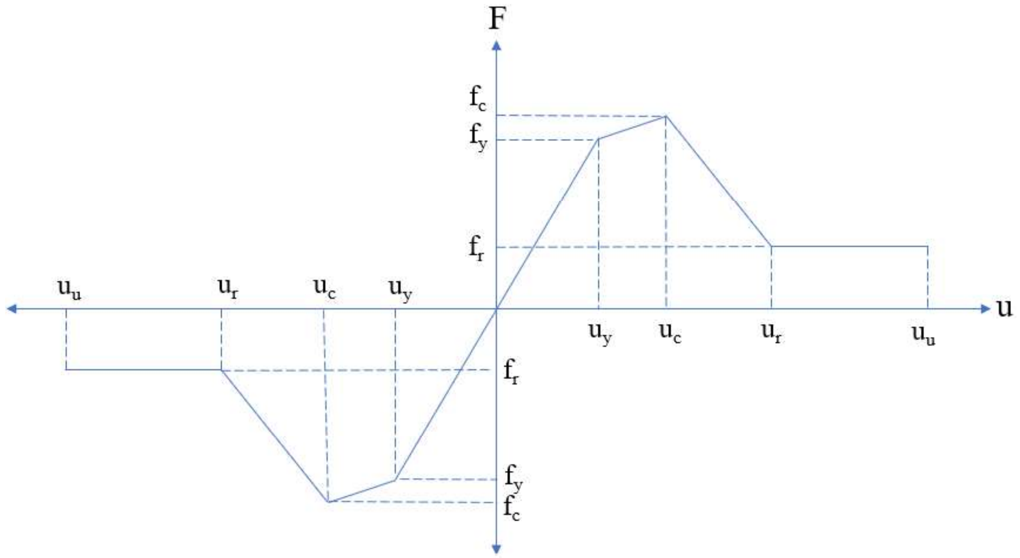

Figure 2.10. Strength and displacement limit parameters in the bilinear curve

In this study, MIMK deterioration model with peak oriented hysteresis response is employed to obtain the form of a base shear versus displacement relationship.

CHAPTER 3

SEISMIC ANALYSIS OF MASONRY STRUCTURE

3.1. General

This chapter focuses on seismic analysis of unreinforced masonry (URM) structures idealized as an equivalent SDOF model, which employs MIMK deterioration model with peak oriented hysteretic response. The selection of ground motion dataset is important to properly observe the effect of the dynamic lateral forces on a URM structure. In order to observe all damage states of a URM structure in an explicit manner, the ground-motion dataset should not only cover high intensity levels but should also have low and moderate levels of seismic intensity. In addition, it is particularly important to use region-specific ground motions for any structure of interest. To represent all seismic intensity levels using recorded ground motions of regional seismic character is not possible given the inherent sparse nature of moderate to large earthquakes. For these purposes, this study is carried out by using the synthetic earthquake dataset, which was developed by Karimzadeh et al. (2017) using ground motion simulation of the 12 November 1999 Düzce Earthquake. In that study, not only the real records of the 1999 Duzce event are simulated but also dummy stations are defined where anticipated ground motions are modeled. In this thesis, the recording stations, which are used to investigate the effects of source, soil types at the stations and distances to the fault are randomly selected from simulated records of the 1999 Duzce earthquake. Then, the filtering of the ground motion dataset is performed. An ESDOF model is used to facilitate seismic analysis with the OpenSees software. In this study, fundamental period, strength ratio, ductility, post-yielding ratio, post-capping ratio, residual strength and hysteresis model degradation parameters are selected as the structural parameters to observe their effects on the URM models under the selected simulated ground motion records. The Newmark method is used to conduct the nonlinear dynamic analysis to obtain the results for all combinations of the structural parameters in the URM models. The statistical evaluations of the structural analyses results will be presented in detail within the next chapter.

3.2. Ground Motion Dataset of the Düzce Earthquake

The selected input ground motion dataset has an important role in obtaining reasonable and physical results from seismic analyses. The following sub-sections explain processes of the generation and selection of the simulated ground motion dataset in detail.

3.2.1. General Information About the Düzce Earthquake

Anatolian plate is located between the Eurasian plate in the north and the African and Arabian plates in the south. North Anatolian Fault (NAF) Zone is the longest and the most active tectonic structure on the Anatolian plate. The Düzce earthquake that occurred on 12 November 1999 is one of the recent major earthquakes generated by the NAF within the last century (Figure 3.1).

The Düzce earthquake is characterized by a right lateral strike-slip fault rupture with a moment magnitude (M_w) of 7.1, and it caused thousands of fatalities and injuries as well as extensive damage to structures (Sucuoglu, 2002).

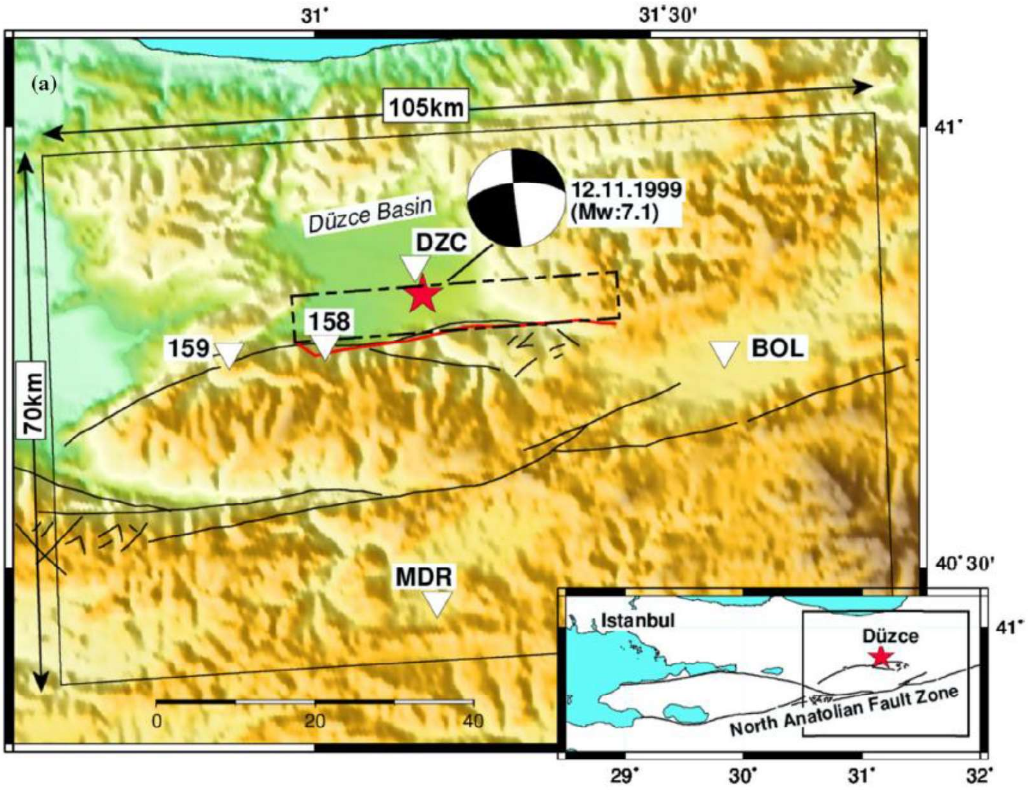

Figure 3.1. The location of the Düzce earthquake (Tanırcan et al., 2017)

3.2.2. Simulated Ground Motion Records of the Düzce Earthquake

Owing to the existence of severe earthquake excitations, many engineering structures are exposed to nonlinear behavior. In order to represent nonlinear behavior of structures in a simplified manner, it is essential to conduct nonlinear time history analyses by using the full-time acceleration records of ground motions. Recently, the simulation techniques for ground motions have been prevailed among the seismologists due to the existence of sparse seismic networks (Askan et al., 2013).

Ground motion simulations used in this study were conducted for the Düzce earthquake as a case study in Karimzadeh et al. (2017) to understand whether simulated ground motion records can be practically and realistically used for the dynamic analysis of MDOF structures. For the simulation of the ground motion records, the stochastic finite-fault method, based on dynamic frequency approach, was utilized. Previously, Ugurhan and Askan (2010) stated that the method can be considered as a suitable method to constitute synthetic ground motions since stochastic technique enables to generate acceleration records containing a wide range of frequencies. Stochastic finite fault method can be conducted at dummy stations, where there are no real records with the simulation parameters. It must be noted that the simulation parameters are first validated at real station locations by comparing against real records. Then, they are used to simulate acceleration records at dummy stations. In the stochastic finite fault method, smaller sub-faults are initially defined on the original rectangular fault plane with discretization. Thus, each sub-fault can be associated with a stochastic point source and the motions of each sub-fault are accumulated to model the acceleration time histories of the 1999 Düzce earthquake at the selected dummy and real stations.

3.2.3. The Selection of the Simulated Time-History Records from the Generated Stations

In the study of Karimzadeh (2016), two different regions around Duzce were designed to model the simulated time-history records. One of them was generated in a larger area with 66 dummy earthquake stations, and another one contains a smaller area with 280 dummy earthquake stations closer to the fault zone. Thus, a total of 344 dummy earthquake stations were considered between the Eastern longitudes 30^0 and 32^0 and the Northern latitudes 40^0 and 42^0. In order to observe the variations in PGA values, the 280 nodes (dummy earthquake stations), which are represented in Figure 3.2, are used in this study.

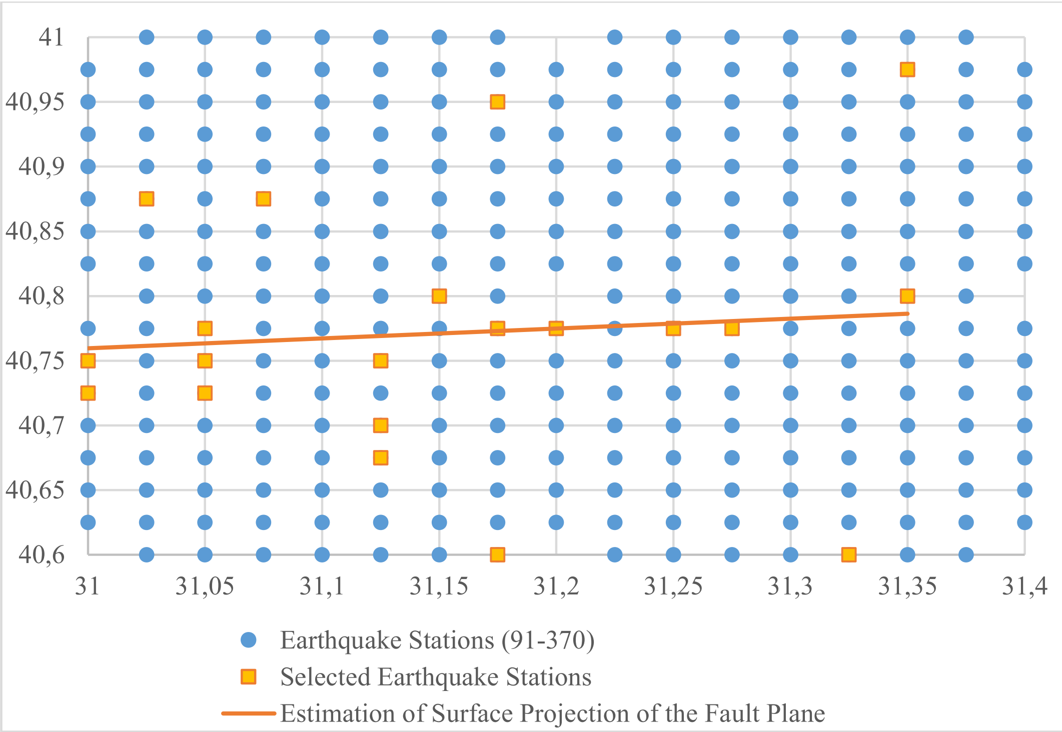

Figure 3.2. The 280 dummy earthquake stations defined in Karimzadeh (2016) in the smaller box within the Duzce region

Scenario events of magnitudes M_w= 5.0, 5.5, 6.0, 6.5, 7.0, 7.1 were previously simulated in Karimzadeh (2016) for two site conditions which are classified as the soft and hard soil type. Out of 280 stations, 20 of them as represented in Figure 3.3, are selected in this study. Therefore, 240 distinctive time-history earthquake records are obtained to carry out nonlinear dynamic analysis of the ESDOF models. The first 120 records represent the soft soil type, including 20 records for each magnitude value. The last 120 records represent the hard soil in the same manner.

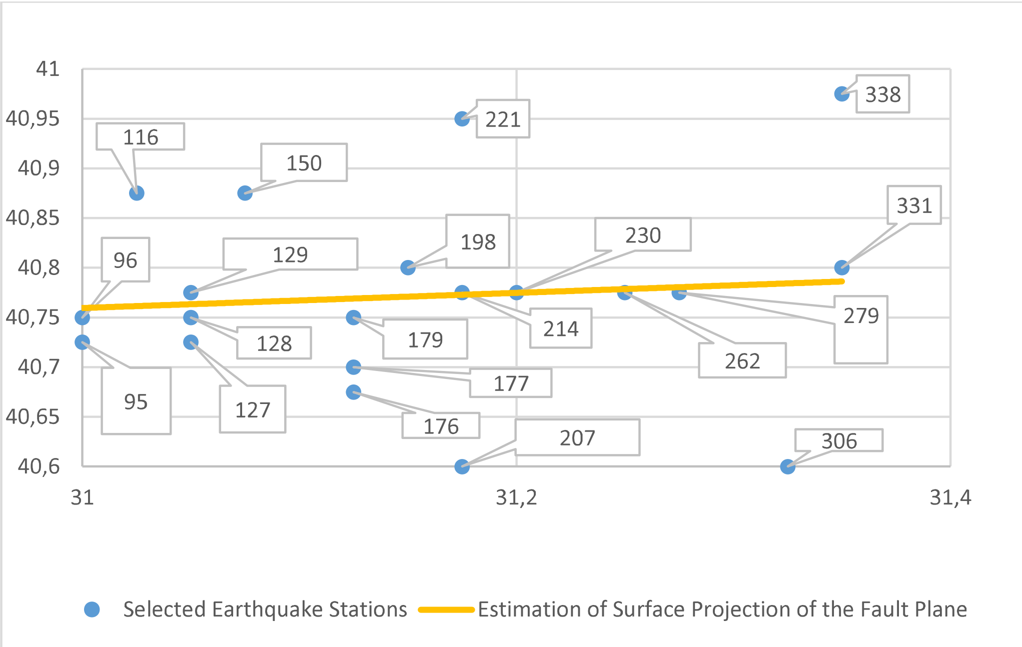

Figure 3.3. The location of the selected earthquake stations with respect to the Duzce fault

PGA is employed as the major parameter to select the earthquake stations and the corresponding stations since it is dominantly effective in representing the seismic response of masonry structures. Therefore, selection of the earthquake stations is carried out by using the PGA values between 0.1g and 1.0g (g is the gravitational acceleration) taken from the magnitude 7.1 scenario for the soft soil conditions. The same stations are used for the entire magnitude range of interest. The PGA values are equally divided to ten intervals to have a minimum of random two PGA values at each interval as given in Table 3.1. The purpose is to cover all the range of seismic response from the elastic behavior to collapse for the ESDOF models considered.

Table 3.1. *PGA values of the selected nodes*

	Soft Soil (PGA Values)						Hard Soil (PGA Values)					
Selected nodes	M5	M5.5	M6	M6.5	M7	M7.1	M5	M5.5	M6	M6.5	M7	M7.1
306	0.01	0.03	0.06	0.07	0.11	0.16	0.01	0.02	0.05	0.06	0.10	0.13
338	0.01	0.04	0.07	0.11	0.14	0.19	0.01	0.03	0.06	0.08	0.16	0.15
207	0.01	0.03	0.07	0.10	0.13	0.21	0.01	0.03	0.06	0.08	0.10	0.14
221	0.02	0.05	0.10	0.13	0.21	0.26	0.01	0.04	0.08	0.10	0.17	0.21
176	0.02	0.05	0.11	0.17	0.22	0.32	0.01	0.04	0.09	0.13	0.17	0.23
150	0.02	0.06	0.15	0.30	0.35	0.39	0.02	0.05	0.12	0.24	0.31	0.34
177	0.02	0.05	0.14	0.18	0.29	0.40	0.02	0.04	0.11	0.14	0.22	0.32
116	0.02	0.04	0.11	0.28	0.43	0.47	0.01	0.03	0.09	0.22	0.35	0.35
128	0.02	0.06	0.11	0.32	0.62	0.55	0.01	0.04	0.09	0.26	0.34	0.50
127	0.02	0.05	0.10	0.23	0.48	0.57	0.01	0.04	0.08	0.19	0.26	0.41
179	0.02	0.08	0.19	0.31	0.44	0.61	0.02	0.06	0.29	0.25	0.55	0.44
262	0.04	0.12	0.25	0.25	0.51	0.65	0.03	0.10	0.19	0.20	0.32	0.46
95	0.01	0.03	0.09	0.21	0.52	0.71	0.01	0.03	0.07	0.17	0.34	0.49
279	0.04	0.10	0.26	0.28	0.48	0.72	0.03	0.08	0.20	0.22	0.30	0.51
230	0.04	0.14	0.37	0.37	0.64	0.78	0.03	0.11	0.30	0.29	0.38	0.56
214	0.02	0.12	0.33	0.33	0.64	0.82	0.02	0.10	0.28	0.26	0.43	0.61
198	0.05	0.10	0.37	0.56	0.91	0.84	0.04	0.08	0.29	0.44	0.55	0.68
96	0.01	0.05	0.11	0.30	0.71	0.88	0.01	0.04	0.08	0.23	0.57	0.69
331	0.02	0.07	0.16	0.23	0.70	0.93	0.02	0.06	0.12	0.18	0.51	0.71
129	0.02	0.05	0.13	0.42	1.00	0.99	0.01	0.04	0.10	0.33	0.51	0.68

Even though ground motions result from complex phenomenon beneath the ground during earthquakes, the differences of PGA values among the earthquake stations for the same moment magnitude are usually due to two fundamental independent variables, namely the site condition and distance of the earthquake stations to the fault. The site classes are defined as a function of the top 30-meter average S wave velocity Vs30 while the distance metric used in this study is Joyner-Boore distance (R_{JB}). In Figure 3.4, the most commonly used source to site distance measurements are represented that R_{JB} is defined as the shortest horizontal distance to the surface projection of the rupture area, epicentral distance metric (i.e. R_{epic} or R_x) is the distance from earthquake epicenter to source and the minimum distance from fault plane to source is stood for R_{RUP}.

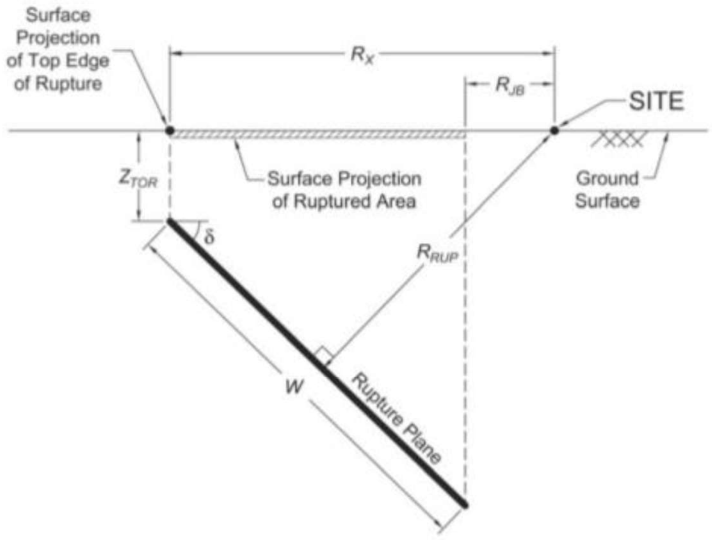

Figure 3.4. The most commonly used fault distances types (Kaklamanos et al., 2011)

Epicentral distance metric has been used widely in the past; however, R_{JB} is a better metric to represent the effect of fault rupture particularly for large earthquakes.

3.2.4. Filtering and Baseline Correction of the Time-History Records

Existence of noise in ground motion records can prevent getting appropriate seismic responses from acceleration time-histories. Therefore, the frequency filtering, one of the popular seismic filtering techniques, can be applied when the frequency of signal and noise are different from each other.

Frequency filtering is being conducted with five major filter types; namely band-pass filter, low pass filter, high pass filter, notch filter, and band reject. Among these, the band-pass filter is the most common filtering technique since a seismic trace can consist of lower and higher frequencies such as ambient noise (Smith, 1958). In order to examine higher and lower period values together in this study, the band-pass filter is preferred to meet the requirements of the filtering. SeismoSignal software is used to filter the time-history data with the band-pass frequency, ranging from 0.10 to 25.0 Hertz.

Guorui and Tao (2015) stated that baseline correction enables seismological studies to have credible displacement, velocity, and acceleration time series. In order to get reasonable outcomes from the baseline correction application, it requires the following two conditions:

(1) The end of velocity time-history of the ground motion record should be zero.

(2) The displacement history approaches a constant value with time.

Linear baseline correction is carried out by utilizing SeismoSignal software as well as the frequency filtering.

3.3. The Modeling of the URM Structures as ESDOF Systems

The URM structures are modeled with the OpenSees software command rules for the node, element, constraint, material property, and element section. The ESDOF models are defined by the model basic command. Each node of the model is described and assigned to construct a nodal object. As shown in Figure 3.5, the element of the model is constituted among the 1st and 2nd nodes.

The single-point homogeneous boundary constraint is assigned to the 1st node as fully fixed support. The hysteretic response is considered with MIMK deterioration model with the peak-oriented to demonstrate the force-displacement relationship of the model under the lateral loads. The section of the object is identified as the uniaxial section that enables to represent a single section force-deformation response quantity. The rotational hinge also captures the nonlinear behavior of the element; therefore, it is used to represent a bilinear hysteretic response based on the MIMK deterioration model.

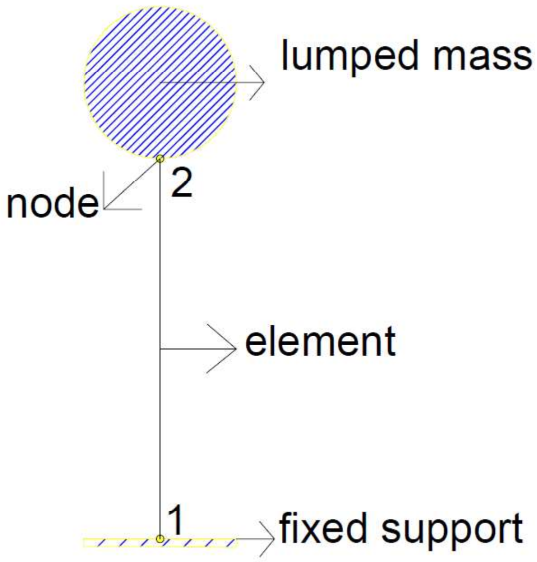

Figure 3.5. The model of URM structure

3.4. ESDOF Parameters for the URM Models

URM structures are seismically vulnerable because they can be destroyed during even moderate earthquakes. Therefore, they have caused serious physical losses during past earthquakes. Masonry structures generally exhibit rigid and brittle behavior, therefore although they have high lateral capacity, if threshold is exceeded during a major earthquake, the structures reaches to the displacement capacity rapidly due to limited ductility.

In this part, the prominent structural parameters, namely fundamental period, strength ratio, ductility ratio, post-yielding ratio, post-capping ratio, residual strength and hysteresis model degradation parameters, are investigated to elaborate their effects on URM structures in terms of seismic vulnerability. In order to conduct a parametric study, the considered parameters are varied in discrete values within a range of minimum and maximum limits, which are determined by the local characteristics of masonry structures. The aforementioned parameters are introduced in the following sub-sections.

3.4.1. Fundamental Period

Fundamental period of the structure (abbreviated as T) is one of the most essential parameters to demonstrate the dynamic behavior of the ESDOF model. Fundamental period of the structure is predicted by utilizing the vibration measurements taken from real structures. It is, then, verified with computational eigenvalue analysis.

There are three commonly used empirical formulas to estimate the fundamental period of masonry structures: the formulation in ASCE (2005), the formulation in Eurocode-8 (1995), and the simple rule of thumb formula in Erberik (2008) for masonry buildings as given in Equations 3.1 -3.3.

According to ASCE (2005):

$$T = 0.02H^{0,75} \tag{3.1}$$

According to Eurocode-8 (1995):

$$T = 0.05H^{0.75} \tag{3.2}$$

According to the basic formulation:

$$T = 0.06N \tag{3.3}$$

where T is a fundamental period of masonry structure, H is the height of the structure, and N is the number of stories. Based on these formulations and the work of Guerrini et al. (2017) on Italian masonry buildings, the parametric values for fundamental period of masonry buildings are selected as 0.05, 0.1, 0.2, 0.3, and 0.4 seconds.

The weight of the ESDOF models is also correlated to the fundamental period of the structure with consideration of the number of stories. Similarly, the fundamental period values are orderly matched with the number of stories as represented in Table

3.2. In addition to this, the weight of the structural model is calculated by multiplying the unit weight of URM buildings, assumed as 15 kN/m^2. This value has been used in some studies including Shahzada et al. (2012), who conducted an experimental study with brick material for two story URM buildings. The area of the plan geometry is assumed as 10x10 m^2 for regular URM building as shown in Figure 3.6.

Table 3.2. *The weight of the structure with respect to the fundamental period*

period (second)	number of stories	width (meter)	length (meter)	unit weight (kN/m^2)	total weight (kN)
0.05	1	10	10	15	150
0.1	2	10	10	15	300
0.2	3	10	10	15	450
0.3	4	10	10	15	600
0.4	5	10	10	15	750

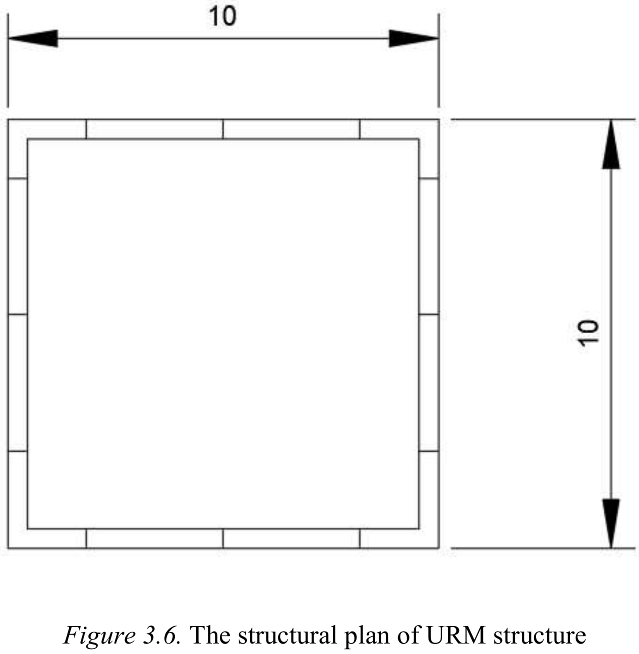

Figure 3.6. The structural plan of URM structure

3.4.2. Strength Ratio

There are few experimental studies to estimate the strength ratio (abbreviated as ɳ) of URM structures. In the literature, Benedetti et al. (1998) carried out the experimental tests with 119 shaking-table tests on 24 non-engineering URM buildings, which were constructed with stone and brick units. The specimen buildings were constructed as half-scale two-story structures. The base shear coefficient, considered as strength ratio, was determined in the range of 0.1-0.3 according to the results of the tests.

Yi et al. (2004) conducted some experimental tests to find out the shear behavior of several URM wall specimens. The authors aimed to specify failure type and propose a strength ratio for the tested URM wall specimens by applying a multivariate regression analysis. According to the test results, the tested walls were primarily influenced by rocking failure mode. In addition, a best fit equation was obtained from the regression analysis with the coefficient of correlation R 0.9889 and the rocking strength / actual strength ratio for the tested specimens was proposed as 1.03.

Tomazevic et al. (2004) performed an experimental study to determine the base shear coefficient of masonry buildings by testing 1/5 scale multi-story URM buildings and confined masonry buildings with different types of masonry materials. The test results revealed that the strength ratios of the tested masonry structures were approximately ranging from 0.5 to 1.9 as illustrated in Figure 3.7.

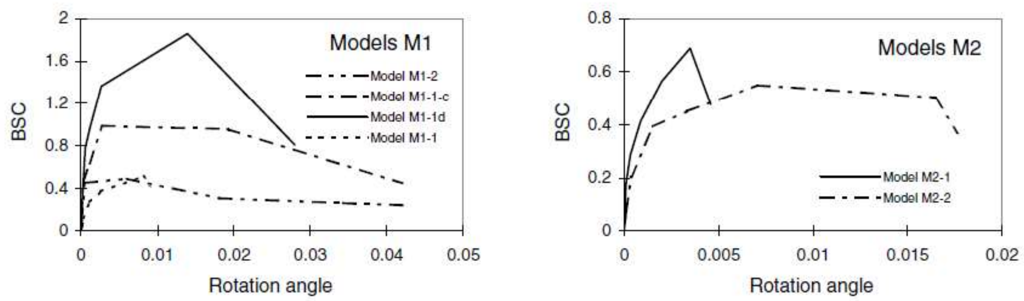

Figure 3.7. Experimental base shear coefficient versus rotation angle relationship (Tomazevic et al., 2004)

The strength ratio of URM buildings in the literature is generally higher than the strength ratio of actual URM buildings constructed in Turkey since material quality, workmanship, quality control, and design standards are not properly implemented in Turkey. If the previous Turkish Earthquake Code (TEC)-2007 is considered to assess the design strength ratio for Turkish masonry structures, the following equation can be employed.

$$\frac{V_b}{W} = \eta = \frac{A_o I S(T)}{R_a} \tag{3.4}$$

where V_b is the base shear force, W is the weight, A_o is the seismic zone coefficient, I is the building importance factor, S(T) is the spectrum coefficient, and R_a is the seismic load reduction factor. In the code, the values R_a=2, S(T)=2.5 and I=1 are proposed to design a masonry building. Since coefficient A_o is a function pf seismic zone in TEC (2007), the values of design strength ratios range between 0.125 and 0.5 as given in Table 3.3.

Table 3.3. *Design strength ratio values according to TEC (2007)*

Seismic Zone	1	2	3	4
Ao	0.4	0.3	0.2	0.1
Vb/W	0.5	0.375	0.25	0.125

Considering all the discussion above, the parametric values of strength ratio for URM structures in this study are considered as 0.1, 0.3, 0.5, 0.7 and 0.9, respectively.

3.4.3. Ductility Ratio

Ductility ratio (abbreviated as μ) is another important structural parameter that represents displacement capacity of structures. The relationship of μ with the maximum displacement is known as

$$\mu = \frac{u_{max}}{u_y} \tag{3.5}$$

where μ is the ductility ratio, u_{max} is the maximum displacement, and u_y is the yield displacement.

In the literature, Zavala et al. (2004) carried out a field test for a full-scale two-story URM building composed of brick units. The test was conducted with a static load. According to the test results which demonstrate hysteresis response of the structures, the authors stated that ductility ratio was approximately obtained as 2.8.

Magenes (2006) conducted nonlinear static analyses of URM buildings ranging from one to three story, with a simple plan and constructed with hollow clay elements. It was aimed to find the ductility ratio and compare the value with the one obtained from the Italian seismic code. According to the results, the ductility of regular URM structures was proposed as 4.4.

Magenes and Penna (2011) carried shaking table tests with three stone masonry building specimens. The buildings were scaled by a 1/2 model. At the end of the tests, ductility ratio was approximately determined from the cyclic force-displacement curves as 5.0 as illustrated in Figure 3.8.

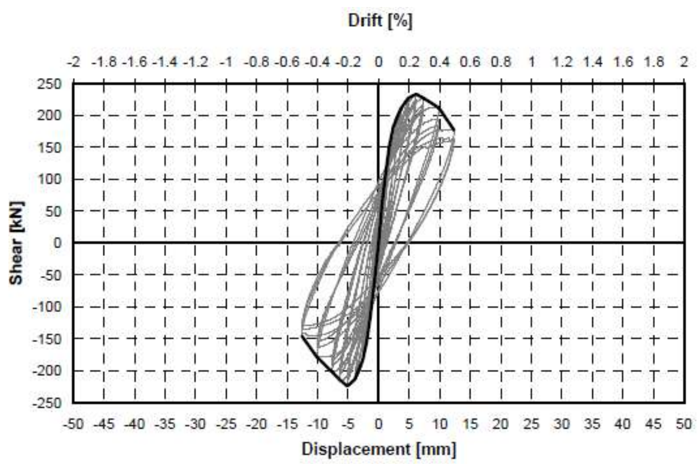

Figure 3.8. Cyclic force-displacement curve (Magenes and Penna, 2011)

Lourenco et al. (2012) conducted shaking table tests with an URM building composed of concrete masonry units. The structure was scaled by a 1/2 model. According to the test results, the ductile ratio of the structure was observed as 5.57.

As stated above, Turkish URM buildings generally have poor material quality and workmanship so the values of structural parameters for Turkish URM structures should be lower than the ones in the countries where the aforementioned studies in the literature have been carried out. Therefore, the parametric values of ductility ratio are respectively assumed as 2.0, 2.5, 3.0, 3.5 and 4.0 in this study.

3.4.4. Other ESDOF Model Parameters

In addition to the major structural parameters for URM buildings in the previous sections, there are also secondary parameters of the employed hysteresis model such as post-yielding ratio, post-capping ratio, residual strength ratio, and model degradation parameter that should be utilized for the parametric study. In this study, the presumed values of these secondary parameters can be stated with 3 different discrete values that the post-yielding ratio (α_s) is assumed as 0.0, 0.05 and 0.1, the post-capping ratio (α_r) is assumed as -0.4, -0.3 and -0.2, the residual strength ratio (λ) is assumed as 0.0, 0.2 and 0.4, and the model degradation parameter (γ) is assumed as 200, 400 and 800. Furthermore, the rate of strength deterioration is taken constant as 1.0, which is the default value in the OpenSees platform.

3.5. Classification of the URM Structural Parameters

Finally, all the selected values for URM buildings are represented in Table 3.4. As seen in Table 3.4, the URM buildings are classified as very rigid, rigid, average, flexible, and very flexible in terms of period while classified as very poor, poor, moderate, high, and very high in terms of seismic performance for the remaining structural parameters.

Table 3.4. *Assigned values of structural parameters for URM buildings in this study*

Vibrational Properties	**Very rigid**	**Rigid**	**Average**	**Flexible**	**Very flexible**
Period (T)	0.05	0.1	0.2	0.3	0.4
Seismic Performance	**Very poor**	**Poor**	**Moderate**	**High**	**Very High**
Strength Ratio (η)	0.1	0.3	0.5	0.7	0.9
Ductility Ratio (μ)	2.0	2.5	3.0	3.5	4.0
Post-yield ratio (α_s)		0	0.05	0.1	
Post-capping ratio (α_r)		-0.4	-0.3	-0.2	
Residual strength ratio (λ)		0	0.2	0.4	
Model degradation parameter (γ)		200	400	800	

There are either 3 or 5 sub-classes with discrete values, depending on the considered structural parameter. Accordingly, major parameters (T, η and μ) have 5 different values whereas secondary parameters (α_s, α_r, λ and γ) have 3 different values. The average (or moderate) values can be considered as the central (or mean) values. Other values are regarded as plus or minus deviations from the central value. In total, 10,125 unique structural combinations can be obtained for the URM model simulations. Besides, 240 different time-acceleration ground motion records are applied to each combination of the structural model. At the end of the structural analyses, 2,430,000 distinctive displacement and force responses are obtained to carry out damage estimation of the structures and statistical approaches. In order to handle this huge response statistics and draw conclusions out of it, some abbreviations are used for the sub-classes of each parameter as given in Table 3.5.

Table 3.5. *The abbreviations for each sub-class of the structural parameters*

	Very rigid	**Rigid**	**Average**	**Flexible**	**Very flexible**
Period (T)	T1	T2	T3	T4	T5
	Very poor	**Poor**	**Moderate**	**High**	**Very High**
Strength Ratio (η)	F1	F2	F3	F4	F5
Ductility Ratio (μ)	M1	M2	M3	M4	M5
Post-yield ratio (α_s)		Y2	Y3	Y4	
Post-capping ratio (α_r)		C2	C3	C4	
Residual strength ratio (λ)		R2	R3	R4	
Model degradation parameter (γ)		D2	D3	D4	

3.6. Structural Nonlinear Dynamic Analysis

As mentioned previously, approximately 2.5 million dynamic analyses are carried out in this thesis in order to investigate the effect of seismological and structural parameters on the seismic performance of URM structures. This is a huge number of analyses and can only be realized in the case of SDOF analysis demanding little computational effort, where a single analysis takes a few seconds. All of the analyses have been carried out with the OpenSees software. The Newmark integration method has been used to obtain the numerical results of SDOF analyses. The following chapters are devoted to the presentation of the seismic analyses results and their statistical evaluation.

CHAPTER 4

ASSESSMENT OF PERFORMANCE FOR URM STRUCTURES

4.1. General

This chapter focuses on the sensitivity analysis regarding the effect of different seismological and structural parameters on seismic performance of URM structures. Structural modeling and idealization of URM structures were discussed in Chapter 2 and the modeling parameters were determined in Chapter 3. In this chapter, results of the dynamic analyses are evaluated using a parametric approach and the significance of each parameter is assessed in a detailed manner. In this study, the limit states (LS) are defined in terms of the yielding displacement (u_y), capping displacement (u_c), residual displacement (u_r) and ultimate displacement (u_u) for each structural simulation. These limit states are indeed the bounds of the damage states (DS), which are employed to determine the performance levels of URM models. These damage states are used to assess the influence of different seismological and structural parameters on the seismic performance of URM models.

4.2. Attainment of Limit and Damage States

Limit states are predefined specific performance thresholds, which are expressed in terms of a local or a global structural parameter such as capacity, stress, displacement, strain, rotation, etc. They have been commonly used within the last decades in performance-based design and analysis methodologies, seismic risk assessment studies, earthquake damage and loss estimation approaches. Exceedance of LS leads to the conditional performance of that specific structure, called as a damage or performance state.

The concept of LS is employed to define DS due to the exceedance or non-exceedance criteria, meaning that LS-1 is a threshold between DS-1 and DS-2, LS-2 between DS-2 and DS-3 and LS-3 between DS-3 and DS-4. Table 4.1 shows the relationship between LS and DS for a generic case. Hence if there are three LS defined, this means there should be four damage states ranging from the elastic behavior to collapse.

Table 4.1. *General Definitions of Limit and Damage States*

LS	Definition of Limit State	DS	Definition of Damage State
LS-1	Immediate Occupancy	**DS-1**<LS-1	Very limited structural damage
LS-2	Damage Control	LS-1<**DS-2**<LS-2	Moderate damage-repairable
LS-3	Life Safety	LS-2<**DS-3**<LS-3	Significant damage – non repairable
LS-4	Collapse Prevention	LS-3<**DS-4**	Severe damage / partial collapse

Different limit state definitions have been used in the literature. Calvi (1999) employed LS to assess the seismic risk of the SDOF model of masonry and reinforced concrete structures. In that study, LS-1 was considered as 0.1%, LS-2 was identified as the closer ratio to LS-1, LS-3 as 0.3% in terms of the drift ratio for masonry structures. He defined the first DS as “no damage”, the second DS as “minor structural damage”, the third DS as “significant structural damage” and the fourth DS as “collapse” for masonry structures.

Collins and Stojadinovic (2000) conducted performance-based design (PBD) with a reliability-based approach. As demonstrated in Figure 4.1, they used different LS definitions to match the structural performance with the performance objective.

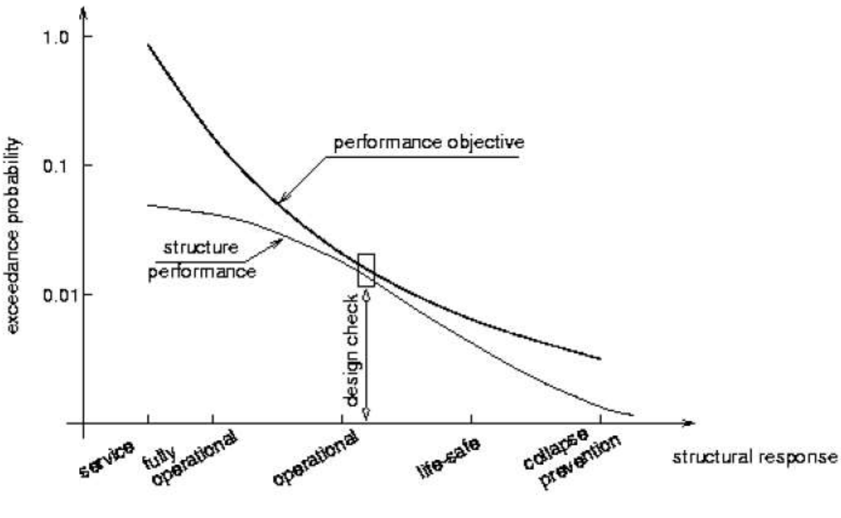

Figure 4.1. Performance-based design with reliability-based approach (Collins and Stojadinovic, 2000)

Bazzurro et al. (2004) stated that the identification of DS levels is essential to describe the vulnerability of buildings before the occurrence of a seismic event. Therefore, they used nonlinear static analyses up to the failure point of the buildings. The purpose of this study was to determine the probabilistic performance of structures by using fragility curves developed with predefined LS.

In the study of Erberik (2008), seismic vulnerability of mid-rise and low-rise reinforced concrete buildings was assessed by generating fragility curves. The buildings were converted from MDOF models to SDOF models to simplify the structural analysis. Three limit states, termed as the “serviceability”, “damage control” and “collapse prevention”, were defined by using the structural characteristics of the considered class of structures. At end of the study, the damage estimated with the fragility curves was compared with the actual damage observed during the 1999 Duzce earthquake.

Yakut and Solmaz (2012) studied the seismic performance of reinforced concrete frame structures in order to propose equations about the relationship between structural parameters via using nonlinear regression analyses. In order to get these equations, the seismic codes, namely Eurocode 8 (2003), FEMA 356 (2000) and TEC (2007), were used to define LS of the structures during nonlinear static analyses, which were carried out with the OpenSees software.

Mouyiannou et al. (2014) carried out nonlinear dynamic analysis to identify DS levels of stone masonry buildings, which were represented by SDOF models. The analyses were conducted with the TREMURI program. The results of structural analyses are represented in Figure 4.2. In their study, three LS were considered to evaluate the seismic risk of stone masonry structures as they were deemed risky between LS-3 and LS-4. Therefore, the DS of the structure was assumed as collapse after LS-3 is exceeded.

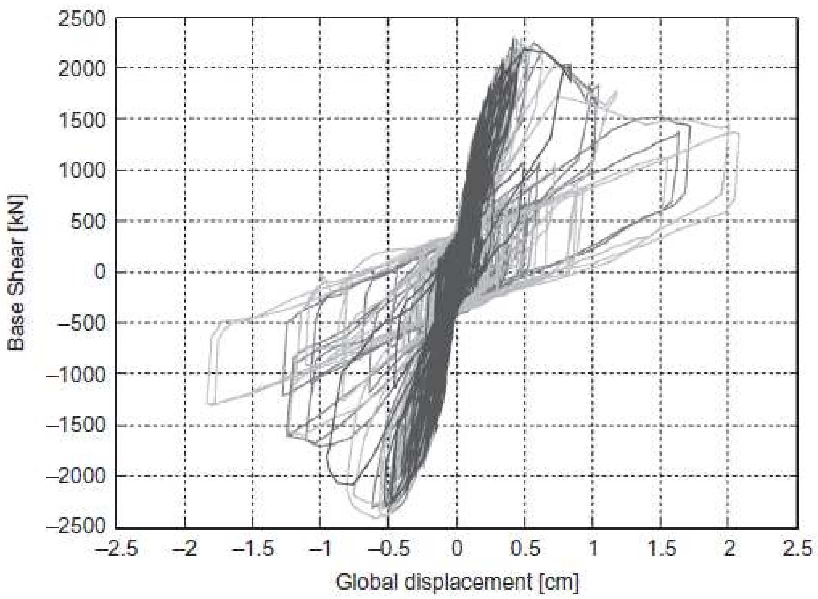

Figure 4.2. The results of nonlinear dynamic analysis (Mouyiannou et al., 2014)

Petry and Beyer (2014) performed quasi-static cyclic tests to find out the force-displacement capacity of the URM walls. LS of the walls were defined by using

FEMA 306 (1998). This study was performed in order to explain the behavior of the walls in different failure modes as shear and flexural. At end of the tests, the walls were classified according to their displacement capacity.

Chaudhari and Dhoot (2016) stated that PBD provides life safety and minimum economic losses by assessing the seismic performance of structures. The main target of the study was to estimate maximum displacement capacity with the base shear so that the damage levels of the structures can be identified with the performance levels shown in Figure 4.3.

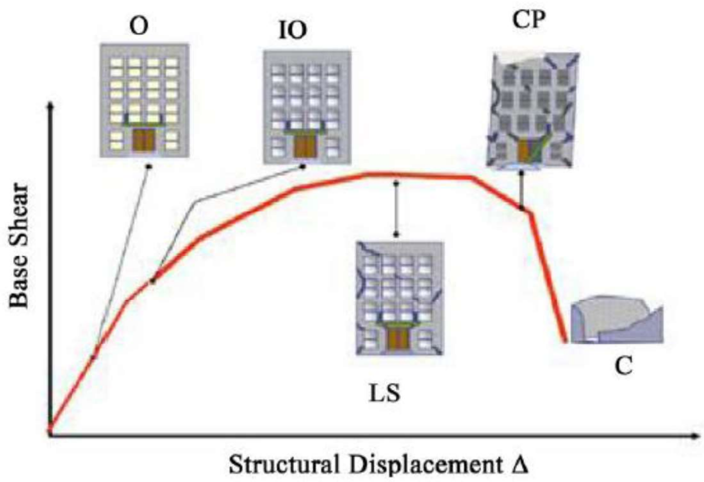

Figure 4.3. Performance-based design of structures (Chaudhari and Dhoot, 2016)

As discussed in the previous chapter, the MIMK with peak-oriented hysteresis model (Ibarra et al., 2015) is employed in this study to carry out the dynamic analysis of the idealized (equivalent SDOF) masonry building models. Accordingly, the limit states are selected to be yield displacement (u_y), capping displacement (u_c) and residual displacement (u_r), or shortly LS-1, LS-2 and LS-3, respectively. This means that there are four DS, which are denoted as “none/light damage”, “moderate damage”, “extensive/heavy damage” and “collapse” between these LS. After each dynamic analysis, the maximum displacement values obtained are compared with LS values and the performance level of the ESDOF model is determined for different values of selected seismological and structural parameters. This means that there is a performance level (or DS) output for every dynamic analysis. The following sections present the results of this parametric study by examining the effect of each parameter on the seismic performance of the ESDOF models.

As shown in Table 3.5 and 3.6, discrete values are assigned to 7 different structural parameters related with the considered hysteresis model. Among these, period, strength ratio and ductility ratio have 5 different values whereas the remaining parameters have 3 different values, each containing a central (average) value and deviations from this central value for both favorable and unfavorable conditions. If all different combinations of structural simulations are considered, it makes up to 10,125 cases. In terms of seismological parameters, magnitude is considered with 6 discrete values (5.0, 5.5, 6.0, 6.5, 7.0, 7.1), R_{JB} distance has 5 different intervals (0-5 km, 5-10 km, 10-15 km, 15-20 km, 20-25 km) and finally there are two different soil conditions (hard, soft) as obtained from the simulated ground motion database. When 20 different earthquake stations are selected for the synthetic records with 6 different magnitudes and 2 different soil conditions, the total number of records used in the dynamic analyses is 240. Hence when structural simulations are subjected to this selected set of records, the total number of analyses becomes 2,430,000. This is also equal to the number of response data in terms of DS, which is considered to interpret the results of the parametric study presented in the following sections.

4.3. Sensitivity Analyses

Sensitivity analysis is essential to investigate the influence of the seismological and the structural parameters on DS. In this study, sensitivity analyses are conducted by considering all of the possible discrete values of a selected structural parameter while keeping the other parameters constant at their central (average) values. In addition to this, combinations of the structural parameters that yield the most favorable and unfavorable conditions for soft and hard soil type are also used to examine the effects of the magnitude and distance on seismic performance. The mean values of DS (i.e. DSM) given in the following tables are obtained by taking the mean of all DS values obtained from dynamic analyses for that specific combination of parameters. In order to quantify the mean value, weighting factors are provided for DS-1, DS-2, DS-3, DS-4 as 1.0, 2.0, 3.0 and 4.0, respectively.

First, the results from the combination of parameters with the most unfavorable values, stated as T1-F1-M1-Y2-C2-R2-D2, are presented for soft soil conditions in Figure 4.4, and the DSM values for each magnitude and R_{JB} distance interval are also given in Table 4.2. This is the combination of parameters for which the lowest level of performance is expected from dynamic analyses.

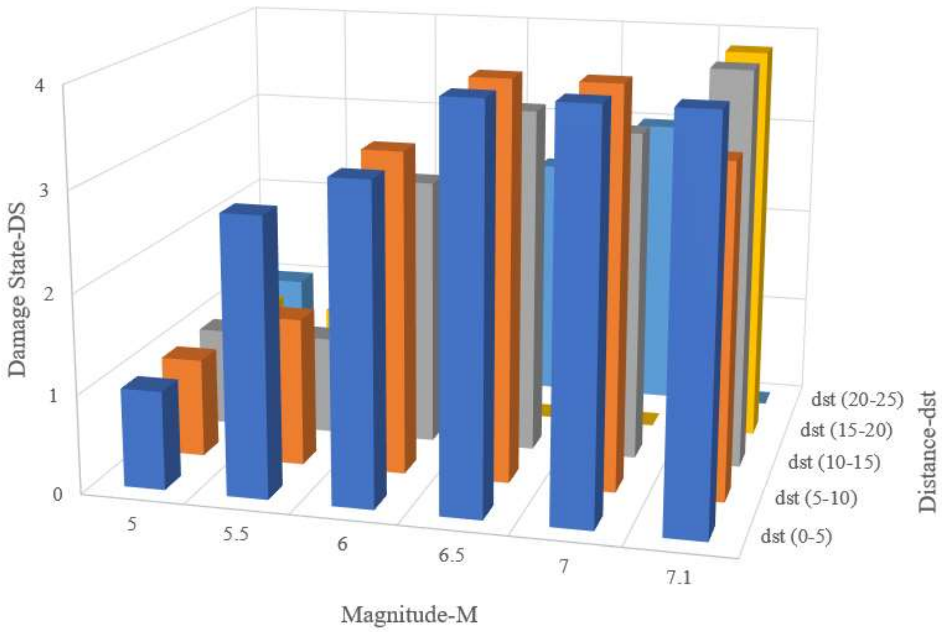

Figure 4.4. The performance assessment for the structural combination T1-F1-M1-Y2-C2-R2-D2 under soft soil conditions

In Table 4.2, value of 1.0 means that all the structural simulations have behaved within the elastic limit (no damage) for the corresponding magnitude-distance interval pair. Abbreviation "N.A" stands for the condition that there is no data for that specific pair of seismological values. Accordingly, the given values in the table reveal that for near fault-distances and large magnitude events, the structural models can easily experience collapse (i.e. value of 4.0) or heavy damage (i.e. 3.0<DSM<4.0).

Table 4.2. *The DSM values for T1-F1-M1-Y2-C2-R2-D2 in soft soil conditions*

	Distance interval (km)				
Magnitude	0-5	5-10	10-15	15-20	20-25
5	DS-1 (1.0)	DS-1 (1.00)	DS-1 (1.00)	DS-1 (1.00)	DS-1 (1.00)
5.5	DS-3 (2.80)	DS-2 (1.50)	DS-1 (1.00)	DS-1 (1.00)	DS-1 (1.00)
6	DS-4 (3.20)	DS-4 (3.25)	DS-3 (2.71)	DS-2 (1.50)	DS-2 (1.50)
6.5	DS-4 (4.00)	DS-4 (4.00)	DS-4 (3.50)	N.A	DS-3 (2.50)
7	DS-4 (4.00)	DS-4 (4.00)	DS-4 (3.33)	N.A	DS-3 (3.00)
7.1	DS-4 (4.00)	DS-4 (3.33)	DS-4 (4.00)	DS-4 (4.00)	N.A

For hard soil conditions, the DSM values for the same structural combination of parameters are presented in Figure 4.5 while the mean values of DS for each magnitude and R_{JB} distance interval are given in Table 4.3. The mean values show that there is a similar trend between the DSM values and the two seismological parameters just like the one for soft soil conditions in Table 4.2. When the values in Table 4.2 and 4.3 are compared, it is observed that there is not a consistent trend between the seismic performance of these deficient URM models under soft and hard soil conditions.

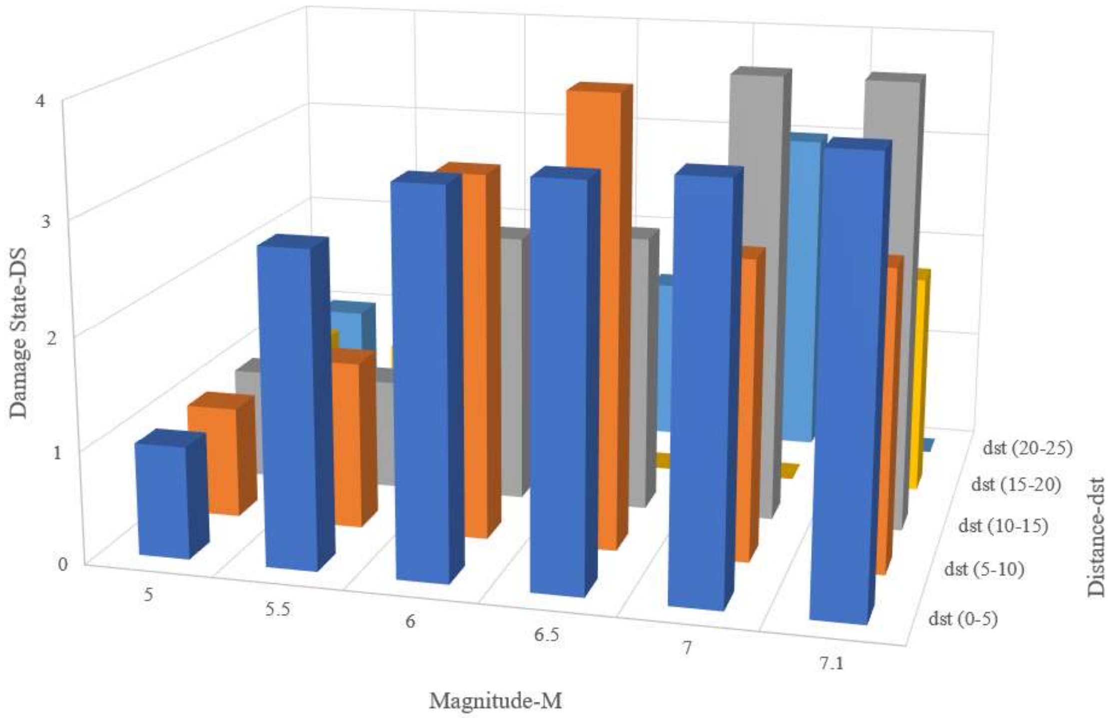

Figure 4.5. The performance assessment for the structural combination T1-F1-M1-Y2-C2-R2-D2 under hard soil conditions

Table 4.3. *The DSM values for T1-F1-M1-Y2-C2-R2-D2 in hard soil conditions*

	Distance interval (km)				
Magnitude	0-5	5-10	10-15	15-20	20-25
5	DS-1 (1.00)	DS-1 (1.00)	DS-1 (1.00)	DS-1 (1.00)	DS-1 (1.00)
5.5	DS-3 (2.80)	DS-2 (1.50)	DS-1 (1.00)	DS-1 (1.00)	DS-1 (1.00)
6	DS-4 (3.40)	DS-4 (3.25)	DS-3 (2.43)	DS-1 (1.00)	DS-1 (1.00)
6.5	DS-4 (3.50)	DS-4 (4.00)	DS-3 (2.50)	N.A	DS-2 (1.50)
7	DS-4 (3.58)	DS-3 (2.66)	DS-4 (4.00)	N.A	DS-3 (3.00)
7.1	DS-4 (3.85)	DS-3 (2.66)	DS-4 (4.00)	DS-2 (2.00)	N.A

Next, results from the combination of parameters with central (mean) values, stated as T3-F3-M3-Y3-C3-R3-D3, are represented for soft soil conditions in Figure 4.6, while the DSM values for each magnitude and R_{JB} distance interval is given in Table 4.4. This is the combination of parameters for which average performance is expected from dynamic analyses.

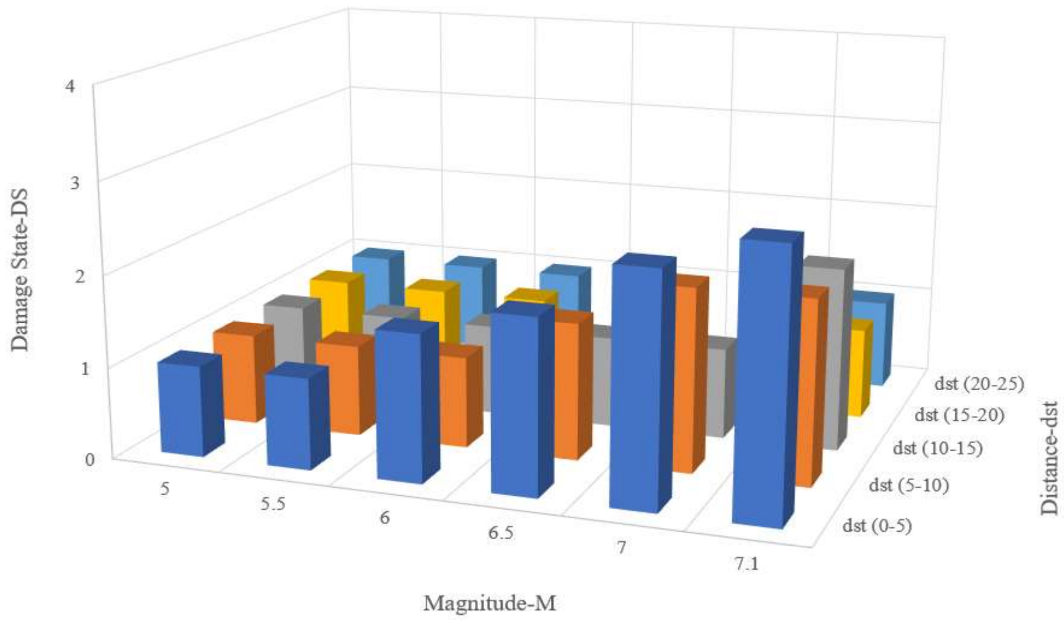

Figure 4.6. The performance assessment for the structural combination T3-F3-M3-Y3-C3-R3-D3 under soft soil conditions

The DSM values obtained from this analysis indicate that ESDOF models with average values of parameters exhibit satisfactory seismic performance with no inelastic action except for large magnitudes and close distances in soft soil conditions.

Table 4.4. *The DSM values for T3-F3-M3-Y3-C3-R3-D3 in soft soil conditions*

	Distance interval (km)				
Magnitude	0-5	5-10	10-15	15-20	20-25
5	DS-1 (1.00)	DS-1 (1.00)	DS-1 (1.00)	DS-1 (1.00)	DS-1 (1.00)
5.5	DS-1 (1.00)	DS-1 (1.00)	DS-1 (1.00)	DS-1 (1.00)	DS-1 (1.00)
6	DS-2 (1.60)	DS-1 (1.00)	DS-1 (1.00)	DS-1 (1.00)	DS-1 (1.00)
6.5	DS-2 (1.90)	DS-2 (1.50)	DS-1 (1.00)	N.A.	DS-1 (1.00)
7	DS-3 (2.50)	DS-2 (2.00)	DS-1 (1.00)	N.A.	DS-1 (1.00)
7.1	DS-3 (2.85)	DS-2 (2.00)	DS-2 (2.00)	DS-1 (1.00)	DS-1 (1.00)

For hard soil conditions, the DSM values for the same structural combination of parameters are represented in Figure 4.7 while the mean values of DS for each magnitude and R_{JB} distance interval is given in Table 4.5. The mean values show similar trends with the ones obtained in the case of soft soil conditions.

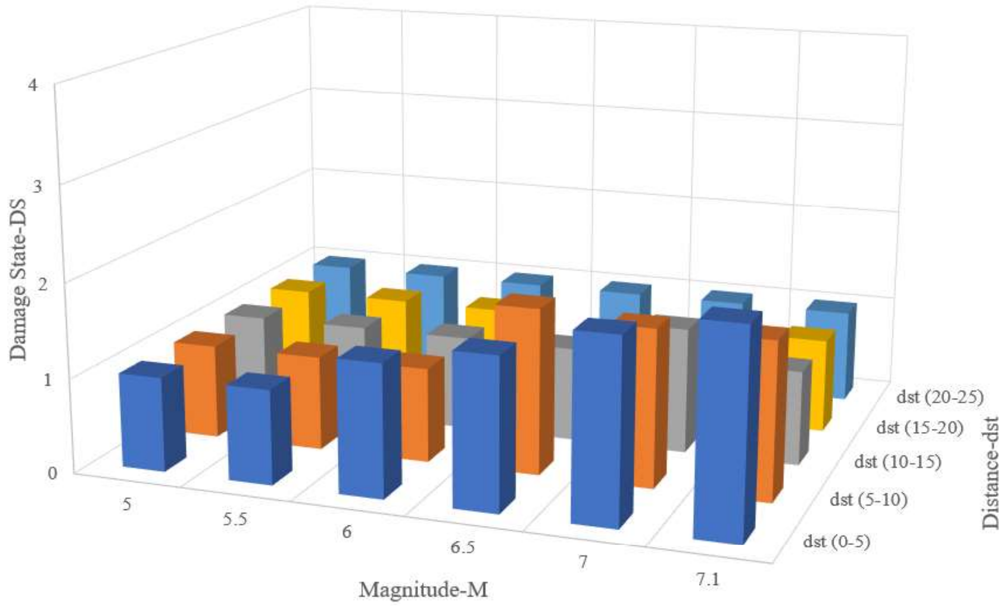

Figure 4.7. The performance assessment for the structural combination T3-F3-M3-Y3-C3-R3-D3 under hard soil conditions

Table 4.5. *The DSM values for T3-F3-M3-Y3-C3-R3-D3 in hard soil conditions*

	Distance interval (km)				
Magnitude	0-5	5-10	10-15	15-20	20-25
5	DS-1 (1.00)	DS-1 (1.00)	DS-1 (1.00)	DS-1 (1.00)	DS-1 (1.00)
5.5	DS-1 (1.00)	DS-1 (1.00)	DS-1 (1.00)	DS-1 (1.00)	DS-1 (1.00)
6	DS-2 (1.40)	DS-1 (1.00)	DS-1 (1.00)	DS-1 (1.00)	DS-1 (1.00)
6.5	DS-2 (1.60)	DS-2 (1.75)	DS-1 (1.00)	N.A	DS-1 (1.00)
7	DS-2 (1.92)	DS-2 (1.66)	DS-2 (1.33)	N.A	DS-1 (1.00)
7.1	DS-3 (2.14)	DS-2 (1.66)	DS-1 (1.00)	DS-1 (1.00)	DS-1 (1.00)

Finally, the results from the combination of parameters with the most favorable values, stated as T5-F5-M5-Y4-C4-R4-D4, are presented for soft soil conditions in Figure 4.8

while the DSM values for each magnitude and R_{JB} distance interval is given in Table 4.6. This is the combination of parameters for which the highest level of performance is expected from dynamic analyses.

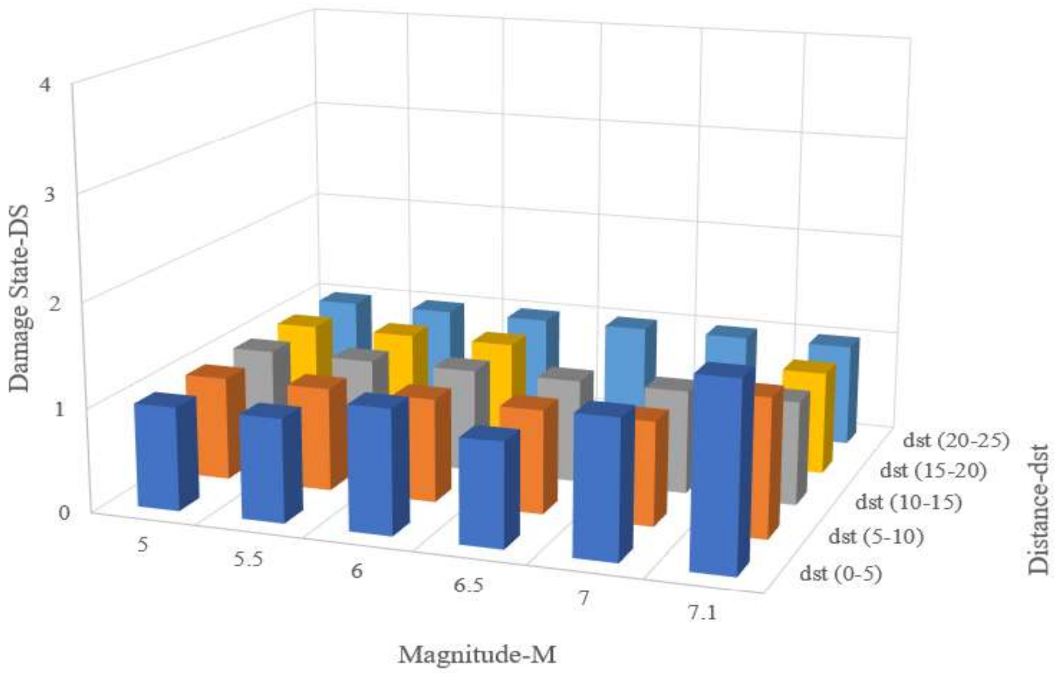

Figure 4.8. The performance assessment for the structural combination T5-F5-M5-Y4-C4-R4-D4 under soft soil conditions

The results indicate that the ESDOF models with the most favorable values of parameters generally behave in the elastic range with some exceptional cases, in which the elastic limit is exceeded for large magnitudes and close distances.

Table 4.6. *The DSM values for T5-F5-M5-Y4-C4-R4-D4 in soft soil conditions*

	Distance interval (km)				
Magnitude	0-5	5-10	10-15	15-20	20-25
5	DS-1 (1.00)	DS-1 (1.00)	DS-1 (1.00)	DS-1 (1.00)	DS-1 (1.00)
5.5	DS-1 (1.00)	DS-1 (1.00)	DS-1 (1.00)	DS-1 (1.00)	DS-1 (1.00)
6	DS-2 (1.20)	DS-1 (1.00)	DS-1 (1.00)	DS-1 (1.00)	DS-1 (1.00)
6.5	DS-1 (1.00)	DS-1 (1.00)	DS-1 (1.00)	N.A.	DS-1 (1.00)
7	DS-2 (1.33)	DS-1 (1.00)	DS-1 (1.00)	N.A.	DS-1 (1.00)
7.1	DS-2 (1.78)	DS-2 (1.33)	DS-1 (1.00)	DS-1 (1.00)	DS-1 (1.00)

For hard soil conditions, the DSM values for the same structural combination of parameters are presented in Figure 4.9 and mean values of DS for each magnitude and R_{JB} distance interval are given in Table 4.7. Similar to the results in soft soil conditions, the ESDOF models do not exhibit any inelastic behavior except two cases, in which $M_w \geq 7.0$ and $0 < R_{JB} < 5$km.

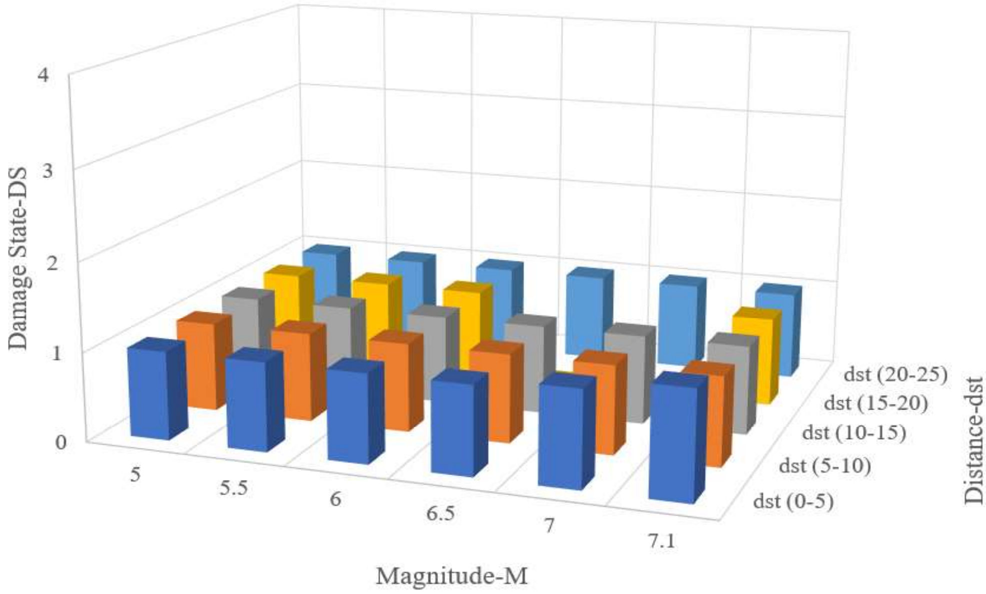

Figure 4.9. The performance assessment for the structural combination T5-F5-M5-Y4-C4-R4-D4 under hard soil conditions

Table 4.7. *The DSM values for T5-F5-M5-Y4-C4-R4-D4 in hard soil conditions*

	Distance interval (km)				
Magnitude	0-5	5-10	10-15	15-20	20-25
5	DS-1 (1.00)	DS-1 (1.00)	DS-1 (1.00)	DS-1 (1.00)	DS-1 (1.00)
5.5	DS-1 (1.00)	DS-1 (1.00)	DS-1 (1.00)	DS-1 (1.00)	DS-1 (1.00)
6	DS-1 (1.00)	DS-1 (1.00)	DS-1 (1.00)	DS-1 (1.00)	DS-1 (1.00)
6.5	DS-1 (1.00)	DS-1 (1.00)	DS-1 (1.00)	N.A.	DS-1 (1.00)
7	DS-2 (1.08)	DS-1 (1.00)	DS-1 (1.00)	N.A.	DS-1 (1.00)
7.1	DS-2 (1.21)	DS-1 (1.00)	DS-1 (1.00)	DS-1 (1.00)	DS-1 (1.00)

According to the results, it can be stated that

- The damage level of the structures generally increases with larger magnitude values.
- If R_{JB} distance increases, the effect of the ground excitation becomes smaller causing a decrease in the damage levels.
- The site conditions are generally effective on damage levels with magnitude values M_w>6.0 within the distance interval (0-5) km. In general, shifting from soft to hard soil conditions decreases the damage level of the structures for the same magnitude and R_{JB} distance interval.
- Considering Tables 4.2-4.7, DSM is prone to decrease from the lowest performance level to the highest performance level of the structural parameters, respectively.
- The DSM values are unexpectedly higher in some farther R_{JB} distance intervals than the closer ones. Sucuoğlu (2002) stated that larger ground motion amplitudes can be obtained at farther earthquake stations in the case of Düzce earthquake. This observation was explained with the relative role of directivity of the fault rupture. It is dominantly observed in the magnitude of 7.0 and 7.1 for the case of most unfavorable values of structural parameters.

In the second phase of the sensitivity analysis, the influence of each structural parameter is investigated individually while all of the other parameters are kept constant at their central (average) values. The first parameter to be investigated is period (T) with 5 discrete values, i.e. T=0.05, 0.1, 0.2, 0.3 and 0.4 sec. The other structural parameters have the following constant values: η=0.5, μ=3, α_s=0.05, α_r=-0.3, λ=0.2 and γ=400. The linear trendlines of DS versus T relationships for different values of magnitude and R_{JB} in soft and hard soil conditions are shown in Figures 4.10-4.13. The discrete values of DS and T forms a grid network with a cluster of data at each node and the trendlines are obtained in accordance with the number of data points at each related node of this grid.

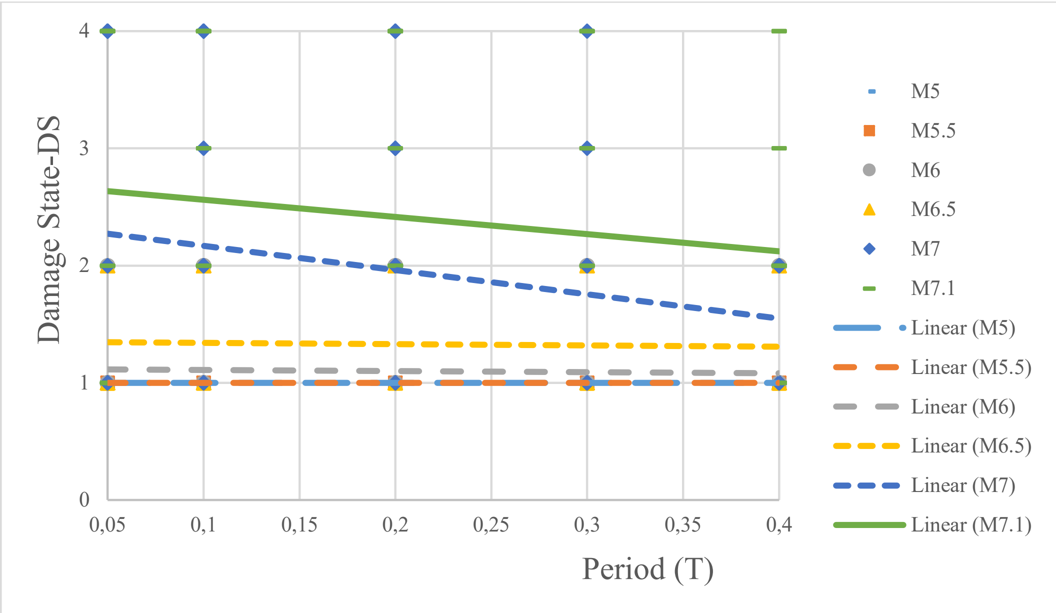

Figure 4.10. Trendlines of each magnitude with T values in terms of DS for soft soil

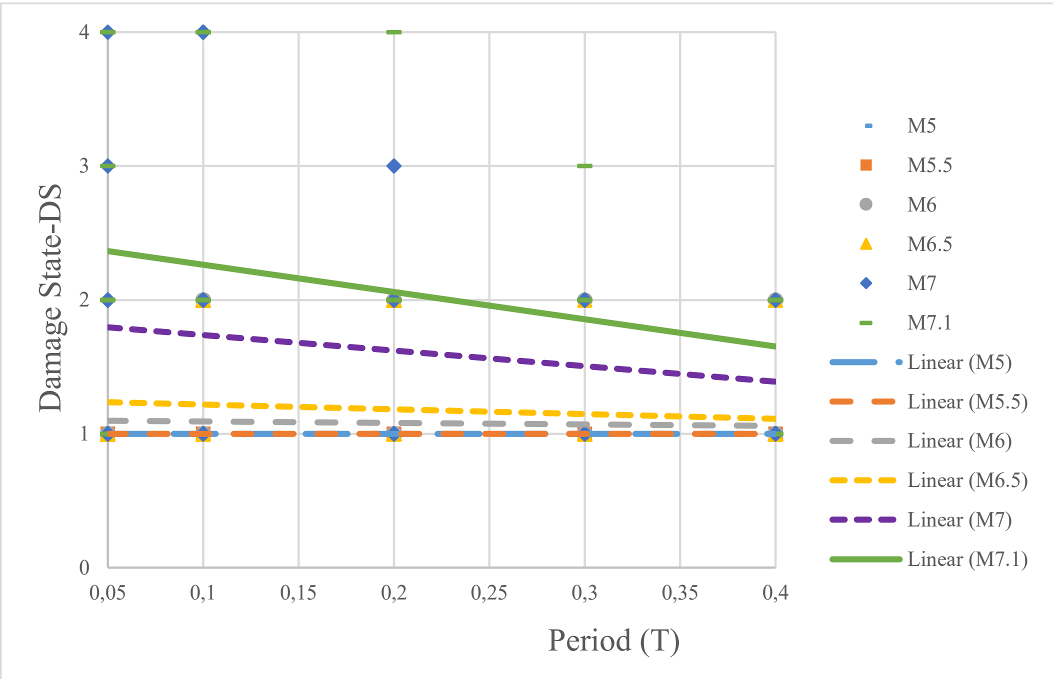

Figure 4.11. Trendlines of each magnitude with T values in terms of DS for hard soil

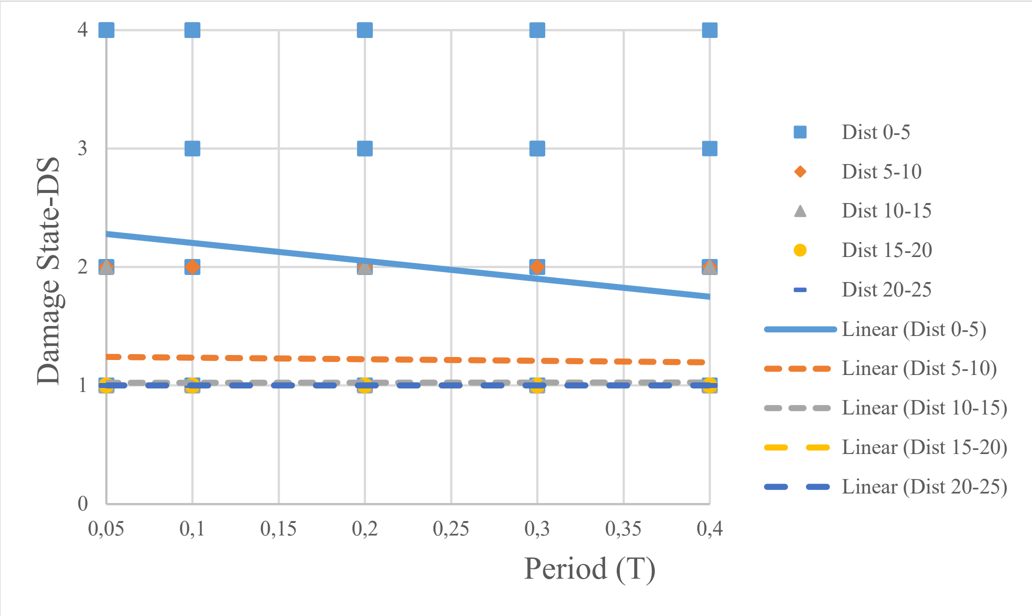

Figure 4.12. Trendlines of R_{JB} intervals with T values in terms of DS for soft soil

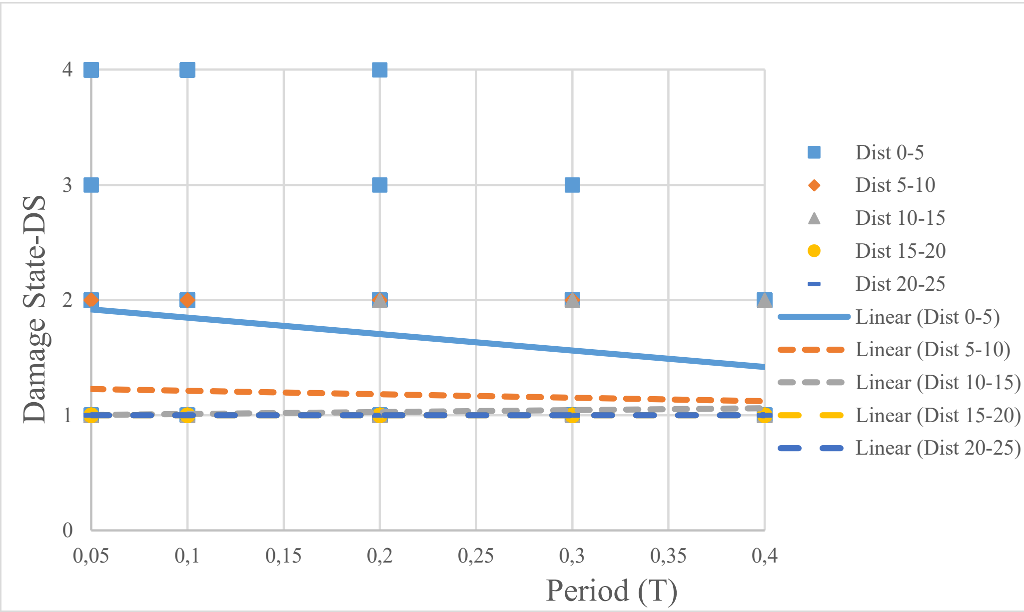

Figure 4.13. Trendlines of R_{JB} intervals with T values in terms of DS for hard soil

Considering the trendlines in Figures 4.10-4.13, the following observations can be stated:

- The change in period values is not effective on the DS values for the magnitude of 5.0 and 5.5 and the R_{JB} distance intervals of 15-20 and 20-25 km. It slightly affects the DS values for the magnitude values of 6.0 and 6.5 and the R_{JB} distance intervals of 5-10 and 10-15 km. For the moment magnitude values of 7.0 and 7.1 and the R_{JB} distance interval 0-5 km, it is highly sensitive on the DS. These generalizations are valid for both soil conditions.
- DS generally decreases with T values varying from 0.05 up to 0.4 depending on the magnitudes and R_{JB} distance intervals.
- DS is generally prone to decrease with T values as it shifts from soft soil to hard soil condition.

The second parameter to be investigated is the strength ratio (η) with 5 discrete values, i.e. η=0.1, 0.3, 0.5, 0.7 and 0.9 sec. The other structural parameters have the following constant values: T=0.2 sec, μ=3, α_s=0.05, α_r=-0.3, λ=0.2 and γ=400. The linear trendlines of the DS versus η relationship for different values of magnitude and R_{JB} in soft and hard soil conditions are shown in Figures 4.14-4.17.

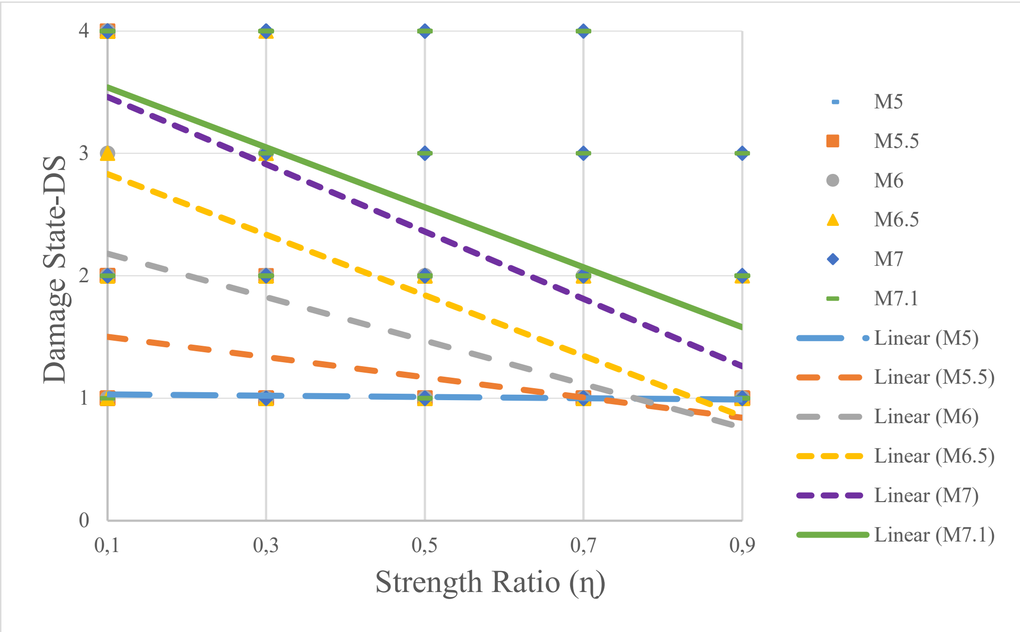

Figure 4.14. Trendlines of each magnitude with η values in terms of DS for soft soil

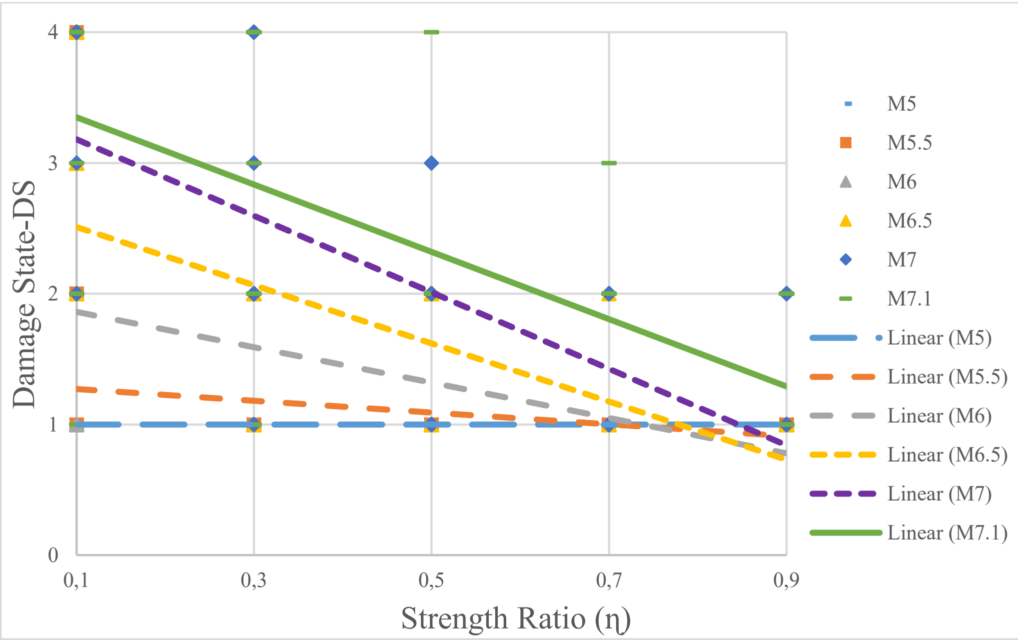

Figure 4.15. Trendlines of each magnitude with η values in terms of DS for hard soil

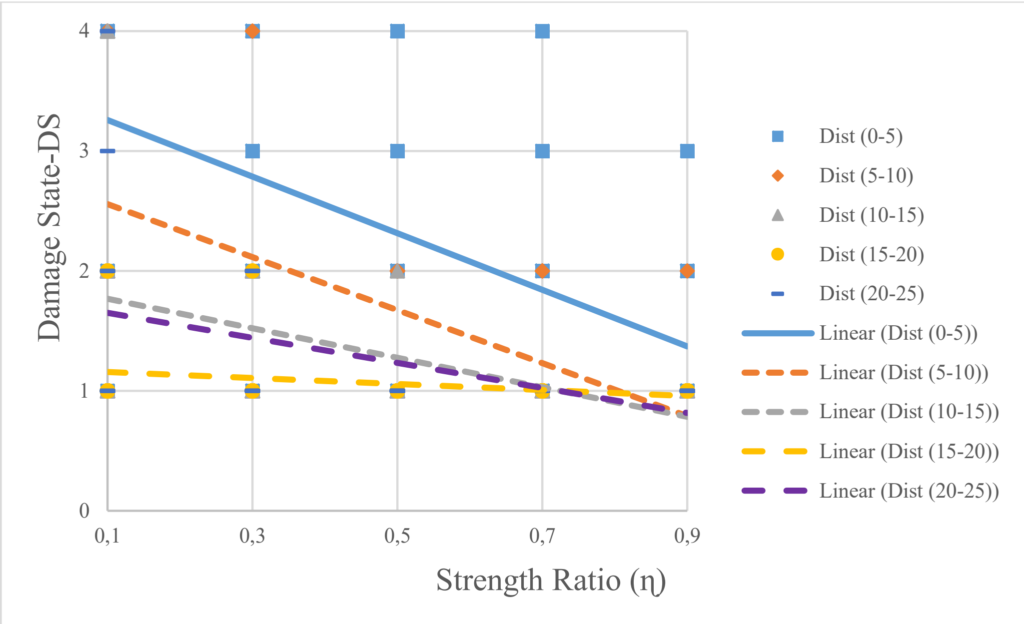

Figure 4.16. Trendlines of R_{JB} intervals with η values in terms of DS for soft soil

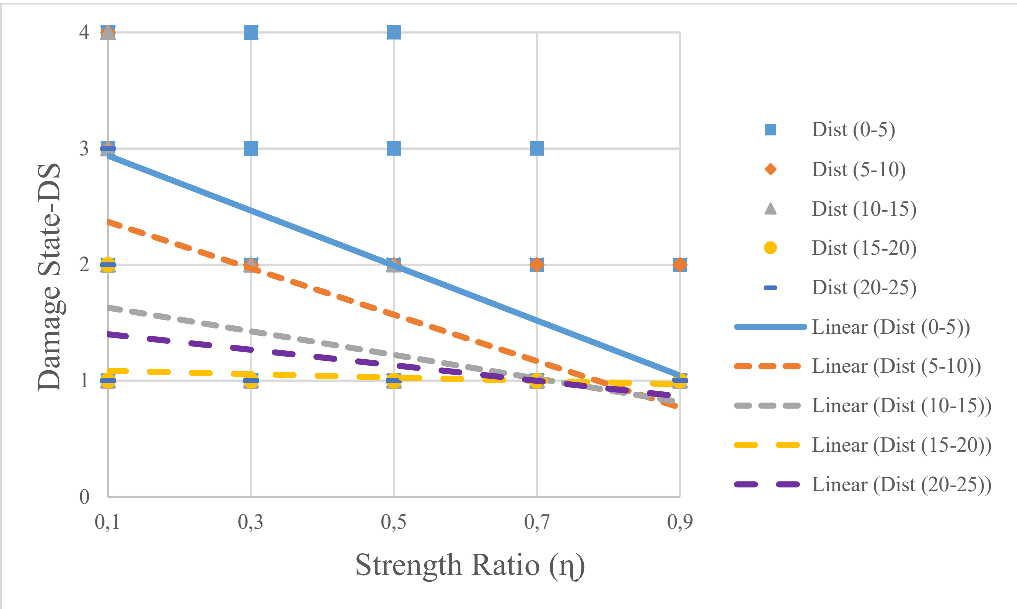

Figure 4.17. Trendlines of R_{JB} intervals with η values in terms of DS for hard soil

Considering the trendlines in Figures 4.14-4.17, the following observations can be stated:

- The change in strength ratio values is less effective on the DS values for the magnitude value of 5.0 and the R_{JB} distance interval of 15-20 km. In general, the sensitivity of strength ratio on DS increases with the magnitude varying from 5.5 to 7.1 and the R_{JB} distance intervals changing from 20-25 to 0-5 km. The interval of 15-20 km is normally expected to have a closer or slightly higher sensitivity than 20-25 km; however, there are a smaller number of records in the interval 15-20 km due to the selection of the earthquake stations in terms of PGA. Overall, strength ratio has more sensitivity on DS when compared to the period parameter.
- DS explicitly decreases with η values varying from 0.1 to 0.9 for all magnitudes and R_{JB} distance intervals except for the magnitude of 5.0 in both soil conditions.
- DS has a tendency to decrease with η values by shifting from soft soil to hard soil conditions.

The third parameter to be investigated is the ductility ratio (μ) with 5 discrete values, i.e. μ =2.0, 2.5, 3.0, 3.5 and 4.0. The other structural parameters have the following constant values: T=0.2 sec, η=0.5, α_s=0.05, α_r=-0.3, λ=0.2 and γ=400. The linear trendlines of the DS versus μ relationship for different values of magnitude and R_{JB} in soft and hard soil conditions are shown in Figures 4.18-4.21.

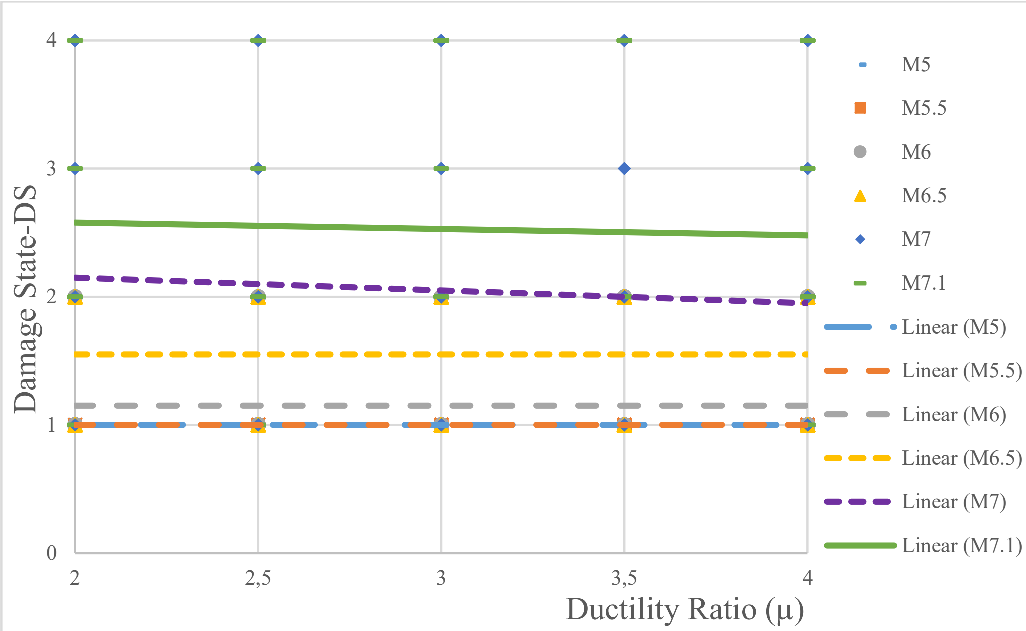

Figure 4.18. Trendlines of each magnitude with μ values in terms of DS for soft soil

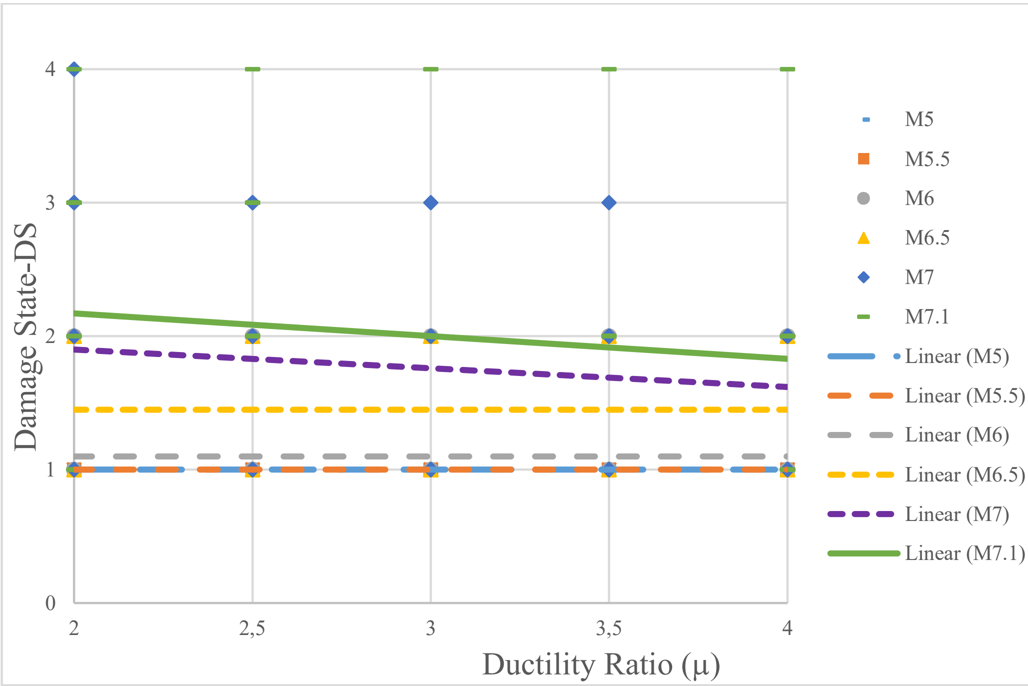

Figure 4.19. Trendlines of each magnitude with μ values in terms of DS for hard soil

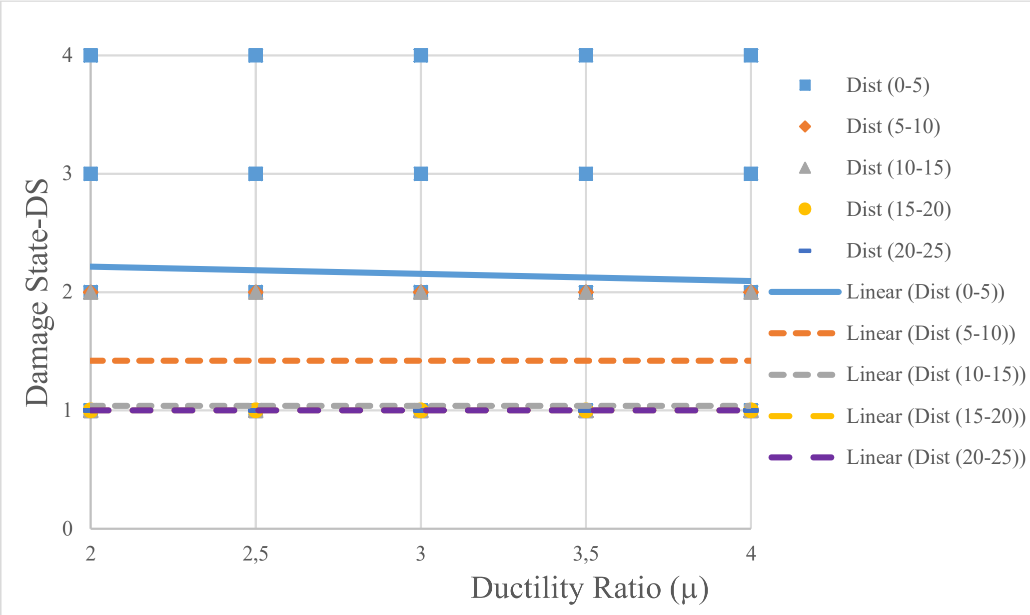

Figure 4.20. Trendlines of R_{JB} intervals with μ values in terms of DS for soft soil

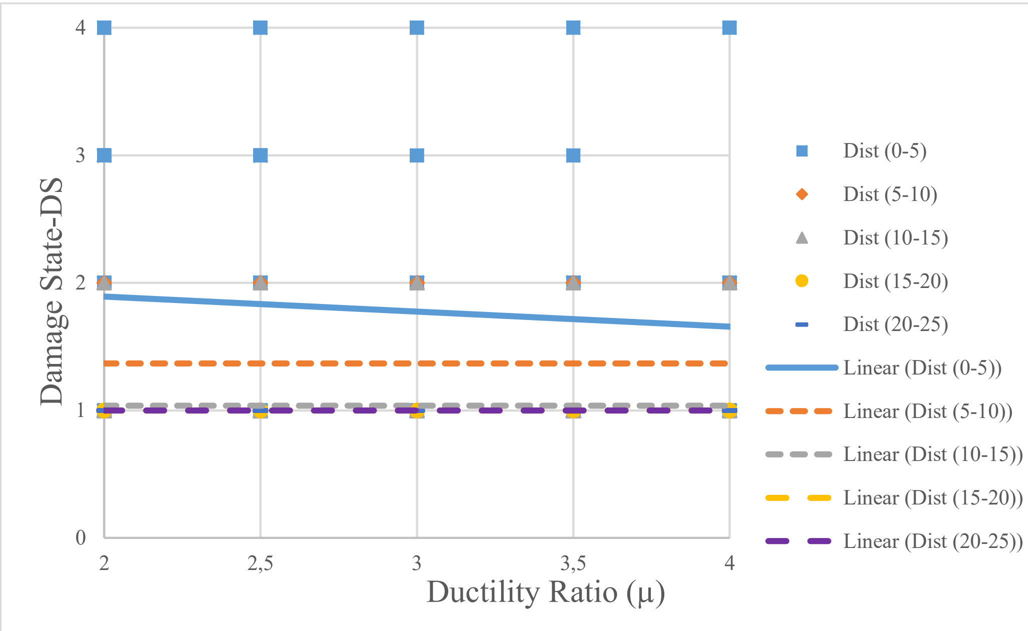

Figure 4.21. Trendlines of R_{JB} intervals with μ values in terms of DS for hard soil

Considering the trendlines in Figures 4.18-4.21, the following observations can be stated:

- The change in ductility values is not sensitive to DS for the magnitude values varying from 5.0 to 6.5 and R_{JB} distance intervals ranging from 20-25 to 5-10 km. Ductility is found to be only slightly sensitive for the magnitude of 7.0 and 7.1 and the R_{JB} distance interval of 0-5 km.
- DS generally tends to decrease with μ values from 2.0 to 4.0 for all of the magnitudes and R_{JB} distance intervals.
- DS has a slight tendency to decrease with μ values by shifting from soft soil to hard soil conditions.

The fourth parameter to be investigated is the post-yielding ratio (α_s) with 3 discrete values, i.e. α_s= 0.0, 0.05 and 0.1. The other structural parameters have the following constant values: T=0.2 sec, η=0.5, μ=3.0, α_r=-0.3, λ=0.2 and γ=400. The linear trendlines of the DS versus α_s relationship for different values of magnitude and R_{JB} in soft and hard soil conditions are shown in Figures 4.22-4.25.

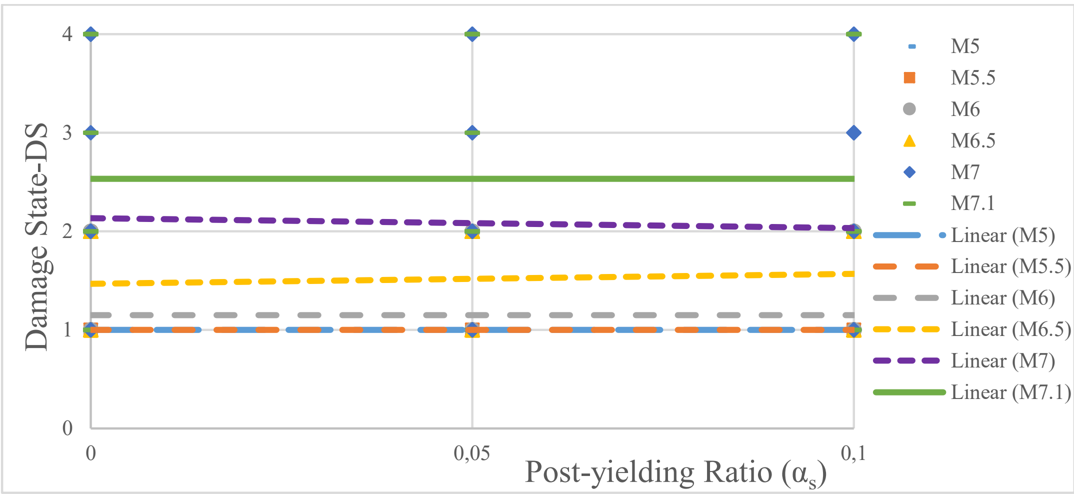

Figure 4.22. Trendlines of each magnitude with α_s values in terms of DS for soft soil

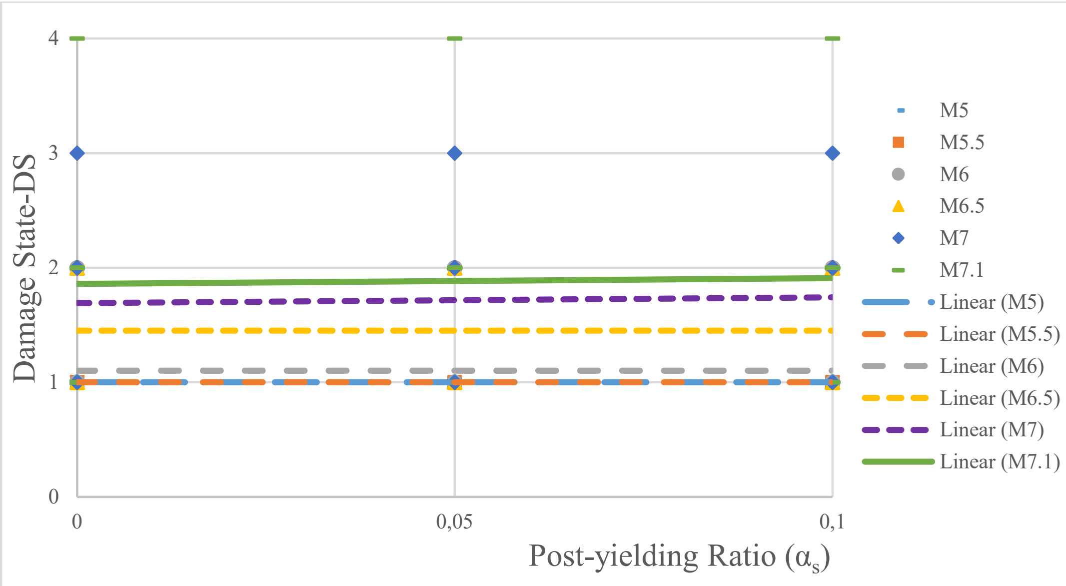

Figure 4.23. Trendlines of each magnitude with α_s values in terms of DS for hard soil

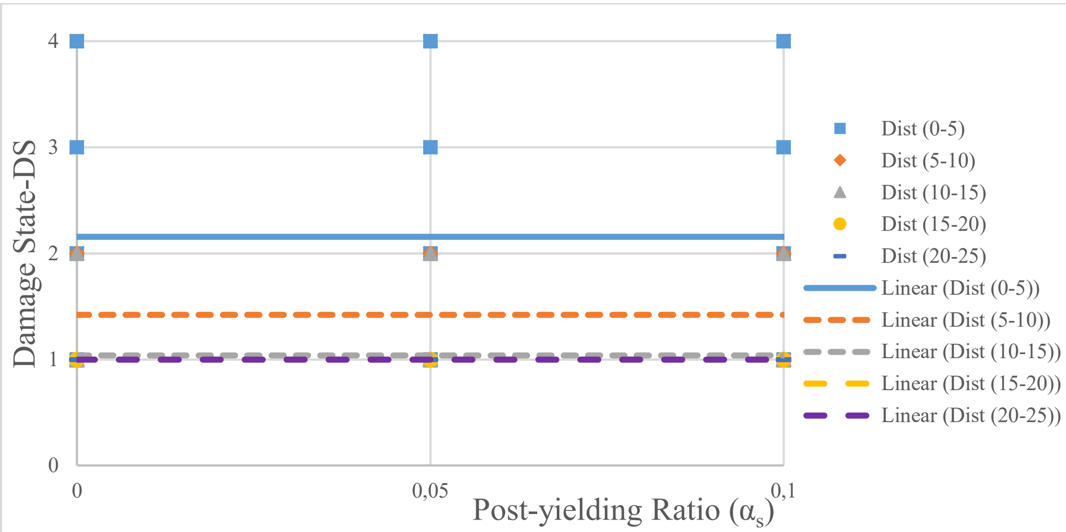

Figure 4.24. Trendlines of R_{JB} intervals with α_s values in terms of DS for soft soil

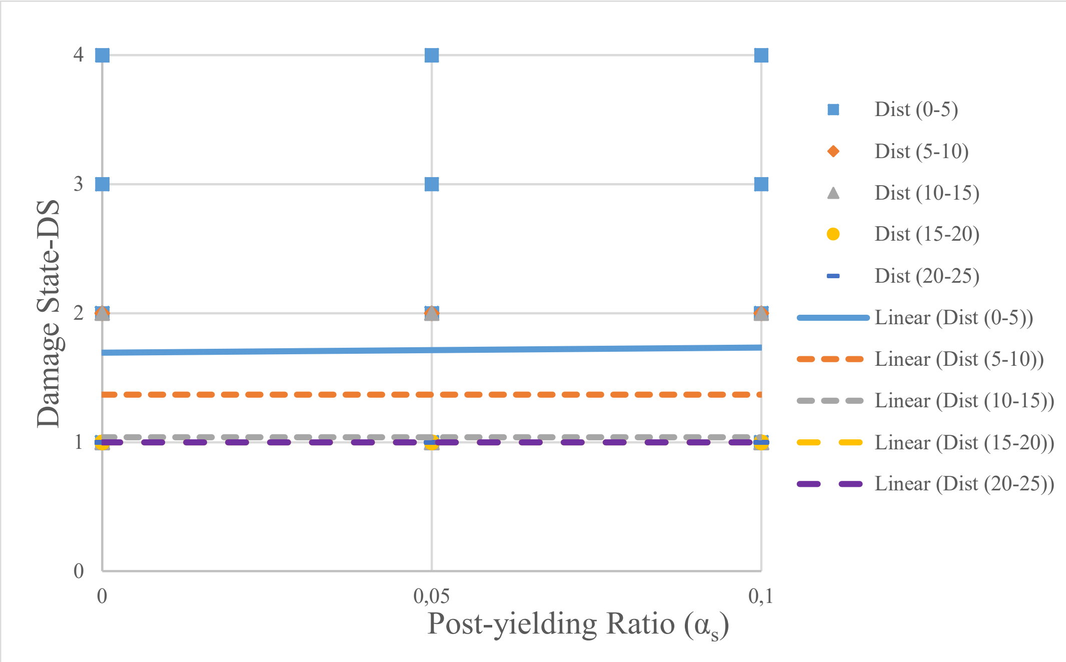

Figure 4.25. Trendlines of R_{JB} intervals with α_s values in terms of DS for hard soil

Considering the trendlines in Figures 4.22-4.25, the following observations can be stated:

- The change in post-yielding ratio values is observed not to be sensitive to DS for all magnitudes and R_{JB} distance intervals.
- DS slightly tends to decrease with α_s values by shifting from soft soil to hard soil conditions.

The fifth parameter to be investigated is the post-capping ratio (α_r), with 3 discrete values, i.e. α_r=-0.4, -0.3 and -0.2. The other structural parameters have the following constant values: T=0.2 sec, η=0.5, μ=3.0, α_s=0.05, λ=0.2 and γ=400. The linear trendlines of the DS versus α_r relationship for different values of magnitude and R_{JB} in soft and hard soil conditions are shown in Figures 4.26-4.29.

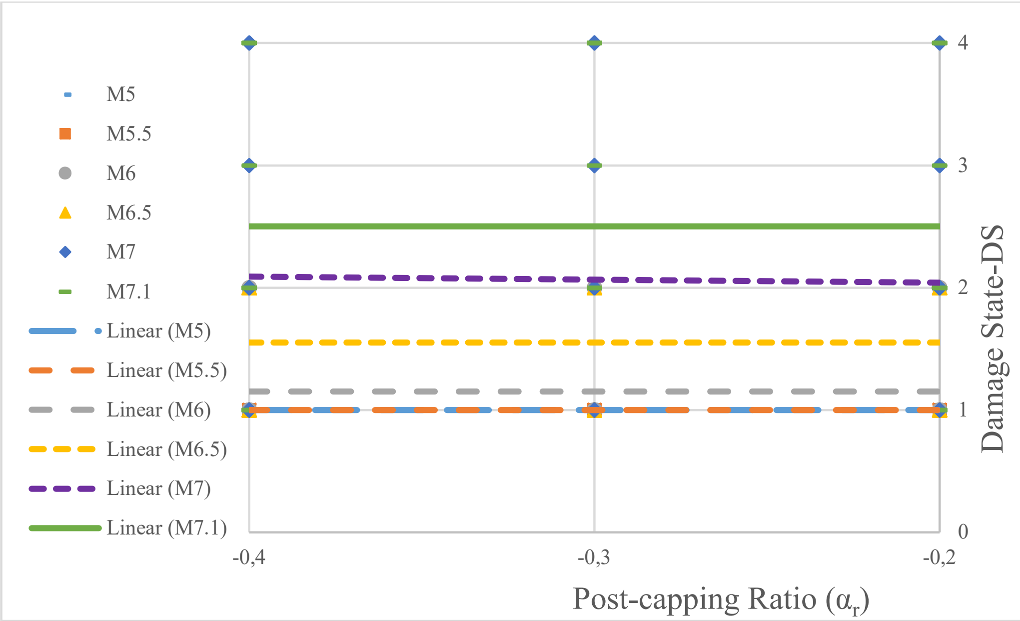

Figure 4.26. Trendlines of each magnitude with α_r values in terms of DS for soft soil

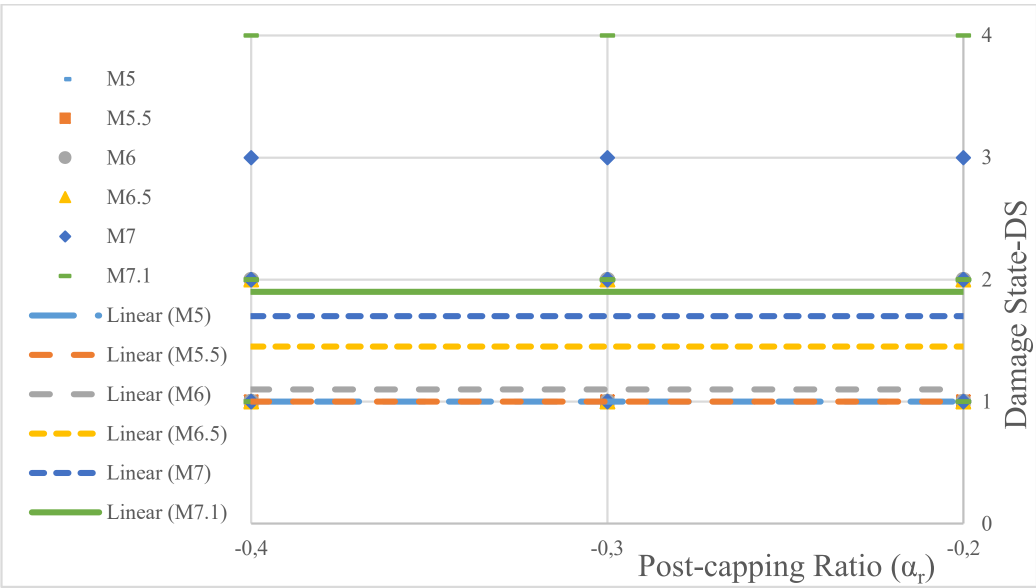

Figure 4.27. Trendlines of each magnitude with α_r values in terms of DS for hard soil

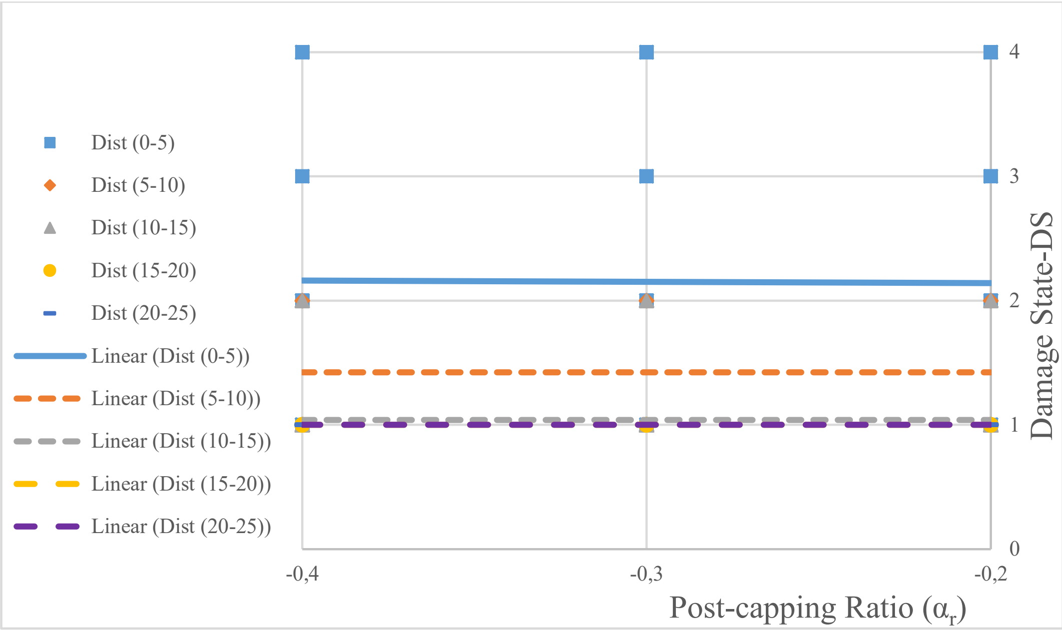

Figure 4.28. Trendlines of R_{JB} intervals with α_r values in terms of DS for soft soil

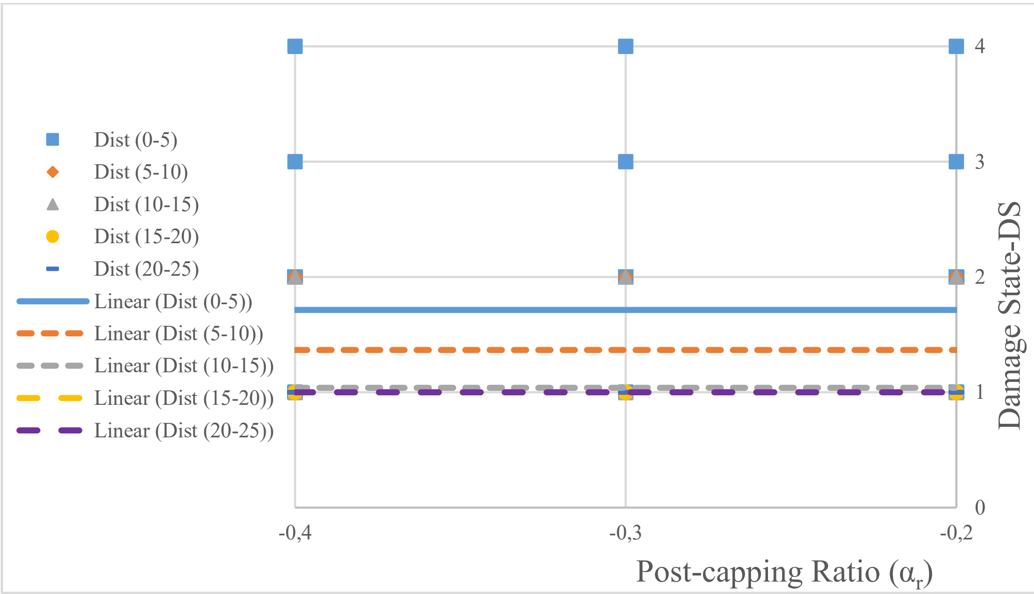

Figure 4.29. Trendlines of R_{JB} intervals with α_r values in terms of DS for hard soil

Considering the trendlines in Figures 4.26-4.29, the following observations can be stated:

- The change in post-capping ratio is observed not to be sensitive to DS for all of the magnitudes and R_{JB} distance intervals.
- DS has a slight tendency to decrease with α_r values by shifting from soft soil to hard soil conditions.

The sixth parameter to be investigated is the residual strength ratio (λ) with 3 discrete values, i.e. λ=0.0, 0.2 and 0.4. The other structural parameters have the following constant values: T=0.2 sec, η=0.5, μ=3.0, α_s=0.05, α_r=-0.3, γ=400. The linear trendlines of the DS versus λ relationship for different values of magnitude and R_{JB} in soft and hard soil conditions are shown in Figures 4.30-4.33.

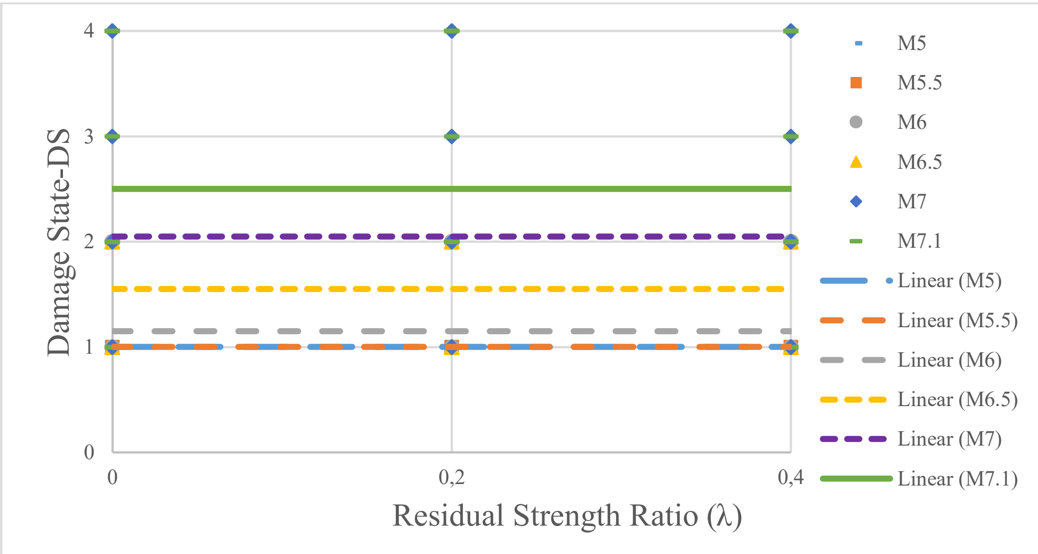

Figure 4.30. Trendlines of each magnitude with λ values in terms of DS for soft soil

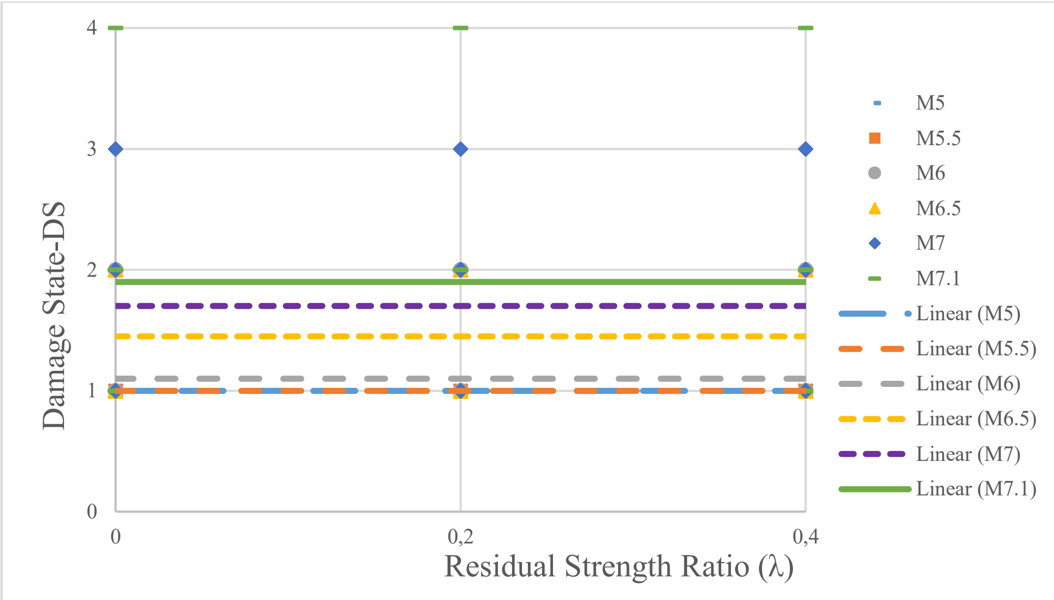

Figure 4.31. Trendlines of each magnitude with λ values in terms of DS for hard soil

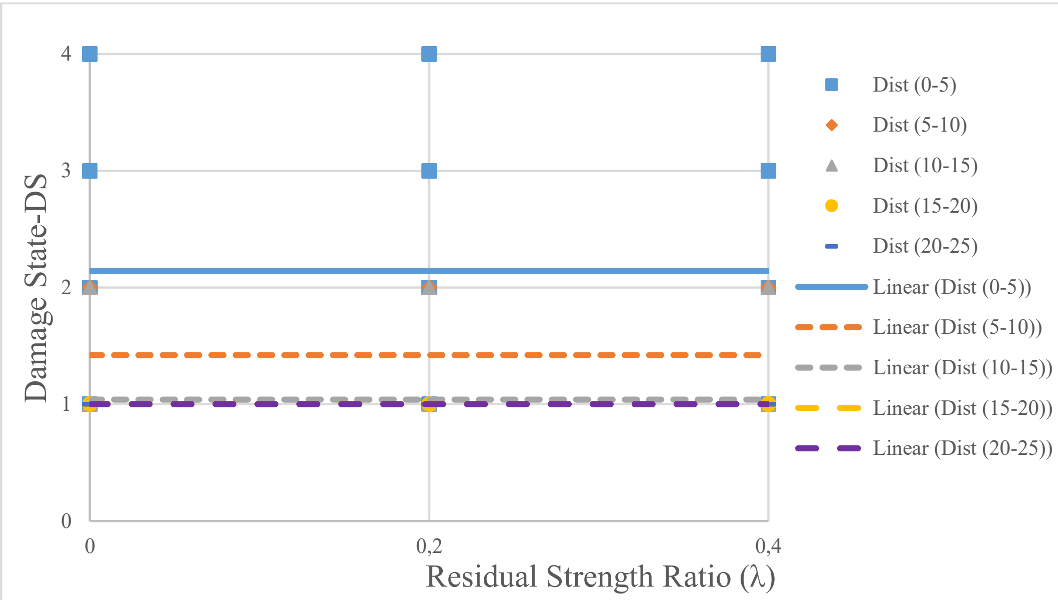

Figure 4.32. Trendlines of R_{JB} intervals with λ values in terms of DS for soft soil

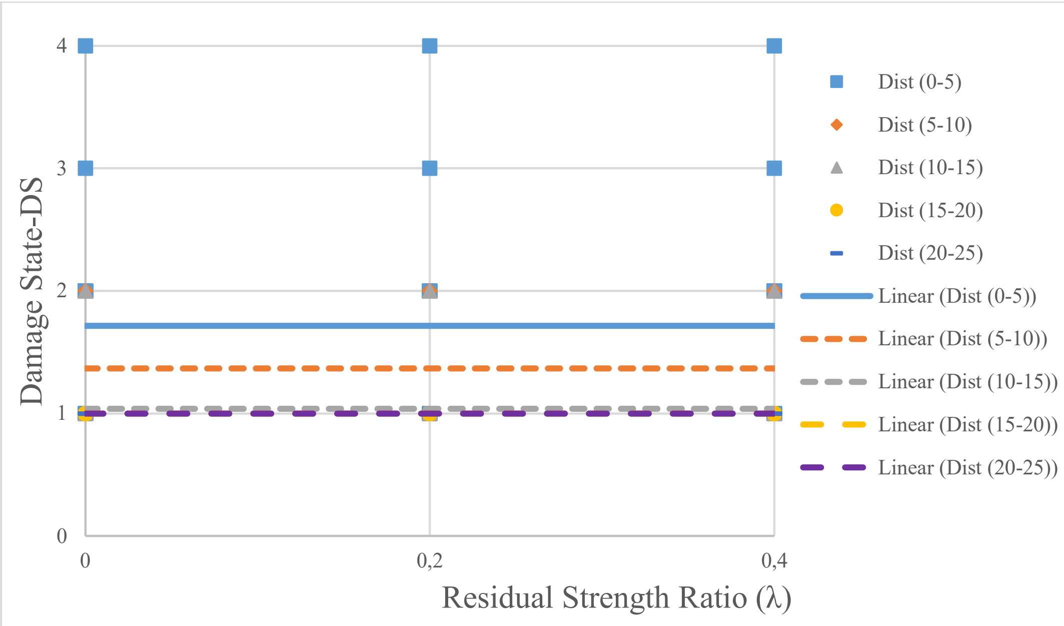

Figure 4.33. Trendlines of R_{JB} intervals with λ values in terms of DS for hard soil

Considering the trendlines in Figures 4.30-4.33, the following observations can be stated:

- The change in residual strength ratio is absolutely not sensitive to DS for all magnitudes and R_{JB} distance intervals.
- DS has a slight tendency to decrease with λ values by shifting from soft soil to hard soil conditions.

The seventh and the last parameter to be investigated is the degradation parameter (γ) with 3 discrete values, i.e. γ=200, 400 and 800. The other structural parameters have the following constant values: T=0.2 sec, η=0.5, μ=3.0, α_s=0.05, α_r=-0.3, λ=0.2. The linear trendlines of the DS versus γ relationship for different values of magnitude and R_{JB} in soft and hard soil conditions are shown in Figures 4.34-4.37.

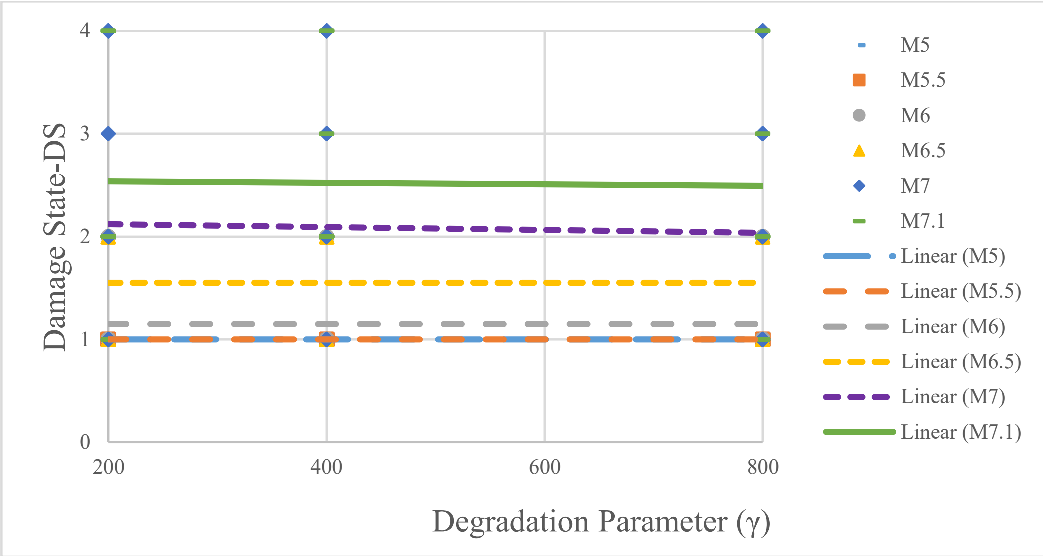

Figure 4.34. Trendlines of each magnitude with γ values in terms of DS for soft soil

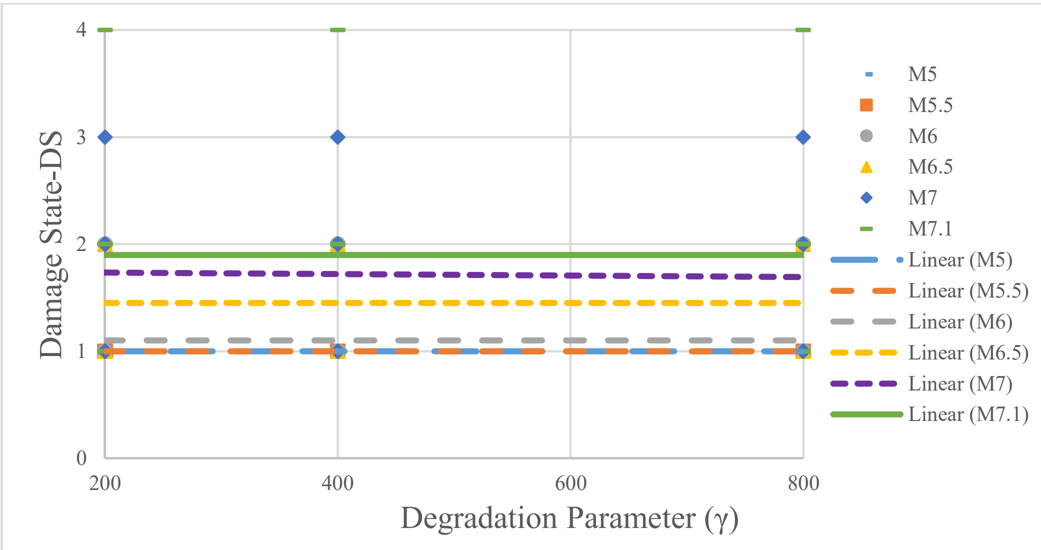

Figure 4.35. Trendlines of each magnitude with γ values in terms of DS for hard soil

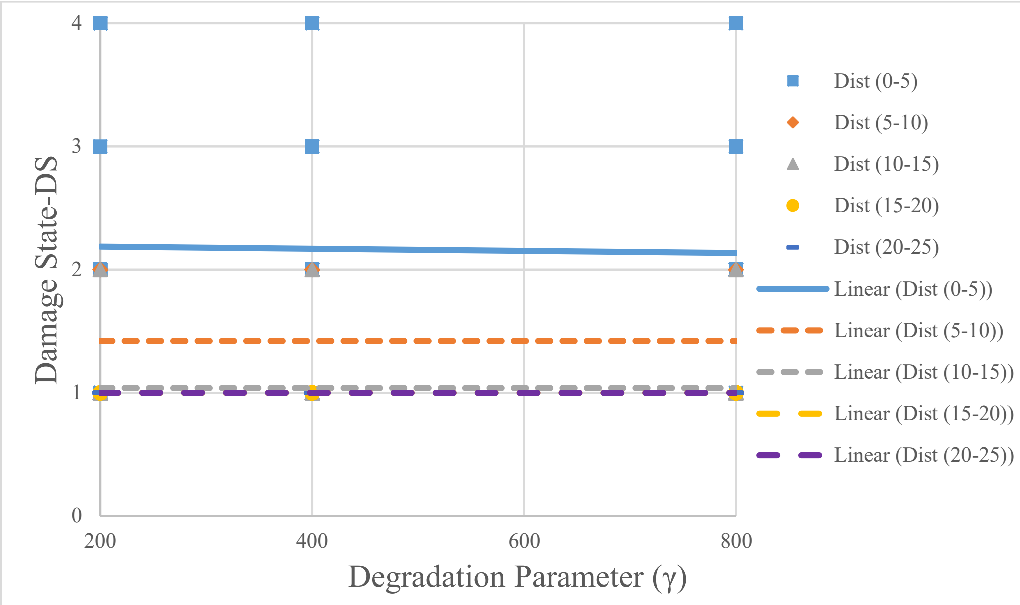

Figure 4.36. Trendlines of R_{JB} intervals with γ values in terms of DS for soft soil

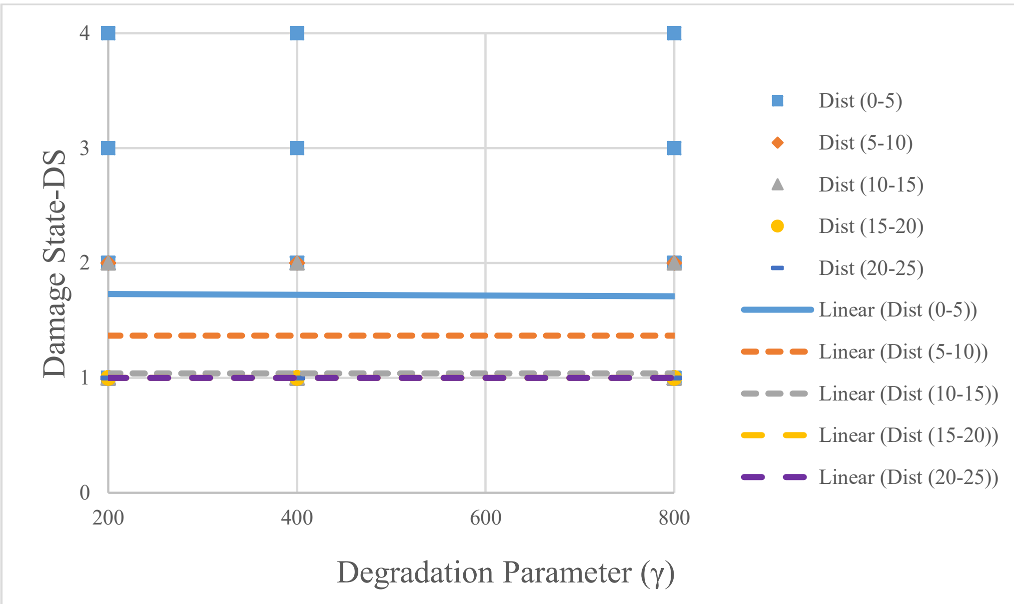

Figure 4.37. Trendlines of R_{JB} intervals with γ values in terms of DS for hard soil

Considering the trendlines in Figures 4.34-4.37, the following observations can be stated:

- The change in degradation parameter is found to be not sensitive to DS for all magnitudes and R_{JB} distance intervals.
- DS generally becomes constant with varying γ values for all of the magnitudes and R_{JB} distance intervals.
- DS has a slight tendency to decrease with γ values by shifting from soft soil to hard soil conditions.

4.4. Estimation of the Damage State Probabilities

Determination of the damage state probabilities for the URM buildings models in terms of PGA and magnitude for soft and hard soil conditions is the last study in this chapter. In Karimzadeh et al. (2018), the assessment of performance level of structures was carried out with using the target limit states, which were identified by determining the displacement capacity of the equivalent SDOF models. With this approach, the conditional probability of exceeding the predefined LS can be generated by determining the probabilities of being in a damage state at a predetermined PGA or magnitude value in accordance with the relationship between LS and DS in Table 4.1. To demonstrate the changes of DS with the PGA and magnitude values, the probability density function (PDF) for each damage state is generated by using the normal distribution function and it is calculated with the mean and standard deviation of the PGA and magnitude values for the performance level of interest. In this study, the log-normal distributions of DS, which are constituted with fitting them to each node of normal distributions of DS in a grid network, are employed to represent all of the probabilistic meaning of DS with merely changing in positive PGA and magnitude values.

Figures 4.38-4.41 are related to soft soil conditions with PGA values ranging from 0.1g to 1.0g and magnitude values from M_w5.0 to M_w7.1. The curves as represented in Figure 4.39 and 4.41 represent the probability of exceedance values of LS of interest at each ground motion intensity level.

As shown in Figure 4.38, the occurrence probabilities of DS-1, DS-2, DS-3 and DS-4 are highly observed between 0.1g and 0.2g, 0.3g and 0.4g, 0.4g and 0.5g, 0.5g and 0.6g, respectively. This shows that the mean PGA value of being in a damage state is increasing while DS is shifting from 1 to 4 as expected.

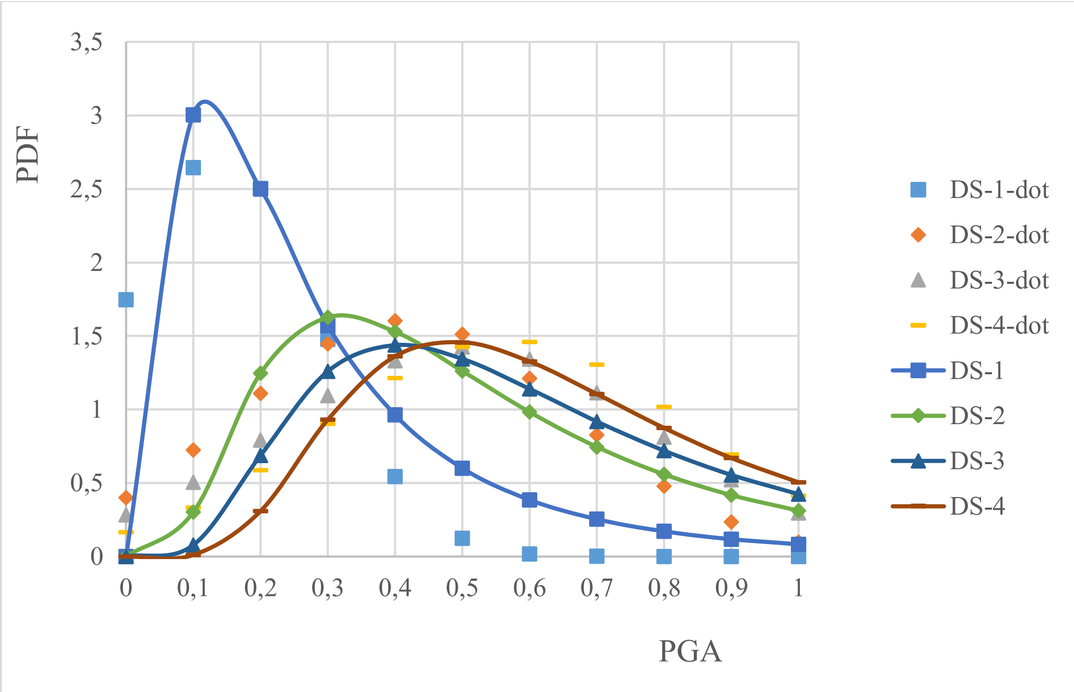

Figure 4.38. PDF of the log-normal distributions of DS with changing PGA values for soft soil conditions

In Figure 4.39, the LS curve is obtained by calculating the number of incidents that exceed the corresponding DS that is normalized by the total number of incidents for each ground motion intensity. Then, this is repeated for all LS to yield a set of curves. From the figure it is observed that LS-2 and LS-3 are very close to each other so that they can be treated as a single LS. This is expected since masonry structures have limited ductility and a narrow margin of safety between the first inelastic action and the collapse state.

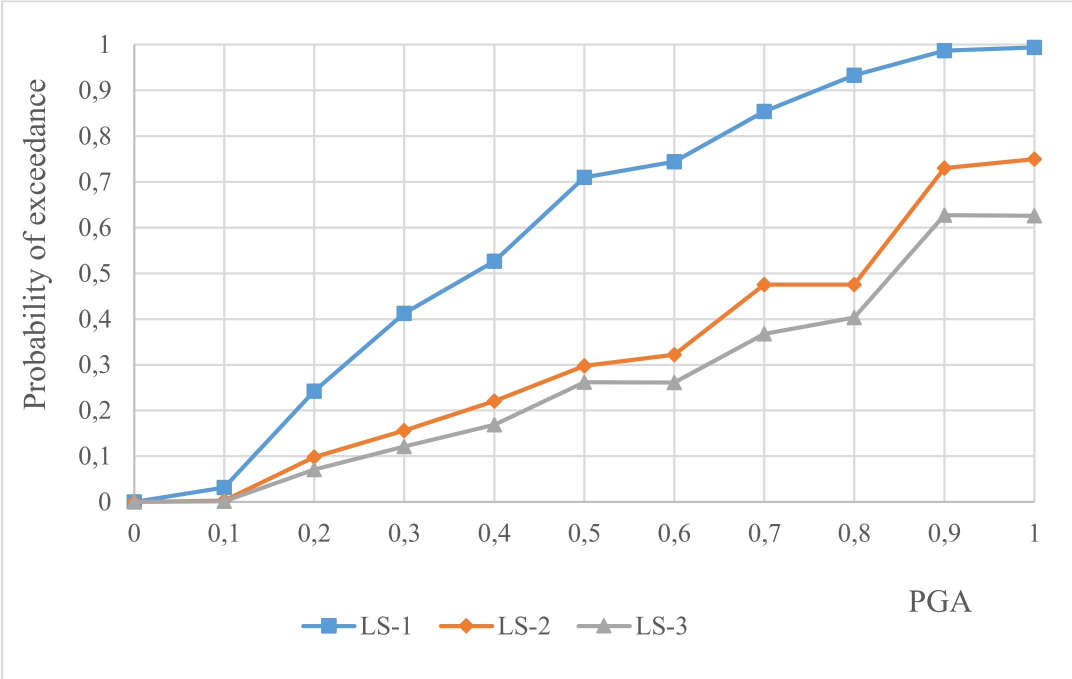

Figure 4.39. The generation of LS boundaries with PGA values for soft soil conditions

Figure 4.40 presents the probability distributions of each DS this time for magnitude. Since the data is only valid for 6 discrete magnitude values, it is not possible to obtain good fits for this case. The trends reveal that masonry structures are expected to be in DS-1 for earthquakes with magnitude of 5.5-6.0 whereas they are expected to be in DS-4 for earthquakes with magnitude close to 7.0. In between, DS-2 and DS-3 seem to be close to each other with characteristic magnitude between 6.5 and 7.0.

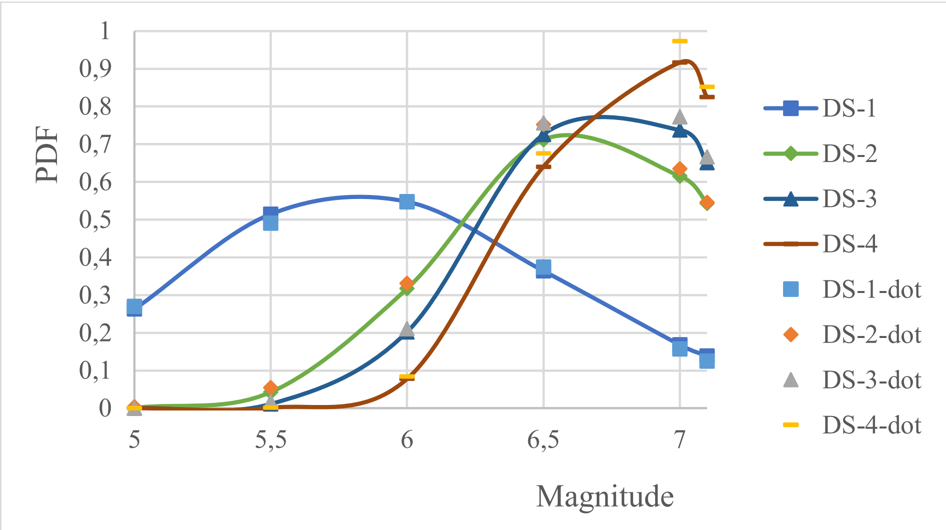

Figure 4.40. PDF of the log-normal distributions of DS with changing magnitude values for soft soil conditions

Figure 4.41 gives the probabilities of exceeding each LS for discrete values of magnitude, just like it has been carried out for PGA. There is a similar trend in which LS-2 and LS-3 are close to each other again as expected.

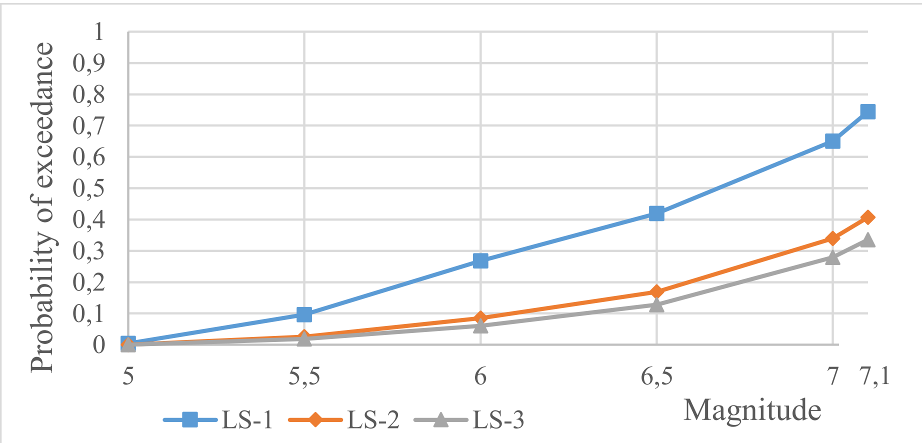

Figure 4.41. The generation of LS boundaries with magnitude values for soft soil conditions

Figures 4.42-4.45 show the similar plots related to hard soil conditions, which consist of PGA values ranging from 0.1g to 0.8g and magnitude values from M_w5.0 to M_w7.1.

As shown in Figure 4.42, the probability of DS-1, DS-2, DS-3 and DS-4 are highly observed between 0.1g and 0.2g, 0.2g and 0.3g, 0.2g and 0.3g, 0.3g and 0.4g, respectively.

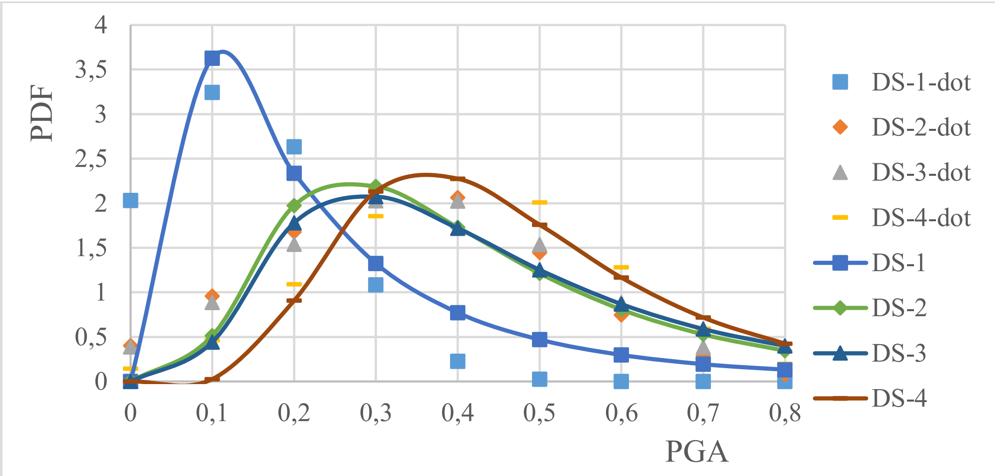

Figure 4.42. PDF of the log-normal distributions of DS with changing PGA values for hard soil conditions

It should be pointed out that the second and third limit state have a tendency to be constant between 0.7g and 0.8g owing to the existence of fewer data of DS between 0.7g and 0.8g as seen in Figure 4.43.

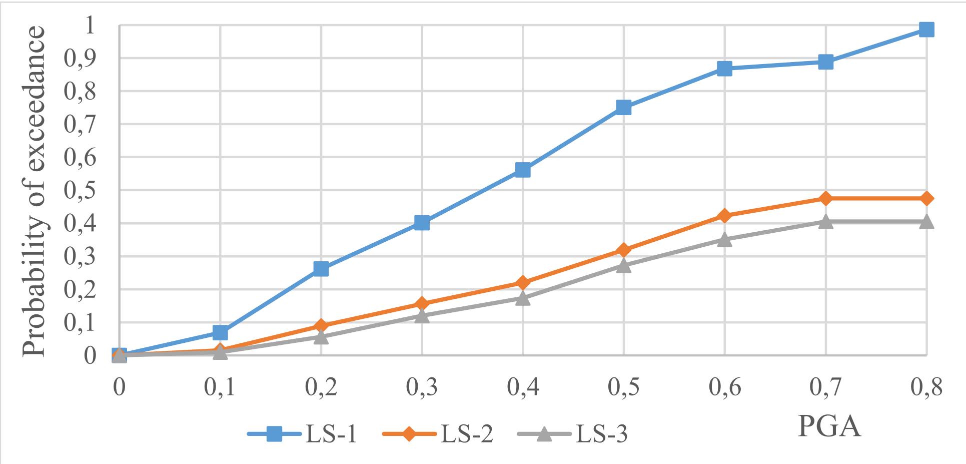

Figure 4.43. The generation of LS boundaries with PGA values for hard soil conditions

As shown in Figure 4.44, DS-1 is obtained with M_w5.0, DS-2 and DS-3 with M_w5.5 and DS-4 with M_w6.0. Considering Figure 4.45, once again it can be stated that the performance assessment of the URM structures can be carried out with two distinct limit states considering all cases of ground motion intensity measures.

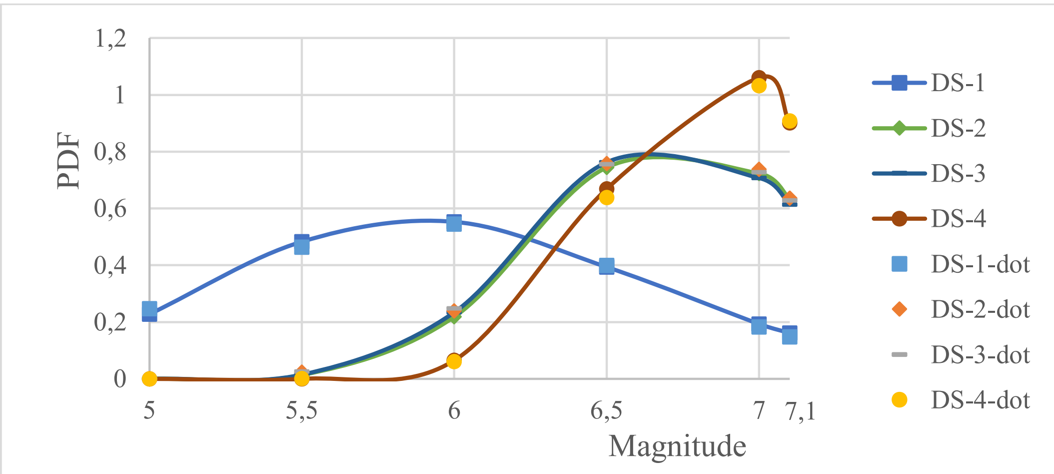

Figure 4.44. PDF of the log-normal distributions of DS with changing magnitude values for hard soil conditions

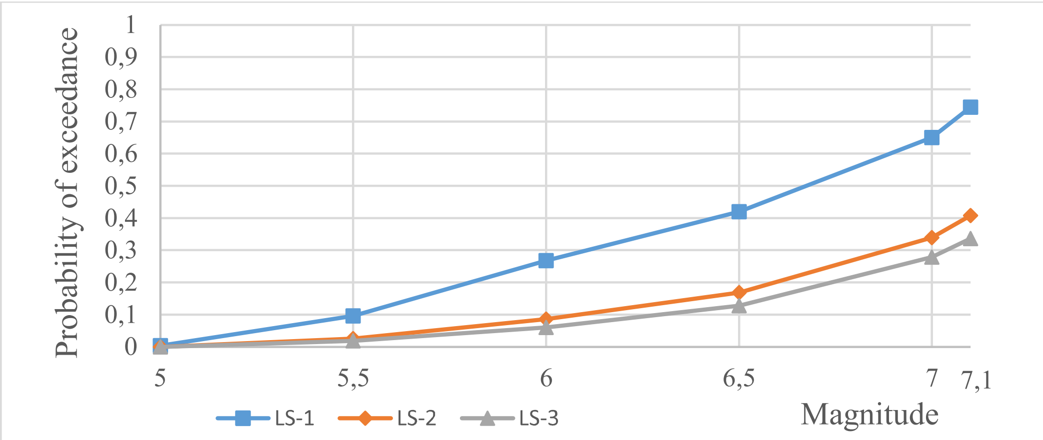

Figure 4.45. The generation of LS boundaries with magnitude values for hard soil conditions

4.5. Comparisons of the Performance Levels for Structural Combinations

Comparing the probability of exceedance curves for each LS in terms of PGA values for soft and hard soil conditions as shown in Figure 4.46, the following outcomes can be stated:

- The influence of soil conditions on the probability exceedance of the LS of interest does not seem to be significant with changing PGA. It should also be noted that different quantities of data at the same PGA value for both site conditions lead to the undesired trend in the interval of 0.7g and 0.8g.
- The recorded maximum PGA value is observed as 1.0g in soft soil conditions while reducing to 0.8g in hard soil conditions.

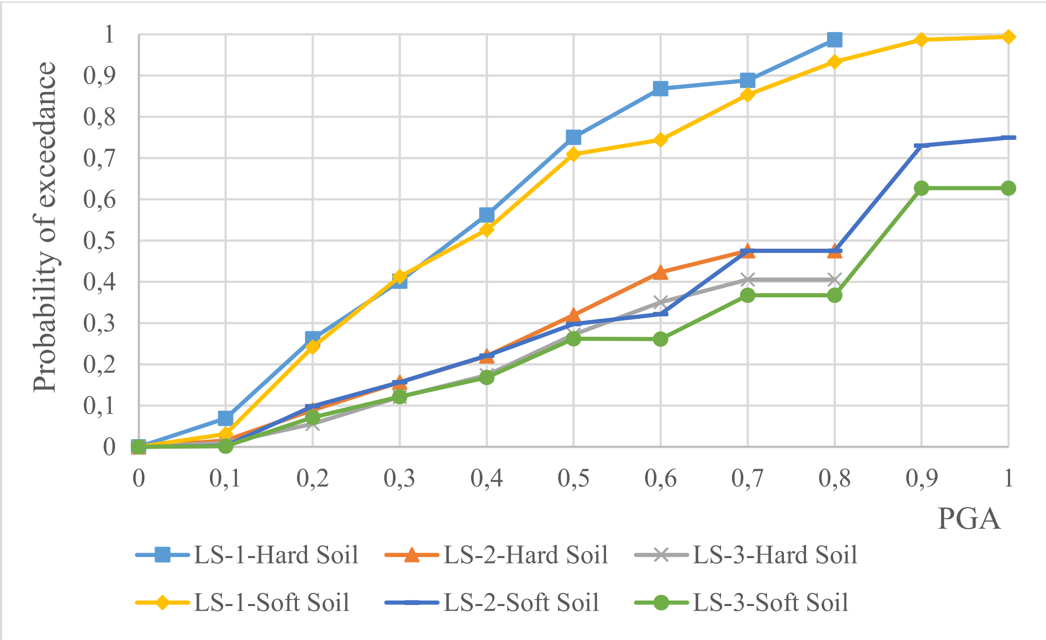

Figure 4.46. Comparison of LS with changing PGA values for both soil conditions

Comparing the same probability of exceedance curves with changing magnitude values for soft and hard soil conditions as shown in Figure 4.47, the following results can be stated:

- Considering the influence of soil conditions on the performance levels of structural simulations, it can be stated that except a slight difference for LS-1 the probabilities of other LS are nearly similar for both site conditions. Furthermore, the probability of exceedance of all boundaries of LS with changing the magnitude values in hard soil conditions has a tendency to reduce when compared with the case of soft soil conditions.
- Masonry models are slightly more vulnerable to simulated ground motions in soft soil conditions for all LS, especially for higher magnitudes. The differences seem to be at most 10% for magnitude value of 7.0.

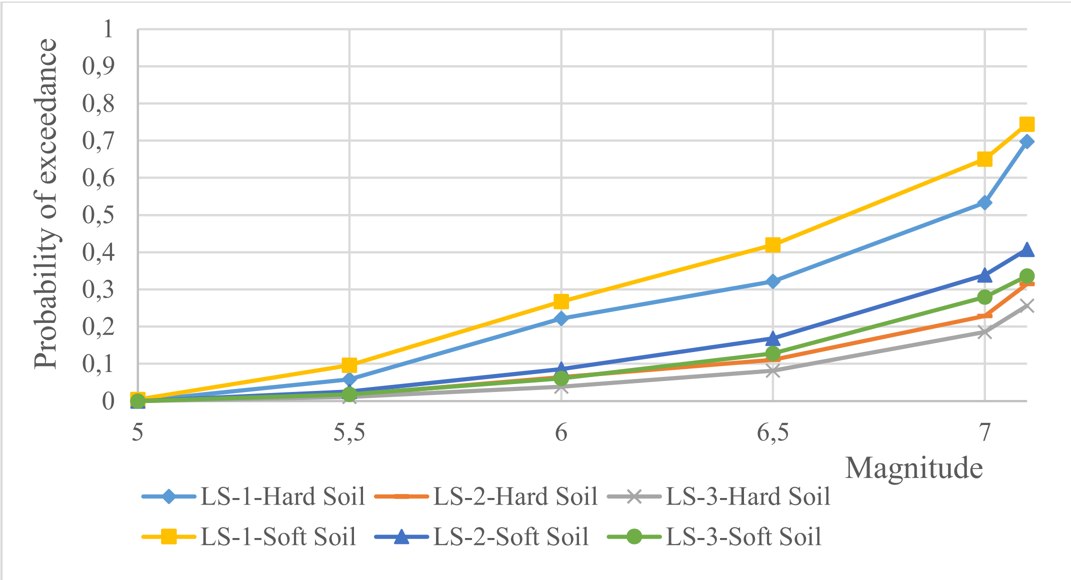

Figure 4.47. Comparison of LS with changing magnitude values for both soil conditions

CHAPTER 5

STATISTICAL EVALUATION OF SEISMIC PERFORMANCE OF URM STRUCTURES

There are various statistical methods to collect and analyze numerical data in large quantities as demonstrated in Table 5.1. In this study, three statistical methods are selected among them to conduct statistical assessment of seismic performance of URM buildings. The selected methods are discriminant analysis, multiple regression analysis and principal component analysis. Discriminant analysis is more appropriate to determine effective independent variables on DS since the dependent variable is categorical in this study. Multiple regression analysis is employed to find out the best prediction for DS with the independent variables. Principal component analysis is also preferred to compare the influences of independent variables on DS by reducing the dimensionality of the data. The selected three statistical methods in this study approach to the results with the different ways and the purpose of these three statistical methods is to compare their suitability for this case study.

Table 5.1. *The model types of statistical analyses*

Descriptive Models	**Regression & Predictive Models**	**Classification Models**
Principal Component Analysis	Multiple Linear Regression	Support Vector Machine
Basic Statistics	Principal Component Regression	Linear Discriminant Analysis
Clustering	Partial Least Squares Regression	Partial Least Squares - Discriminant Analysis

The main purpose of this chapter is to determine the most effective seismological or structural parameters on damage state via these statistical methods. The relationships between the dependent variable (i.e. DS) and independent variables, consisting of the seismological and structural parameters, are investigated by discriminant and multiple regression analyses. Finally, principal component analysis is employed to examine the relationships between each group of damage state and independent variables of interest.

In this study, the linear combination in an equation, which is a combination of several variables such that no variable is multiplied by either itself or another, is employed to represent the relationships between DS and independent variables by conceptualizing them in a simple way and conducting the calculations readily. Besides, a large amount of data as 2.430.000 distinct seismic responses in terms of displacement obtained after nonlinear dynamic analyses can be expressed with the statistical tools by using the linear combination in order to explain the influences of each independent variable on DS in a simple manner.

5.1. Discriminant Analysis

Discriminant analysis (DA) is a multivariate technique to classify the relative weights of independent variables between the groups of a case. This analysis enables to obtain a discriminant relationship between dependent and independent variables as given in Equation 5.1, which is a linear combination of independent variables to define a dependent variable:

$$Z_i = W_1X_1 + W_2X_2 + \ldots\ldots + W_nX_n \tag{5.1}$$

where Z_i is the score of discriminant relationship i, W_n is the discriminant coefficient of independent variable n, and X_n is the n^{th} independent variable.

In this study, DA is employed to obtain the independent variables that discriminate DS successfully or that are the most effective on DS. The independent variables consist of seismological parameters, which are magnitude, soil condition and R_{JB} distance, and the structural parameters, namely period, strength ratio, ductility ratio, post-yielding ratio, post-capping ratio, residual strength ratio and hysteresis model degradation parameter. Discrete performance values of the independent variables for each ESDOF model are used in the SPSS software, which enables to analyze big datasets and run statistical tests. DA fundamentally identifies a discriminant relationship to determine the most effective parameter on a dependent variable. The statistical significance of the analysis depends on two parameters, termed as the eigenvalue (λ_e) and Wilks' lambda (Λ). According to Bruin (2006), the eigenvalue and Wilks' lambda can be estimated with the canonical correlation (cc), which are used to identify and measure the associations between the independent parameters and DS as follows:

$$\lambda_e = (cc)^2 / (1-(cc)^2) \tag{5.2}$$

$$\Lambda = 1- (cc)^2 \tag{5.3}$$

The eigenvalue with a canonical correlation value closer to 1.0 represents the best discriminant relationship of DS with the independent variables. In other words, a large eigenvalue is considered as an indicator of a strong relationship.

The Wilks' lambda, which takes a value between 0.0 and 1.0, becomes acceptable when it takes a smaller value and close to 0.0 for a strong discriminant relationship. The significance value also contributes to determine whether the difference between the groups is significant or not. The results of the DA are presented in Tables 5.2-5.5.

According to Table 5.2, three reasonable discriminant relationships are obtained. The first relationship should be selected as its eigenvalue is greater than 1.0 and the canonical correlation of the eigenvalue at the first relationship is the closest to 1.0. It is also observed that the first relationship has a 96.7% of the discriminating ability as far as three continuous discriminant relationships are considered. Dividing the eigenvalue of the relationship to the sum of all eigenvalues determines the percentage of variance.

Table 5.2. *Eigenvalues of the discriminant relationship*

Relationship of DS	Eigenvalue	% of Variance	Cumulative %	Canonical Correlation
1	1.299	96.7	96.7	0.752
2	.036	2.7	99.4	0.188
3	.008	0.6	100.0	0.087

Since the significance of the relationships obtained from the chi-square test, which is carried out to determine the discriminating ability of the relationships, is equal to 0.0, all of these three relationships extracted in the DA seem to be reasonable to interpret the relationships of the dependent variable (i.e. DS). However, one of them has the most accurate relationship when Wilks' lambda values are compared as given in Table 5.3. Accordingly, the first damage state relationship for the structural simulations seems more suitable than others.

Table 5.3. *Wilks' lambda values of the discriminant relationships*

Test of Relationship(s)	Wilks' Lambda	Chi-square	df	Significance
1 through 3	0.417	2128298.682	30	0.000
2 through 3	0.958	105484.680	18	0.000
3	0.992	18462.286	8	0.000

The following discriminant relationship of DS is obtained from Table 5.4.

$$Z = -0.687M_w + 0.141S + 0.513R_{JB} + 0.105T + 0.812\eta + 0.027\mu + 0.001\alpha_s + 0.003\alpha_r - 0.015\lambda + 0.006\gamma \quad (5.4)$$

Table 5.4. *Coefficients of the independent variables for each relationship*

	Relationship 1	Relationship 2	Relationship 3
Magnitude (M_w)	-.687	.367	-.100
Soil (S)	.141	.126	-.046
Distance (R_{JB})	.513	-.081	-.017
Period (T)	.105	.632	.452
Strength Ratio (η)	.812	.444	-.133
Ductility Ratio (μ)	.027	.320	-.683
Post-yielding Ratio (α_s)	.001	.111	.171
Post-capping Ratio (α_r)	.003	.057	.488
Residual Strength Ratio (λ)	-.015	-.089	-.139
Degradation Parameter (γ)	.006	.033	.071

where M_w, S, R_{JB}, T, η, μ, α_s, α_r, λ and γ stand for magnitude, soil condition, Joyner and Boore distance, period, strength ratio, ductility ratio, post-yielding ratio, post-capping ratio, residual strength ratio and degradation parameter, respectively.

Considering Equation 5.4, it is observed that the strength ratio, magnitude of the earthquake and source-to-site distance are the most effective parameters for the URM structures, respectively.

Period is also known as an important structural parameter for the identification of seismic behavior during an earthquake excitation. However, the strength ratio of URM structures seems to dominate its influence in this study. The influences of other structural parameters, namely ductility, residual strength ratio, post-yielding ratio, post-capping ratio and hysteresis model degradation parameter do not appear significant for the URM structures.

According to Table 5.5, 77.5% of DS-1 is correctly classified, whereas this percentage is 56.3%, 53.6% and 68.2% for DS-2, DS-3 and DS-4, respectively. Totally, 71.7% of original grouped cases is correctly classified. It is observed that the DS-1 and DS-4 are better classified due to their more certain nature as compared to the intermediate damage states.

Table 5.5. *Classification of the results between the groups of DS*

		DS	Predicted Group Membership 1.00	2.00	3.00	4.00	Total
	Count	1.00	1252896	269369	72578	22220	1617063
		2.00	20975	256936	120661	57867	456439
		3.00	0	17454	39878	17000	74332
		4.00	2	22010	67618	192536	282166
	%	1.00	77.5	16.7	4.5	1.4	100.0
		2.00	4.6	56.3	26.4	12.7	100.0
		3.00	0.0	23.5	53.6	22.9	100.0
		4.00	0.0	7.8	24.0	68.2	100.0

5.2. Multiple Regression Analysis

Multiple regression analysis (MRA) is used to predict the value of a dependent variable based on the values of two or more independent variables. This method is the most common form of simple linear regression. MRA also enables to determine the overall fit of the model and the relative contribution of each of the predictors to the total variance.

The multiple regression relationship as given in Equation 5.5 is similar to the discriminant relationship in terms of the dependent variable, which is identical for both analyses. The main difference among them can be stated that MRA relies on a continuous dependent variable whereas DA relates to a discrete dependent variable along with classifying objects into groups.

$$Y = a + c_1K_1 + \ldots\ldots + c_nK_n \tag{5.5}$$

In Equation 5.5, Y is a predictive value of the dependent variable, c_n is the coefficient of the n^{th} independent variable, K_n is value of the n^{th} independent variable and a is a constant.

In this study, MRA is carried out to construct linear relationships between the dependent variable and the independent variables via the SPSS software. The results of MRA are presented in Tables 5.6-5.8.

In Table 5.6, R (multiple correlation coefficient) is a measure of the strength of the relationship between the independent variables and the dependent variables. The term R^2 is a measurement of the variability in the dependent variable due to the independent variables in the model. The adjusted R-square is another version of R-square which is modified for the number of independent variables in the model. The adjusted R-square increases only if a new predictor improves the model. Its best value it attained when it is closer or equal to the R-square value.

Next, Durbin-Watson statistics, ranging between 0.0 and 4.0, is employed to determine whether an autocorrelation exists or not in the error of the independent variables. If the range of Durbin-Watson is between 1.5 and 2.5, it means there is no autocorrelation. If it is less than 1.5, a positive autocorrelation can be predicted in the error terms. If it is higher than 2.5, a negative autocorrelation can be expected in the error terms. In this study, the value of Durbin-Watson is obtained as 1.002, which is potentially consistent with the nonlinear structural analyses conducted in this study.

Table 5.6. *Model summary of MRA*

Model	R	R Square	Adjusted R Square	Std. Error of the Estimate	Durbin-Watson
1	0.721[a]	0.520	0.520	0.69251	1.002

Table 5.7 provides information about the model significance via F test when R Square is equal to 0.0. The sum of squares from regression ($SS_{regression}$) and the sum of squares from residual ($SS_{residual}$) are given as follows:

$$SS_{regression} = \sum (Y_{fit} - Y\hat{})^2 \quad (5.6)$$

$$SS_{residual} = \sum (Y - Y_{fit})^2 \quad (5.7)$$

where Y^ is the mean of the dependent variable, Y_{fit} is the value of the dependent variable of the fitted model and Y is the value of the dependent variable. The test statistic (F) is calculated as follows:

$$F = \frac{((SS_{regression}(\text{full model}) - SS_{regression}(\text{reduced model}))/df}{\text{mean square of residual (full model)}} \quad (5.8)$$

where df is the number of degrees of freedom for the regression, the $df_{regression}$ is the total number of the independent variables in an MRA and the $df_{residual}$ is obtained with the $df_{regression}$-1. Considering Table 5.7, the regression model of MRA seems reasonable as the significance value is equal to 0.0.

Table 5.7. *ANOVA in MRA*

Model		Sum of Squares	df	Mean Square	F	Significance
1	Regression	1260760.962	10	126076.096	262891.299	.000[b]
	Residual	1165361.987	2429989	0.480		
	Total	2426122.949	2429999			

The unstandardized coefficients and the standardized coefficients of the independent variables are presented in Table 5.8. Both of them can be employed to predict linear relationship between the dependent and independent variables.

Table 5.8. *Coefficients of the independent variables in MRA*

Model		Unstandardized Coefficients		Standardized Coefficients	t	Significance
		B	Std. Error	Beta		
1	(Constant)	0.316	0.005		58.254	0.000
	Magnitude (M_w)	0.474	0.001	0.363	731.681	0.000
	Soil Type (S)	-0.148	0.001	-0.074	-166.588	0.000
	Distance (R_{JB})	-0.039	0.000	-0.271	-546.071	0.000
	Period (T)	-0.653	0.003	-0.084	-188.148	0.000
	Strength Ratio (η)	-1.632	0.002	-0.462	-1038.870	0.000
	Ductility Ratio (μ)	-0.044	0.001	-0.031	-70.814	0.000
	Post-yielding Ratio (α_s)	-0.146	0.011	-0.006	-13.390	0.000
	Post-capping Ratio (α_r)	-0.041	0.005	-0.003	-7.448	0.000
	Residual Strength Ratio (λ)	0.072	0.003	0.012	26.623	0.000
	Degradation Parameter (γ)	-1.783E-05	0.000	-0.004	-10.010	0.000

The multiple regression relationship as given in Equation 5.9 is generated to obtain the value of the dependent variable of interest by using the unstandardized coefficients.

$$Y' = 0.316 + 0.474M_w - 0.148S - 0.039R_{JB} - 0.653T - 1.632\eta - 0.044\mu - 0.146\alpha_s - 0.041\alpha_r + 0.072\lambda - 0.0000178\gamma \quad (5.9)$$

Strength ratio, magnitude of the earthquake, and source-to-distance are observed to be the first three dominant parameters for the damage states of URM buildings considering the standardized coefficients of the independent variables in MRA. The discrete values of soil conditions in the statistical analyses are used as “1” for soft soil condition, “2” for hard soil condition. Furthermore, 52% of the discrete performance values of the independent variables precisely participate in MRA to express their relationship with DS. As the participation rate of the independent variable to MRA is lower, the discriminant relationship as stated in Equation 5.4 with classification rate as 71.7% seems more reliable to obtain relationships between damage states and the independent variables in this study.

5.3. Principal Component Analysis

Principal component analysis (PCA) focuses on reducing a large set of independent variables into a smaller number of factors. PCA is also known as the factor analysis. The purpose of PCA is to generate a linear combination between the independent variables by extracting the maximum variance from them.

In this study, PCA is carried out to determine which independent variables are the most effective on each group of the DS. The following Tables 5.9-5.13 are presented to explain the correlation between the independent variables for DS-1.

A correlation matrix, which is symmetric, contains the covariances between all possible pairs of variables in the dataset.

Table 5.9. *The correlation Matrix for DS-1*

	M_w	S	R_{JB}	T	η	μ	α_s	α_r	λ	γ
M_w	1.000	.040	-.258	.003	.275	-.003	-.004	-.001	-.003	.001
S	.040	1.000	-.038	.015	-.009	.000	.000	.000	.001	.000
R_{JB}	-.258	-.038	1.000	-.012	-.185	.003	.003	.001	.003	-.001
T	.003	.015	-.012	1.000	-.017	.000	-.001	.000	.002	.001
η	.275	-.009	-.185	-.017	1.000	.003	.004	.001	.003	.000
μ	-.003	.000	.003	.000	.003	1.000	.000	.000	.001	.000
α_s	-.004	.000	.003	-.001	.004	.000	1.000	.000	.000	.000
α_r	-.001	.000	.001	.000	.001	.000	.000	1.000	.000	.000
λ	-.003	.001	.003	.002	.003	.001	.000	.000	1.000	.000
γ	.001	.000	-.001	.001	.000	.000	.000	.000	.000	1.000

a. Only cases for which DS = 1 are used in the analysis phase.

As the correlation between two variables can be influenced by the others, the partial correlation is utilized to identify the relationship between two variables. The Kaiser-Meyer-Olkin measure of sampling adequacy (KMO) index ranges between 0.0 and 1.0 to compare the correlation values between independent variables. If the KMO index approaches 1.0, it means that PCA is completed efficiently; however, if it approaches 0.0, PCA should be reviewed. In this study, the KMO index of DS-1 obtained in Table 5.10 as 0.592, which can be stated as critical for the correlation between the independent variables.

Bartlett's test of sphericity compares the observed correlation matrix with the identity matrix generated from all diagonal elements of the correlation matrix. It is also carried out to determine the overall significance of all correlations within a correlation matrix. In order to measure the overall correlation between the independent variables, the determinant of the correlation matrix is computed. To classify the independent variables as highly correlated, the determinant of the correlation matrix should approach 0.0. In Table 5.10, as the significance is equal to 0.0 via chi-square test, PCA for DS-1 is acceptable.

Table 5.10. *KMO and Bartlett's Test for DS-1*

Kaiser-Meyer-Olkin Measure of Sampling Adequacy.		0.592
Bartlett's Test of Sphericity	Approx. Chi-Square	269743.138
	df	36
	Significance	0.000

The communality explains the proportion of variance for each independent variable by looking at the extraction values of the independent variables. If the extraction values of the independent variables are close to 0.0, the independent variables are not well represented in PCA. According to the results of Table 5.11, the post-capping ratio and hysteresis model degradation parameter have the lower participation ratio for PCA in DS-1.

Table 5.11. *The communalities for DS-1*

	Initial	Extraction
Magnitude (M_w)	1.000	0.565
Soil (S)	1.000	0.507
Distance (R_{JB})	1.000	0.453
Period (T)	1.000	0.482
Strength Ratio (η)	1.000	0.497
Ductility Ratio (μ)	1.000	0.512
Post-yielding Ratio (α_s)	1.000	0.683
Post-capping Ratio (α_r)	1.000	0.170
Residual Strength Ratio (λ)	1.000	0.516
Degradation Parameter (γ)	1.000	0.122

In Table 5.12, the numbers of components represent the numbers of the independent variables of which the relationship with DS-1 is studied in PCA. The initial eigenvalues are the variances of the principal components. The first component has the highest eigenvalue owing to the presence of the highest variance. The extraction sum of squared loading explains the extracted components required to assess PCA by using the eigenvalue, which should be greater than 1.0. If the eigenvalue of the component is less than 1.0, the components are not extracted due to the low variance. In the study, four components are extracted to evaluate PCA for DS-1 with respect to the eigenvalues of the components.

Table 5.12. *The total variance of DS-1*

Component	Initial Eigenvalues			Extraction Sums of Squared Loadings		
	Total	% of Variance	Cumulative %	Total	% of Variance	Cumulative %
1	1.484	14.843	14.843	1.484	14.843	14.843
2	1.022	10.218	25.060	1.022	10.218	25.060
3	1.001	10.010	35.071	1.001	10.010	35.071
4	1.000	10.003	45.074	1.000	10.003	45.074
5	1.000	10.000	55.074			
6	1.000	9.998	65.072			
7	0.999	9.991	75.063			
8	0.984	9.836	84.899			
9	0.809	8.086	92.985			
10	0.701	7.015	100.000			

Considering the results of Table 5.13, coefficients of the first component enable to generate the principal component relationship of DS-1 with the independent variables of interest as given in Equation 5.10 due to the existence of the highest variance. The magnitude of the earthquake, strength ratio and source-to-site distance are dominant parameters for DS-1 for the URM structures. The first three important independent variables are similar to those obtained from the aforementioned statistical approaches because DS-1 is highly observed than other damage states as far as results of the nonlinear structural analyses are considered. It can be also said that the magnitude becomes the most effective parameter in the elastic range (i.e. DS-1):

$$\text{DS-1} = 0.751M_w + 0.680\eta - 0.668R_{JB} + 0.103S + 0.000T - 0.003\lambda - 0.004\mu - 0.001\alpha_r - 0.005\alpha_s + 0.003\gamma \qquad (5.10)$$

Table 5.13. *The component matrix of DS-1*

	Components			
	1	2	3	4
Magnitude (M_w)	0.751	0.000	-0.007	0.002
Strength Ratio (η)	0.680	-0.184	0.032	-0.006
Distance (R_{JB})	-0.668	-0.078	0.016	-0.002
Soil (S)	0.103	0.704	-0.001	-0.029
Period (T)	0.000	0.692	0.043	-0.026
Residual Strength Ratio (λ)	-0.003	0.031	0.702	-0.151
Ductility Ratio (μ)	-0.004	-0.036	0.553	0.454
Post-capping Ratio (α_r)	-0.001	-0.011	0.348	0.220
Post-yielding Ratio (α_s)	-0.005	-0.068	0.281	-0.774
Degradation Parameter (γ)	0.003	0.022	-0.007	0.349

Tables 5.14-5.18 are presented to explain the correlation between the independent variables for DS-2.

Table 5.14. *The correlation Matrix for DS-2*

	M_w	S	R_{JB}	T	η	μ	α_s	α_r	λ	γ
M_w	1.000	.076	-.292	.086	.528	.016	.002	-.003	-.008	.003
S	.076	1.000	-.043	-.061	-.072	-.008	.002	.000	.002	-.002
R_{JB}	-.292	-.043	1.000	-.022	-.575	-.012	-.001	.000	.006	-.001
T	.086	-.061	-.022	1.000	-.065	.001	-.009	.001	.008	.002
η	.528	-.072	-.575	-.065	1.000	-.039	-.008	.005	.012	-.004
μ	.016	-.008	-.012	.001	-.039	1.000	.002	.002	.002	.001
α_s	.002	.002	-.001	-.009	-.008	.002	1.000	-.001	.002	.000
α_r	-.003	.000	.000	.001	.005	.002	-.001	1.000	.002	.000
λ	-.008	.002	.006	.008	.012	.002	.002	.002	1.000	.001
γ	.003	-.002	-.001	.002	-.004	.001	.000	.000	.001	1.000

a. Only cases for which DS = 2 are used in the analysis phase.

In Table 5.15, the KMO index of DS-2 is obtained as 0.518, meaning that its value is less than the KMO index of DS-1, mostly because DS-2 is obtained less frequently than DS-1 according to results of the structural parametric analyses. PCA seems appropriate in accordance with the significance, which is equal to 0.0.

Table 5.15. *KMO and Bartlett's Test for DS-2*

Kaiser-Meyer-Olkin Measure of Sampling Adequacy.		0.518
Bartlett's Test of Sphericity	Approx. Chi-Square	370241.333
	df	45
	Significance	0.000

When Table 5.16 is examined, the post-yielding ratio has only a lower participation ratio than the other independent variables participating with extraction values greater than 0.50 to explain DS-2.

Table 5.16. *The communalities for DS-2*

	Initial	Extraction
Magnitude (M_w)	1.000	0.560
Soil (S)	1.000	0.539
Distance (R_{JB})	1.000	0.601
Period (T)	1.000	0.548
Strength Ratio (η)	1.000	0.794
Ductility Ratio (μ)	1.000	0.755
Post-yielding Ratio (α_s)	1.000	0.239
Post-capping Ratio (α_r)	1.000	0.613
Residual Strength Ratio (λ)	1.000	0.530
Degradation Parameter (γ)	1.000	0.836

In Table 5.17, five components are extracted to define the relationship of DS-2 in accordance with the eigenvalues of the components.

Table 5.17. *The total variance of DS-2*

Component	Initial Eigenvalues			Extraction Sums of Squared Loadings		
	Total	% of Variance	Cumulative %	Total	% of Variance	Cumulative %
1	1.941	19.406	19.406	1.941	19.406	19.406
2	1.064	10.640	30.046	1.064	10.640	30.046
3	1.006	10.063	40.109	1.006	10.063	40.109
4	1.002	10.015	50.124	1.002	10.015	50.124
5	1.000	10.003	60.127	1.000	10.003	60.127
6	1.000	9.996	70.124			
7	0.997	9.966	80.090			
8	0.980	9.802	89.891			
9	0.697	6.974	96.866			
10	0.313	3.134	100.000			

In Table 5.18, the coefficients of the first component represent the correlation between the independent variables due to the existence of the highest variance. Therefore, the strength ratio, source-to-site distance and magnitude of the earthquake are stated as dominant independent parameters in the relationship of DS-2 with the independent variables. As the URM structures are exposed to the strain hardening between LS-1 and LS-2, the strength ratio becomes the most effective parameter in this interval. The principal component relationship of DS-2 for the URM structures is given as follows:

$$DS\text{-}2 = 0.888\eta - 0.774R_{JB} + 0.743M_w + 0.023T + 0.025S - 0.015\mu - 0.006\alpha_s + 0.003\alpha_r + 0.001\lambda - 0.001\gamma \quad (5.11)$$

Table 5.18. *The component matrix of DS-2*

	Components				
	1	2	3	4	5
Strength Ratio (η)	0.888	0.002	-0.062	0.039	-0.019
Distance (R_{JB})	-0.774	0.033	-0.013	0.013	0.006
Magnitude (M_w)	0.743	0.033	0.068	-0.045	0.023
Period (T)	0.023	0.734	0.075	-0.045	0.028
Soil (S)	0.025	-0.702	0.177	0.010	0.119
Ductility Ratio (μ)	-0.015	0.093	0.739	-0.433	-0.109
Post-yielding Ratio (α_s)	-0.006	-0.113	0.386	-0.243	-0.134
Post-capping Ratio (α_r)	0.003	0.010	0.268	0.640	-0.362
Residual Strength Ratio (λ)	0.001	0.074	0.411	0.577	0.149
Degradation Parameter (γ)	-0.001	0.056	0.159	0.076	0.895

Tables 5.19-5.23 are presented to explain the correlation of the independent variables for DS-3.

Table 5.19. *The correlation Matrix for DS-3*

	M_w	S	R_{JB}	T	η	μ	α_s	α_r	λ	γ
M_w	1.000	-.027	-.160	.065	.484	-.030	-.003	.017	.001	.015
S	-.027	1.000	.014	-.062	-.249	-.007	-.007	.001	-.005	-.003
R_{JB}	-.160	.014	1.000	-.065	-.499	-.039	.004	-.015	.001	-.013
T	.065	-.062	-.065	1.000	-.155	-.088	-.039	-.016	.043	.003
η	.484	-.249	-.499	-.155	1.000	-.142	-.030	-.021	.043	-.004
μ	-.030	-.007	-.039	-.088	-.142	1.000	.032	.018	-.001	.009
α_s	-.003	-.007	.004	-.039	-.030	.032	1.000	-.007	.005	.004
α_r	.017	.001	-.015	-.016	-.021	.018	-.007	1.000	.001	-.008
λ	.001	-.005	.001	.043	.043	-.001	.005	.001	1.000	-.004
γ	.015	-.003	-.013	.003	-.004	.009	.004	-.008	-.004	1.000

a. Only cases for which DS = 3 are used in the analysis phase.

As shown in Table 5.20, the KMO index of DS-3 reduces to 0.347, meaning that the obtainment of DS-3 from the nonlinear structural analyses is less than the aforementioned damage states in PCA. Although the measurement of this index for DS-3 is low to express correlations between the independent variables in high accuracy, the analysis model is acceptable since the significance value is equal to 0.0.

Table 5.20. *KMO and Bartlett's Test for DS-3*

Kaiser-Meyer-Olkin Measure of Sampling Adequacy.		0.347
Bartlett's Test of Sphericity	Approx. Chi-Square	64282.137
	df	45.0
	Significance	0.000

As far as Table 5.21 is investigated, the extraction value of magnitude, soil condition, post-yielding ratio and residual strength ratio has lower participation ratio to explain the relationship of DS-3 than other independent variables.

Table 5.21. *The communalities for DS-3*

	Initial	Extraction
Magnitude (M_w)	1.000	0.470
Soil (S)	1.000	0.474
Distance (R_{JB})	1.000	0.509
Period (T)	1.000	0.690
Strength Ratio (η)	1.000	0.848
Ductility Ratio (μ)	1.000	0.558
Post-yielding Ratio (α_s)	1.000	0.437
Post-capping Ratio (α_r)	1.000	0.667
Residual Strength Ratio (λ)	1.000	0.481
Degradation Parameter (γ)	1.000	0.864

According to the results given in Table 5.22, five components are extracted to express the relationship of DS-3 in accordance with the eigenvalues of the components.

Table 5.22. *The total variance of DS-3*

Component	Initial Eigenvalues			Extraction Sums of Squared Loadings		
	Total	% of Variance	Cumulative %	Total	% of Variance	Cumulative %
1	1.835	18.354	18.354	1.835	18.354	18.354
2	1.125	11.247	29.601	1.125	11.247	29.601
3	1.023	10.225	39.826	1.023	10.225	39.826
4	1.013	10.125	49.951	1.013	10.125	49.951
5	1.005	10.048	59.999	1.005	10.048	59.999
6	0.990	9.901	69.900			
7	0.967	9.666	79.567			
8	0.958	9.580	89.146			
9	0.827	8.266	97.412			
10	0.259	2.588	100.000			

Table 5.23 shows that the coefficients of the first component represent an effective correlation between the independent variables due to the highest variance. Therefore, the strength ratio, magnitude of the earthquake and source-to-site distance are prominent parameters in the relationship of DS-3 with the independent variables, respectively. Since the URM structures are exposed to the necking between LS-2 and LS-3, the strength ratio can become the most effective parameter in this range as well as DS-2. The principal component relationship of DS-3 for the URM structures is given as follows:

$$DS\text{-}3 = 0.909\eta + 0.669M_w - 0.668R_{JB} - 0.022T - 0.144\mu - 0.040\alpha_s - 0.300S + 0.047\lambda - 0.001\alpha_r + 0.017\gamma \quad (5.12)$$

Table 5.23. *The component matrix of DS-3*

	Components				
	1	2	3	4	5
Strength Ratio (η)	0.909	0.095	-0.028	-0.066	-0.090
Magnitude (M_w)	0.669	-0.043	-0.100	0.025	0.102
Distance (R_{JB})	-0.668	-0.109	0.027	-0.129	-0.183
Period (T)	-0.022	-0.755	0.197	0.190	0.212
Ductility Ratio (μ)	-0.144	0.572	0.306	0.288	0.184
Post-yielding Ratio (α_s)	-0.040	0.334	0.534	-0.125	-0.151
Soil (S)	-0.300	0.138	-0.512	0.061	0.315
Residual Strength Ratio (λ)	0.047	-0.226	0.470	0.452	-0.061
Post-capping Ratio (α_r)	-0.001	0.151	-0.225	0.762	0.114
Degradation Parameter (γ)	0.017	0.028	0.245	-0.260	0.858

Tables 5.24-5.28 are presented to present correlation of the independent variables for DS-4.

Table 5.24. *The correlation Matrix for DS-4*

	M_w	S	R_{JB}	T	η	μ	α_s	α_r	λ	γ
M_w	1.000	.029	-.167	.108	.275	.031	.013	.014	.000	-.006
S	.029	1.000	-.015	-.041	-.151	-.010	-.003	-.003	.003	.003
R_{JB}	-.167	-.015	1.000	-.103	-.322	-.035	-.019	-.008	.003	.001
T	.108	-.041	-.103	1.000	-.154	-.027	.000	-.025	-.009	-.020
η	.275	-.151	-.322	-.154	1.000	-.062	-.028	-.031	-.005	-.012
μ	.031	-.010	-.035	-.027	-.062	1.000	-.013	.007	-.003	-.003
α_s	.013	-.003	-.019	.000	-.028	-.013	1.000	-.004	-.002	-.001
α_r	.014	-.003	-.008	-.025	-.031	.007	-.004	1.000	.001	.000
λ	.000	.003	.003	-.009	-.005	-.003	-.002	.001	1.000	.000
γ	-.006	.003	.001	-.020	-.012	-.003	-.001	.000	.000	1.000

a. Only cases for which DS = 4 are used in the analysis phase

As shown in Table 5.25, when the KMO index of DS-4, which is calculated as 0.425, is compared with values of other damage state relationships, its value for DS-4 is less than the value of DS-1 and DS-2 and higher than the value of DS-3. Even though the relationship between DS-4 and the independent variables of interest is not more reliable due to the low variance in this analysis, the significance value of the model is obtained as 0.0, meaning that the model of analysis is acceptable.

Table 5.25. *KMO and Bartlett's Test for DS-4*

Kaiser-Meyer-Olkin Measure of Sampling Adequacy.		0.425
Bartlett's Test of Sphericity	Approx. Chi-Square	92836.870
	df	45.0
	Significance	0.000

Considering the results in Table 5.26, the extraction value of post-yielding ratio, post capping ratio and degradation parameter has lower participation ratio to explain the relationship of DS-4.

Table 5.26. *The communalities for DS-4*

	Initial	Extraction
Magnitude (M_w)	1.000	0.509
Soil (S)	1.000	0.796
Distance (R_{JB})	1.000	0.525
Period (T)	1.000	0.855
Strength Ratio (η)	1.000	0.775
Ductility Ratio (μ)	1.000	0.624
Post-yielding Ratio (α_s)	1.000	0.334
Post-capping Ratio (α_r)	1.000	0.241
Residual Strength Ratio (λ)	1.000	0.769
Degradation Parameter (γ)	1.000	0.268

According to Table 5.27, five components are extracted to represent the relationship of DS-4 in PCA by comparing each eigenvalue of the components.

Table 5.27. *The total variance of DS-4*

Component	Initial Eigenvalues			Extraction Sums of Squared Loadings		
	Total	% of Variance	Cumulative %	Total	% of Variance	Cumulative %
1	1.525	15.254	15.254	1.525	15.254	15.254
2	1.115	11.151	26.405	1.115	11.151	26.405
3	1.039	10.386	36.791	1.039	10.386	36.791
4	1.016	10.161	46.952	1.016	10.161	46.952
5	1.001	10.007	56.959	1.001	10.007	56.959
6	0.999	9.986	66.944			
7	0.994	9.936	76.880			
8	0.990	9.897	86.778			
9	0.832	8.317	95.095			
10	0.491	4.905	100.000			

In Table 5.28, the coefficients of the first component represent the best correlation between the independent variables due to its highest variance. Therefore, the strength ratio, source-to-site distance and magnitude of the earthquake are outstanding independent variables in the relationship of DS-4. The principal component relationship of DS-4 for the URM structures is given as follows:

$$DS\text{-}4 = 0.789\eta - 0.687R_{JB} + 0.630M_w + 0.049T - 0.175S - 0.021\alpha_r - 0.009\mu + 0.001\alpha_s - 0.013\lambda - 0.030\gamma \quad (5.13)$$

Table 5.28. *The component matrix of DS-4*

	Components				
	1	2	3	4	5
Strength Ratio (η)	0.789	-0.383	-0.065	0.041	0.011
Distance (R_{JB})	-0.687	-0.189	-0.125	-0.045	0.022
Magnitude (M_w)	0.630	0.278	0.177	0.058	0.019
Period (T)	0.049	0.854	-0.317	-0.145	0.045
Soil (S)	-0.175	0.278	0.638	0.527	0.059
Post-capping Ratio (α_r)	-0.021	-0.042	0.409	-0.252	-0.093
Ductility Ratio (μ)	-0.009	0.100	0.520	-0.580	-0.079
Post-yielding Ratio (α_s)	0.001	0.144	-0.117	0.429	-0.340
Residual Strength Ratio (λ)	-0.013	-0.052	0.084	0.193	0.849
Degradation Parameter (γ)	-0.030	-0.120	0.146	0.298	-0.377

5.4. Evaluations of the Results Obtained from the Statistical Analyses

In this section, the relationships between different DS values and the independent variables of interest obtained via the mentioned statistical analyses methods are evaluated. It is observed that the most three effective parameters, named as the strength ratio, magnitude of the earthquake and source-to-site distance, are the same for all of the statistical analyses. However, there are some differences in terms of their priority emerged from the classification rate of each DS in discriminant analysis, the participation rate of each independent variable in the DS in multiple regression analysis and extraction value of an independent variable in the related DS in principal component analysis.

The most three effective parameters for each statistical analysis can be consecutively stated as follows: The strength ratio, magnitude of the earthquake and source-to-site distance for DA and MRA; the magnitude of the earthquake, strength ratio and source-to-site distance for PCA of DS-1; the strength ratio, source-to-site distance and magnitude of the earthquake for PCA of DS-2 and DS-4; the strength ratio, magnitude of the earthquake and source-to-site distance for PCA of DS-3. These differences in the order of significance for the same parameters may be attributed to the differences in the statistical methodologies.

Finally, the modeling uncertainty involved in the structural simulations may have also influenced the outcomes such as the low extraction value of an independent variable and the low classification rate of the group of DS and DA is the most appropriate statistical method for this case study.

CHAPTER 6

SUMMARY AND CONCLUSIONS

6.1. Summary

This study mainly focuses on seismic performance assessment of URM structures subjected to simulated ground motion records for Düzce region. The simulation parameters were previously validated with the records of the 1999 Düzce (M_w=7.1) earthquake. With this fundamental aim, the structural model is initially generated in a simplified manner by converting the MDOF system into an ESDOF model. The performance values of structural parameters, which are fundamental period, strength ratio, ductility, post-yielding ratio, post-capping ratio, residual strength ratio, and degradation parameter, are obtained by previous experimental and analytical studies in addition to the global and local earthquake design regulations for URM structures. The ESDOF model is employed to obtain limit states in terms of displacement with MIMK hysteresis model while the damage states of the structural simulations obtained through dynamic analyses are utilized to compare the global seismic response statistics and the pre-defined limit states. In order to obtain ground motion records from the simulated ground motion database, the dummy earthquake stations are randomly selected to have at least two PGA values in each interval between 0.1g to1.0g at M_w=7.1 in soft soil condition. The same procedure is applied for all cases. With 240 different acceleration-time records, 10125 unique structural simulations, which represents the combination of each performance value of the structural parameters, are carried out to determine seismic responses of URM buildings.

During the study, the DS of an ESDOF model is determined by comparing the results of nonlinear structural analyses and the pre-defined limit states in terms of displacement. Sensitivity analysis is employed to observe changes in DS with changing discrete values of each structural parameter under different earthquake magnitudes and R_{JB} distance intervals for soft and hard soil conditions. After that, the probabilistic estimation of performance levels of URM structures for each magnitude of the earthquake and PGA value is carried out in different soil conditions. Discriminant and multiple regression analysis are conducted in order to obtain relationships between the dependent variable (i.e. DS) and independent variables, namely the magnitude of an earthquake, soil condition, R_{JB} distance and all of the structural parameters. Another method, which is called as principal component analysis is used to focus on the determining relationships between each DS and the independent variables.

The results of this study can be used as a reference to evaluate the potential damage to URM structures. Besides, they can be employed to take precautions in order to mitigate earthquake losses.

6.2. Conclusions

Considering all the limitations and simplifications employed in this study, the following conclusions can be drawn from the results of seismic performance analysis of URM structures:

- The strength ratio seems to be the most effective independent variable, which affects the DS of URM structures; hence, it should be majorly considered in seismic design and assessment of URM structures. In addition, the strength ratio leads to an increased effect of fundamental period, which is the second most effective structural parameter.
- The earthquake magnitude is found to be the second most effective independent variable that determines DS of URM structures according to discriminant analysis and multiple regression analysis. Seismic damage initially begins to appear around M_w=5.5 for URM structures. In general, DS decreases with higher performance values of the structural parameters. For

instance, the mean value of DS for the lowest performance values of the structural parameters with the M_w=7.1 is 3.85 and it is 1.78 for the same earthquake when the highest performance values are used.

- Source-to-site distance is the third most effective variable on the DS-score of URM structures according to discriminant analysis and multiple regression analysis. As expected, source-to-site distance highly affects performance level of the URM structures. In this study, the effect of R_{JB} distance becomes pronounced with M_w=6.0.
- Soft and hard soil conditions have the same mean DS values for M_w=5.0 and 5.5. The influence of site condition begins to increase with M_w=6.0 and slight differences are observed with changing magnitudes.
- The fault rupture directivity effects lead to the occurrence of higher DS values at dummy stations far from the fault plane. In this study, the variation of mean DS values at different R_{JB} distance intervals demonstrated directivity effects under the same earthquake magnitudes.
- Ductility is an essential structural parameter to represent the displacement capacity of structures and the capability of absorption of earthquake energy. However, URM structures represent brittle behavior under seismic excitations. According to the numerical results in this study, URM structures have tendency to be in DS-1, DS-2 and DS-4. Thus, the effect of ductility for URM structures is observed to be less than the effects of the strength ratio and fundamental period.
- Other structural parameters as the post-yielding ratio, post-capping ratio, residual strength ratio, and degradation parameter are found to be non-effective variables on the DS of URM structures. For instance, even though higher degradation parameter enables to absorb more energy in a hysteretic curve, a URM structure has lower energy absorption capacity due to its material characteristic and thus its DS value is not affected by this parameter.

- The results of this study verify that URM structures are under high seismic risk even in the case of moderate ground motion intensities. Therefore, new masonry buildings should be constructed according to the current seismic regulations and the existing masonry buildings should be retrofitted to enhance their strength and displacement capacity.
- Furthermore, strength seems to be the most important structural parameter for rigid and brittle URM structures. If the capacity is not exceeded during ground shaking, the building survives without severe damage. However, if the capacity is exceeded, then the structure generally gets heavy damage or collapses since the safety margin in the inelastic range is narrow due to limited ductility and energy dissipation capacity. This means URM structures should be designed or evaluated by using force-based approaches and sufficient force capacity should be ensured in all the cases rather than the displacement capacity.

6.3. Future Studies

Following recommendations can be made for potential future studies:

- Further detailed models of URM structures can be employed to get more accurate results about the seismic performance of this structure type. Although it causes significant computational effort, historical URM structures particularly require to be analyzed with a detailed modeling approach. Therefore, in the future studies, seismic vulnerability of such structures can be investigated by using refined models and simulations.
- The parametric study can be extended to include other structure types such as reinforced concrete and steel buildings. The inherent structural characteristics of these buildings can be obtained from available studies and can be employed to assess their seismic performance.

- Ground motions from one region are employed in this study. In a future effort, simulated motions from different areas can also be employed.

REFERENCES

American Society of Civil Engineers (ASCE) (2005). Minimum Design Loads for Buildings and Other Structures. ASCE/SEI 7-05

Applied Technology Council (1985). "Earthquake Damage Evaluation Data for California", ATC-13, Redwood City, California.

Applied Technology Council (ATC) (1996). *Seismic Evaluation and Retrofit for Concrete Buildings*, ATC-40, Redwood City, California.

Askan, A., Sisman, F. N. and Ugurhan, B. (2013). Stochastic strong ground motion simulations in sparsely monitored regions: A validation and sensitivity study on the 13 March 1992 Erzincan (Turkey) earthquake. Soil Dynamics & Earthquake Engineering (0267-7261), 55, 170–181.

Asteris, P. G., Skentou, A. D., Moropoulou, A., Apostolopoulou, M., Mohebkhah, A., Cavaleri, L., Rodrigues, H., and Varum, H. (2019). Stochastic vulnerability assessment of masonry structures: Concepts, modeling and restoration aspects. Applied Sciences (Switzerland), 9(2).

ATC (1998) FEMA-306: Evaluation of earthquake damaged concrete and masonry wall buildings. Basic Procedures Manual, Applied Technology Council (ATC), Washington, U.S.

Bazzurro, P., Cornell, C.A., Menun, C. and Motahari, M. (2004). 'Guidelines for Seismic Assessment of Damaged Buildings', Proceedings of the 13th World Conference on Earthquake Engineering, No. 1708, Vancouver, Canada.

Benedetti, D., Carydis, P. and Pezzoli, P. (1998). Shaking Table Tests on 24 Simple Masonry Buildings. Earthquake Engineering and Structural Dynamics, 27(1), 67–90.

Bruin., J. (2006). Newtest: "Command to compute new test". UCLA: Statistical Consulting Group. htttp://stats.idre.ucla.edu/stata/ado/analysis/.

Calvi, G. M. (1999). "A Displacement-Based Approach for Vulnerability Evaluation of Classes of Buildings", Journal of Earthquake Engineering, 3(3): 411-438.

CEN (1995). Eurocode 8: *Design provisions for earthquake resistance of structures, Part 1-2: General rules and rules for buildings – General rules for buildings*. ENV 1998-1-2:1995, Brussels

Chaudhari, D. and Dhoot, G. (2016). Performance Based Seismic Design of Reinforced Concrete Building. Open Journal of Civil Engineering, 6, 188-194.

Chopra A.K. and Goel R.K. (2001). 'A modal pushover analysis procedure for estimating seismic demands for buildings: Theory and preliminary evaluation.' PEER Report 2001/2003, Pacific Earthquake Engineering Research Center, College of Engineering, University of California, Berkeley.

Chopra, A.K. and Goel, R.K. (2000). Capacity-demand-diagram methods based on inelastic design spectrum. Earthquake Spectra, 15(4), 637–655.

Clough, R.W. and Johnston, S.B. (1966). "Effect of Stiffness Degradation on Earthquake Ductility Requirements", Proceedings, Second Japan National Conference on Earthquake Engineering: 227-232.

Collins, K. and Stojadinovic, B. (2000). Limit States for Performance-based Design. Proc. 12 WCCE. Auckland, New Zealand.

Council of Europe (1998). "European Macroseismic Scale", edited by G. Grünthal, Centre Europèen de Géodynamique et de Séismologie, Luxembourg.

D'Ayala, D., Spence, R., Oliveira, C., and Pomonis, A. (1997). "Earthquake Loss Estimation for Europe's Historic Town Centers". Earthquake Spectra, 13(4): 773-793.

EERI, 1996. Post-Earthquake Investigation Field Guide: Learning from Earthquakes. Oakland, CA: Earthquake Engineering Research Institute.

Erberik et al. (2013). Characteristics of Unreinforced Masonry Buildings in Antakya Through Field Survey. 2nd Turkish Conference on Earthquake Engineering and Seismology, Antakya, Turkey, 25-27 September.

Erberik, M. A. (2008). Fragility-based assessment of typical mid-rise and low-rise RC buildings in Turkey. Engineering Structures, 30(5), 1360–1374

Erberik, M. A. (2008). Generation of fragility curves for Turkish masonry buildings considering in-plane failure modes. Earthquake Engineering and Structural Dynamics, 37(3), 387–405.

Erberik, M. A.[a)] (2010). Seismic Risk Assessment of Masonry Buildings in Istanbul for Effective Risk Mitigation. EARTHQUAKE SPECTRA, 26(4), 967–982.

European Committee for Standardization (2003). Eurocode 8: Design of Structures for Earthquake Resistance, Part 3: Strengthening and Repair of Buildings, Eurocode 8, Brussels.

Fajfar P. (2000). 'A nonlinear analysis method for performance-based seismic design', Earthquake Spectra, Vol.16, No. 3, 573-592.

Fajfar P. and Fischinger M. (1988). 'N2 – A Method for Non-linear Seismic Analysis of Regular Structures.' Proc. 9th World Conf. on Earthquake Engineering, Tokyo/Kyoto, Vol. 5, 111-116.

Federal Emergency Management Agency (FEMA) (2000). Prestandart and Commentary for the Seismic Rehabilitation of Buildings, FEMA-356, Washington, D.C.

Federal Emergency Management Agency, FEMA (1997). FEMA-273: *NEHRP guidelines for the seismic rehabilitation of buildings*, Washington DC.

Freeman S.A., Nicoletti J. P. and Tyrell J.V. (1975). ‘Evaluations of Existing Buildings for Seismic Risk - A Case Study of Puget Sound Naval Shipyard, Bremerton, Washington’, Proceedings of U.S. National Conference on Earthquake Engineering, Berkeley, U.S.A., 113-122.

Freeman, S.A. (2004). “Review of the Development of the Capacity Spectrum Method”, ISET Journal of Earthquake Technology, Vol. 41, No. 1, 438-451.

Graziotti, F., Penna, A., Bossi, E. and Magenes, G. (2014). Evaluation of displacement demand for unreinforced masonry buildings by equivalent SDOF systems. Proceedings of the 9th International Conference on Structural Dynamic, EURODYN, Porto-Portugal, 365–372.

Guerrini, G., Graziotti, F., Penna, A. and Magenes, G. (2017). Improved Evaluation of Inelastic Displacement Demands for Short-Period Masonry Structures. Earthquake Engineering and Structural Dynamics, 46(9), 1411–1430.

Guorui, H. and Tao, L. (2015). Review on Baseline Correction of Strong Motion Accelerogram. International Journal of Science, Technology and Society. Vol. 3, No.6, 309-314.

Hermandez-Montes E., Kwon O.-S. and Aschheim M. (2004). ‘An energy-based formulation for first- and multiple-mode nonlinear static (pushover) analyses’, Journal of Earthquake Engineering, 8(1), 69-88.

Ibarra L.F., and Krawinkler, H. (2005). “Global collapse of frame structures under seismic excitations”, Rep. No. TB 152, The John A. Blume Earthquake Engineering Center, Stanford University, Stanford, CA.

Ibarra L.F., Medina R. A., and Krawinkler H. (2005). “Hysteretic models that incorporate strength and stiffness deterioration”, Earthquake Engineering and Structural Dynamics, 34(12), 1489-1511.

Ingham, J., and Griffith, M. (2011). Damage to unreinforced masonry structures by seismic activity. Structural Engineer, 89(3), 14–15.

Kaklamanos, J., Baise, L. G. and Boore, D. M. (2011). Estimating unknown input parameters when implementing the NGA ground-motion prediction equations in engineering practice. Earthquake Spectra, 27(4), 1219–1235.

Karimzadeh Naghshineh, S. (2016). 'Use of simulated strong ground motion records in earthquake engineering applications', PhD Thesis, Graduate School of Natural and Applied Sciences, Civil Engineering Department, Middle East Technical University, Ankara/Turkey

Karimzadeh, S., Askan, A. and Yakut, A. (2017). Assessment of Simulated Ground Motions in Earthquake Engineering Practice: A Case Study for Duzce (Turkey). Pure and Applied Geophysics, 174(9), 3589–3607.

Karimzadeh, S., Erberik, M. A., Yakut, A. and Askan, A. (2018). Seismic damage assessment based on regional synthetic ground motion dataset: a case study for Erzincan, Turkey. Natural Hazards, 92(3), 1371–1397.

Kotanidis C. and Doudoumis I.N. (2008). 'Energy-Based Approach of Static Pushover Analysis', The 14th World Conference on Earthquake Engineering, China/Beijing.

Krawinkler H. and Seneviratna G. (1998). 'Pros and Cons of a Pushover Analysis for Seismic Performance Evaluation', Engineering Structures, 20, 452-464.

Lang, K. (2002). "Seismic Vulnerability of Existing Buildings", Swiss Federal Institute of Technology, Zurich.

Lang, K., and Bachmann, H. (2003). On the Seismic Vulnerability of Existing Unreinforced Masonry Buildings. Journal of Earthquake Engineering, 7(3), 407-426.

Lignos, D.G. and Krawinkler, H. (2012). “Development and Utilization of Structural Component Databases for Performance-Based Earthquake Engineering", Journal of Structural Engineering, ASCE, doi: 10.1061/(ASCE)ST.1943-541X.0000646.

Lourenço, P. B., Avila, L., Vasconcelos, G., Alves, J. P., Mendes, N. and Costa, A. C. (2012). Experimental Investigation on the Seismic Performance of Masonry Buildings Using Shaking Table Testing. Bulletin of Earthquake Engineering, 11(4), 1157–1190.

Lourenço, P. B., Rots, J. G., and Blaauwendraad, J. (1998). Continuum model for masonry: Parameter estimation and validation. Journal of Structural Engineering, 124(6), 642–652.

Magenes, G. (2006). Masonry building design in seismic areas: Recent experiences and prospects from a European standpoint, The First European Conference on Earthquake Engineering and Seismology, Geneva, Switzerland, 3-8 September, keynote k9.

Magenes, P. and Penna, A. (2011). Seismic Demand and Assessment of Masonry Buildings in Europe: Recent Research and Code Development Issues. 9th Australasian Masonry Conference Queenstown, New Zealand.

Mouyiannou, A., Rota, M., Penna, A. and Magenes, G. (2014). Identification of Suitable Limit States from Nonlinear Dynamic Analyses of Masonry Structures. Journal of Earthquake Engineering, 18(2), 231–263.

National Institute of Building Science (NIBS) (1999). Earthquake Loss Estimation Methodology, HAZUS99 Technical Manual. Report prepared for the Federal Emergency Management Agency, Washington D.C.

Parducci A., Comodini F., Lucarelli M., Mezzi M. and Tomassoli E. (2006). ‘Energy-Based Nonlinear Static Analysis’, 1st European Conference on Earthquake Engineering and Seismology Paper 1178, Geneva, Switzerland.

Paret T.F., Sasaki K.K., Eilbeck D.H. and Freeman S.A. (1996). ‘Approximate Inelastic Procedures to Identify Failure Mechanisms from Higher Mode Effects’, Proceedings of the 11th World Conference on Earthquake Engineering, No. 966, Acapulco, Mexico.

Petry, S. and Beyer, K. (2015). Limit states of modern unreinforced clay brick masonry walls subjected to in-plane loading. Bulletin of Earthquake Engineering, 13(4), 1073–1095.

Pomonis, A., Gaspari, M., and Karababa, F. S. (2014). Seismic vulnerability assessment for buildings in Greece based on observed damage data sets. Bollettino Di Geofisica Teorica Ed Applicata, 55(2), 501–534.

Shahzada, K., Khan, A. N., Elnashai, A. S., Ashraf, M., Javed, M., Naseer, A. and Alam, B. (2012). Experimental Seismic Performance Evaluation of Unreinforced Brick Masonry Buildings. EARTHQUAKE SPECTRA, 28(3), 1269–1290.

Smith, M. K. (1958). Review of Methods of Filtering Seismic Data. Geophysics, 23, 44–57.

Sucuoğlu, H. (2002). Engineering Characteristics of the Near-Field Strong Motions from the 1999 Kocaeli and Düzce Earthquakes in Turkey. Journal of Seismology, (3), 347-355.

Sucuoğlu, H., and Yazgan, U. (2003). Simple Survey Procedures for Seismic Risk Assessment in: Urban Building Stocks, Seismic Assessment and Rehabilitation of Existing Buildings, NATO Science Series IV/29, 97-118.

Tama, Y. S., Solak, A., Çetinkaya, N., Şen, G., Yılmaz, S., and Kaplan, H. (2013). Damages to unreinforced masonry buildings by the Van earthquakes of 23 October and 9 November 2011. Natural Hazards and Earth System Sciences, Vol 13, Iss 2, 329-337.

Tanırcan, G., Bekler, F. N., Meral Özel, N. and Dalguer, L. (2017). Dynamic Rupture Modelling of the 1999 Düzce, Turkey Earthquake. Pure and Applied Geophysics, 174(9), 3343–3355.

Themelis, S. (2008). 'Pushover analysis for seismic assessment and design of structures', PhD Thesis, The School of Built Environment, Heriot-Watt University, Edinburg UK

Tomazevic, M., Bosiljkov, V. and Weiss, P. (2004). "Structural Behavior Factor for Masonry Structures." 13th World Conf. on Earthquake Engineering., Paper No. 2642 Vancouver, B.C., China.

Turkish Earthquake Code, (2007). Specifications for the Buildings to be Constructed in Disaster Areas. Ministry of Public Works and Settlement, Ankara, Turkey.

Ugurhan, B. and Askan, A. (2010). Stochastic Strong Ground Motion Simulation of the 12 november 1999 Düzce (Turkey) Earthquake Using a Dynamic Corner Frequency Approach. Bulletin of the Seismological Society of America, 100(4), 1498–1512.

Walsh, K., Cummuskey, P., Dizhur, D., and Ingham, J. (2014). Seismic Characterization of Unreinforced Masonry Buildings in Auckland, New Zealand.

Yakut, A. and Solmaz, T. (2012). 'Performance-based Displacement Limits for Reinforced Concrete Columns under Flexure', Proceedings of the 15th World Conference on Earthquake Engineering. Lisbon, Portugal.

Yi, W.-H., Oh, S.-H. and Lee, J.-H. (2004). Shear Capacity Assessment of Unreinforced Masonry Wall. 13th World Conf. on Earthquake Engineering, Paper No. 1698, Vancouver, B.C., Canada.

Zavala, C., Honma, C., Gıbu, P., Gallardo, J. and Huaco, G. (2004). "Full Scale on Line Test on Two Story Masonry Building Using Handmade Bricks." 13th World Conf. on Eartquake Engineering., Paper No. 2885, Vancouver, B.C., China